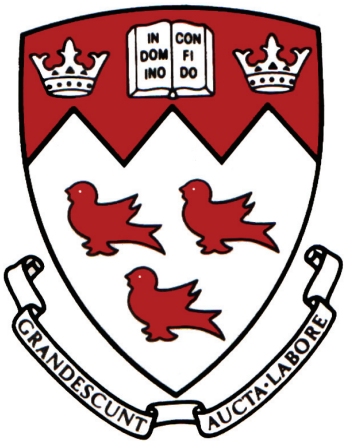
AN INVESTIGATION OF SOIL-TUNNEL INTERACTION IN MULTI-LAYER GROUND

BY

MIGUEL ANTONIO NUNES



DEPARTMENT OF CIVIL ENGINEERING & APPLIED MECHANICS

MCGILL UNIVERSITY, MONTRÉAL, QUÉBEC, CANADA

APRIL, 2008

A thesis submitted to McGill University in partial fulfilment of the requirements of the degree of Master of Civil Engineering

© MIGUEL ANTONIO NUNES, 2008

ABSTRACT

Urbanisation is a phenomenon that has continued undisturbed since the rise of the industrial era. As the populations of cities increase so do the needs and demands associated with urban expansion. These include the provision of adequate infrastructure to support and sustain the current quality of life, while also planning prudently for future growth. However this continued intensified land use progressively presents challenges to planners and operators alike. It is for this reason that engineers are opting to use underground space as an alternative means of meeting societal needs without significant disruption to activities at the surface. Tunnels are therefore becoming increasingly useful for inspecting and retrofitting buried facilities; buried transportation routes can be seen in subway lines and tunnelled highways. However these services cannot exist without adequate knowledge of the ground in which they exist. It is therefore imperative that studies be done in order to understand as much as possible the intricacies of soil-tunnel interaction.

A review of the literature has shown that overwhelming attention has been placed on modelling tunnels in isotropic, homogeneous media, whether those models be empirical, analytical, physical or numerical. However soils in nature are neither homogeneous nor isoptropic. Therefore the objective of this thesis was to examine the soil-tunnel interaction within an excavation in layered ground. A flexible aluminum lining sleeve was placed inside of a cavity excavated out of a cohesive medium for the purpose of monitoring the reaction stresses and bending moments arising from contact with the encroaching soil. A granular stratum was introduced within the cohesive soil at varying elevations above a fixed tunnel position in order to study the effect of proximity of this layer on the soil-lining response. It was found that the presence of the sandy stratum had an effect on the response when it was located at an elevation of two or less equivalent excavated diameters. At elevations greater than this, the effect was negligible. Stresses and bending moments were reduced by 90% when a layer of sand was introduced at one equivalent excavated diameter above the tunnel as opposed to having no sand layer. Further results involving a numerical model were similar; when the granular layer was one excavated diameter above the tunnel the axial forces were found to be 53% of those calculated when no such layer was present. Soil displacement patterns revealed a related trend, with an increase in soil movement of 17% as the sand layer was moved from one excavated diameter away from the opening to the case where no granular material existed.

RESUME

L'urbanisation est un phénomène qui n'a cessé de croître de manière continue depuis l'apparition de l'ère industrielle. À mesure que les populations citadines augmentent, les besoins et les demandes liés à l'expansion urbaine augmentent également. Ceux-ci incluent l'approvisionnement en infrastructures capable de répondre à la fois aux besoins de la population et à satisfaire sa qualité de vie, tout en projetant prudemment vers l'horizon afin d'anticiper la croissance urbaine. Cependant cette continuelle expansion de terrain aménagé présente graduellement des défis aussi bien aux planificateurs qu'aux opérateurs. C'est pour cette raison que les ingénieurs optent pour l'exploitation des espaces souterrains comme moyen alternatif, dans le but de satisfaire les besoins sociaux sans perturber de manière significative les activités menées en surface. Les tunnels deviennent donc de plus en plus utiles pour l'inspection et la mise à niveau des équipements enterrés; des voies de transport telles que les lignes de métro et les autoroutes souterraines peuvent également être rencontrées. Cependant ces services ne peuvent exister sans une connaissance adéquate du sol dans lequel ils existent. Il est donc impératif que des études soient faites afin de comprendre autant que possible les complexités de l'interaction sol-tunnel.

Une revue de la littérature a montré qu'une attention particulière a été placée sur la modélisation des tunnels dans des milieux isotropes et homogènes aussi bien pour des modèles empiriques, analytiques, physiques ou numériques. Cependant les sols naturels ne sont ni homogènes ni isotrope. Par conséquent l'objectif de cette thèse consistait à examiner l'interaction sol-tunnel dans une excavation réalisée dans un sol stratifié. Un revêtement flexible en aluminium a été introduit à l'intérieur d'une cavité excavée dans un milieu cohésif dans le but de mesurer les efforts de réaction et les moments de flexion résultant du contact avec le sol en mouvement. Une strate granulaire a été introduite dans le sol cohérent à différentes hauteurs au-dessus d'une position fixe du tunnel afin d'étudier l'effet de proximité de cette couche sur la réponse sol -revêtement. Il a été constaté que la présence de la strate sableuse a eu un effet sur la réponse lorsque celle-ci se située à une hauteur équivalente à deux fois ou inférieur aux diamètres excavés. A des hauteurs supérieures, l'effet était négligeable. Les contraintes et les moments de flexion ont été réduits de 90% lorsqu'une couche de sable a été introduite au-dessus du tunnel à une hauteur équivalente à un diamètre excavé en comparaison avec le cas où aucune couche de sable n'était pressente.

D'autres résultats impliquant un modèle numérique ont étaient semblables; lorsque la couche granulaire se située à un diamètre excavé au-dessus du tunnel, les forces axiales représentaient 53% de celles calculées lorsque aucune telle couche n'était présente. Les différents diagrammes de déplacement du sol ont indiqué une tendance commune, avec une augmentation du mouvement du sol de 17% entre le cas ou la couche de sable a été déplacée de l'orifice d'une distance de un diamètre excavé jusqu'au cas où aucun matériel granulaire n'était présent.

ACKNOWLEDGEMENTS

Nothing in my life has ever been made possible without the love and guidance from my parents, Anibal and Sandra Nunes. Their sacrifices are yet to be outweighed by their returns. They left the comfortable trappings of familiar surroundings for the unknown, in order that their children might have the opportunities that they never had. This has always been the impetus for my ambition, and no degree or accolade could ever repay their devotion. Eternal gratitude is theirs. To my little sister, Denise Nunes, who has been with me at every major phase of my life, I thank her for her witty motivation and love.

To my grandfathers, Antonio Nunes and Baliram Maharaj, who were two of the smartest men I have ever known, but whose potential was never realised fully because of ignorance and circumstance. My academic ambition is stayed by their lives. To my grandmothers, Carmen Rivera Nunes and Josephine Maharaj, whose stories could prove inspirational to anyone, and whose sacrifices have enabled me to be where I am today.

To Danielle Johnston, my daily rock and confidante, she has been one of the best friends anyone could ever want or need. Her advice and attentiveness will never be forgotten. To Sonal Gandhi, with whom my academic career began, she has seen my start as an unfocused undergraduate and has helped me make sense of the world along every step of my academic life, and life in general.

To Dr. M.A. Meguid, who gave me an opportunity that not many others might have, I have much thanks. He has provided guidance and has taught me much about academic life. To the technicians, John Bartzcak, Damon Kipperchuk, Marek Przykorski and Ron Sheppard, without whom none of my research could have been realised. A special vote of thanks is given to Joe Colaciello for providing free transportation and delivery. Their knowledge and experience is boundless, and I am extremely grateful. To Dr. William Cook and Jorge Sayat, both of whom lent their expertise, allowing me to overcome the last minor challenges to finish my work.

To Julian Gacek, whose mutual support I shared and appreciated throughout my work. To Sean Monkman, whose experience, support and friendship have enriched my work greatly. Without his sharp wit, academic perspective and entertaining thoughts, much of the past two years would not have been as enjoyable as they were. To Gilles Comeau and Kostadin Velchev, with whom I shared laboratory space, I thank you for your understanding and for sharing our resources. Your support has also been much appreciated. To Salem Bouhairie, for providing advice garnered from a wealth of experience. To Zachary Veaner, Cheehan Leung and Charlotte Chow for their contributions to the preparation of my research. Also, to Kaveh Dekoda for giving assistance when he did not have to do so. To Merouane Menaa, who translated my abstract into French. Finally, I have a special gratitude for Reena Balh. She helped in the early construction phases, and also by being supportive throughout the entirety of my research.

Dei gratia
Ad maiorem Dei gloriam

NOMENCLATURE

LATIN SYMBOLS

c	Shear strength
C	Compressibility
C_c	Co-efficient of curvature
C_u	Co-efficient of uniformity
d-	Denotes a differential quantity
D	Excavated tunnel diameter
E	Modulus of elasticity
F	Flexibility ratio
g	Gravitational constant of the Earth
G_s	Specific gravity
h	Height in general, or height of soil cover above a tunnel
I	Second moment of inertia
K_o	Co-efficient of earth pressure, at-rest
ℓ	Arc length
LL	Liquid limit
m	Degree of stress-dependency
M	Bending moment
N	Axial force
PI	Plasticity index
PL	Plastic limit

p	Stress or pressure intensity
q	Deviatoric stress
r	Radius
R_{int}	Strength factor
R_f	Failure ratio
t	Lining thickness
u	Displacement
w	Ground loss
x	Axis normal to the Cartesian y-z plane
y	Axis normal to the Cartesian x-z plane
z	Axis normal to the Cartesian x-y plane

GREEK SYMBOLS

γ	Unit weight
δ	Displacement
ε	Strain
θ	Angle measured in r-θ space (polar co-ordinates)
ν	Poisson's ratio
σ	Stress or pressure intensity
τ	Shear stress
ϕ	Angle of friction
ψ	Angle of dilatancy

SUBSCRIPTS & SUPERSCRIPTS

-1	Denotes major principal action
-3	Denotes minor principal action
-50	Denotes secant measurements
-a	Denotes an asymptotic value
-f	Denotes a failure mode
-h	Denotes action in a horizontal direction
-o	Denotes an initial or fixed condition
-oed	Denotes a value acquired from Oedometric testing
-r	Denotes action in a radial direction
-ref	Denotes reference conditions
-u	Denotes undrained conditions
-ur	Denotes unloading and reloading action
-v	Denotes action in a vertical direction
-θ	Denotes action in a tangential direction

- TABLE OF CONTENTS -

ABSTRACT ..... **i**

RESUME ..... **ii**

ACKNOWLEDGEMENTS ..... **iv**

NOMENCLATURE ..... **v**

LIST OF FIGURES ..... **xi**

LIST OF TABLES ..... **xv**

CHAPTER 1 – INTRODUCTION **1**

1.1 GENERAL OVERVIEW **1**

1.1.1 THE ANATOMY OF A TUNNEL 1

1.1.2 GROUND-LINING RESPONSE 3

1.1.3 THE PLANE-STRAIN CONDITION 7

1.1.4 PREDICTING RESPONSE 8

1.2 TUNNELLING METHODS **10**

1.2.1 CUT AND COVER 11

1.2.2 TUNNEL BORING MACHINE 11

1.2.3 PIPE-JACKING 13

1.2.4 NEW AUSTRIAN TUNNELLING METHOD 14

1.3 RESEARCH OBJECTIVES **15**

CHAPTER 2 – LITERATURE REVIEW **17**

2.1 INTRODUCTION **17**

2.2 PHYSICAL MODELLING **18**

2.2.1 TECHNIQUES 18

2.2.1.1 Trap-Door Models 19
2.2.1.2 Rigid Tubes 23
2.2.1.3 Pressurised Air Bags 26
2.2.1.4 Polystyrene Foam & Organic Solvent 27
2.2.1.5 Soil Augering 28
2.2.1.6 Miniature TBM 29

2.3 LAYERED GROUND **31**

CHAPTER 3 – EXPERIMENTAL PROGRAMME **33**

3.1 INTRODUCTION **33**

3.2 STRONGBOX **33**

3.2.1 OVERVIEW 34
3.2.2 ELEVATION VIEW 36
3.2.2.1 Details – Side 37
3.2.2.2 Details – Base 38
3.2.2.3 Details – Perspex Face 39
3.2.3 PLAN VIEW 41
3.2.4 END VIEW 42
3.2.5 SUPPORTING COMPONENTS 44
3.2.5.1 Perspex Caps 44
3.2.5.2 Steel Strap Connectors 46
3.2.5.3 Anchoring W-Section 47
3.2.5.4 Casing 47
3.2.5.5 Stool 48
3.2.5.6 Lining 49
3.2.5.7 Hydraulic Jack 50
3.3 A COHESIVE MEDIUM **51**
3.3.1 RATIONALE 51
3.3.2 MIX DESIGN 52
3.3.3 MATERIAL PROPERTIES 53
3.3.3.1 Fine Sand 53
3.3.3.2 Coarse Sand 53
3.3.3.3 Bentonite Clay 54
3.3.3.4 Cement 54
3.3.3.5 Aluminum 54
3.3.4 MIX DENSITY 55
3.4 DATA ACQUISITION **55**
3.4.1 STRAIN GAUGES 56
3.4.2 DATA ACQUISITION SYSTEM 57
3.4.3 SOFTWARE 57
3.5 METHODOLOGY **58**
3.5.1 OBJECTIVES 58
3.5.2 PROCEDURE 58
3.5.3 SAMPLE PREPARATION 60
CHAPTER 4 – EXPERIMENTAL RESULTS **63**
4.1 INTRODUCTION **63**
4.2 OBSERVATIONS **63**
4.2.1 SHEAR STRENGTH 63

4.2.2 MOISTURE CONTENT 64
4.3 DATA 65
4.3.1 TREATMENT 65
4.3.2 CASE 1: CONTROL TEST 68
4.3.3 CASE 2: SAND LAYER 1 DIAMETER ABOVE THE TUNNEL (1D TEST) 70
4.3.4 CASE 3: SAND LAYER 2 DIAMATERS ABOVE THE TUNNEL (2D TEST) 72
4.3.5 CASE 4: SAND LAYER 3 DIAMETERS ABOVE THE TUNNEL (3D TEST) 72
4.4 CALCULATED RESULTS 75
4.4.1 STRESSES 75
4.4.2 BENDING MOMENTS 75
4.5 ANALYSIS 76
CHAPTER 5 – NUMERICAL ANALYSIS 77
5.1 INTRODUCTION 77
5.2 CONSTITUTIVE MODEL 77
5.3 NUMERICAL MODEL 80
5.4 PROPERTIES & ASSUMPTIONS 82
5.5 RESULTS 83
5.6 ANALYSIS 90
5.6.1 DISCUSSION 90
5.6.2 DISCREPANCIES 91
CHAPTER 6 – CONCLUSIONS & RECOMMENDATIONS 93
6.1 CONCLUDING REMARKS 93
6.2 RECOMMENDATIONS FOR FUTURE WORK 99
REFERENCES 101
APPENDIX A 108
APPENDIX B 112
APPENDIX C 115
APPENDIX D 117
APPENDIX E 120
APPENDIX F 130
APPENDIX G 132

LIST OF FIGURES

Figure 1.1: Analogue of beams depicting the re-distribution of stresses when support is removed 2

Figure 1.2: Freshly excavated tunnel with gap surrounding the lining 3

Figure 1.3: Cardinal points of a tunnel 3

Figure 1.4: Stress distribution before the removal of soil (left-hand half-space); stress distribution after soil removal with distorted lining shape (right-hand half-space) (Peck, 1969) 4

Figure 1.5: Bending moment distribution around an infinitely rigid lining as a response to removing soil from within the lining 4

Figure 1.6: Elements at the crown and springline experiencing tensile and compressive action, respectively 6

Figure 1.7: Superposition of various modes which contribute to total deformation patterns of a tunnel. (after González and Sagaseta, 2001) 7

Figure 1.8: Displacement profile showing the development of the plane-strain region where movements converge to a maximum value, u_{max} (left); two-dimensional movement in A'-A' (right) 8

Figure 1.9: Circular tunnel considered by Bobet (2001) 9

Figure 1.10: An example of cut and cover construction 11

Figure 1.11: A typical TBM 12

Figure 1.12: A TBM at the end of the tunnel alignment 13

Figure 1.13: A typical jack 14

Figure 1.14: A schematic of the procedure of pipe-jacking 14

Figure 2.1: The classical Trap-Door Problem (Meguid et al., 2008) 19

Figure 2.2: The classical Trap-Door Problem, left: passive mode; right: active mode. (Vardoulakis et al., 1981) 19

Figure 2.3: Schematic of trap-door apparatus used by Park et al. (1999) 20

Figure 2.4: Settlement troughs for displacements of 1 to 4 mm. (Park et al., 1999) 21

Figure 2.5: Trap-door apparatus with loading plate. (After Nakai et al., 2000) 22

Figure 2.6: Displacement patterns from the axi-symmetric trap-door test. (Adachi et al., 1995) 23

Figure 2.7: Model used by Chambon et al. (1991) 24

Figure 2.8: Left: model used by Sterpi et al., and right: observerd failure mechanism (1996) 25

Figure 2.9: Left: schematic of the apparatus by Kamata and Masimo, and right: observerd complete failure pattern (2003) 26

Figure 2.10: Schematic of the apparatus used by Hagiwara et al (1999) 27

Figure 2.11: The steps of placing a polystyrene cylinder within a sand medium as described by Sharma et al. (2001) 28

Figure 2.12: The equipment used by Chapman et al. (2006) 29

Figure 2.13: The schematic of the miniature TBM. (Nomoto et al. 1999) 30

Figure 2.14: Mechanically adjustable device. (Lee and Yoo, 2006) 30

Figure 2.15: Failure mechanism as a result of the Base Friction Method (Egger and Gindroz, 1979) 31

Figure 3.1: Strongbox as seen from the rear (back steel face showing) 35

Figure 3.2: Strongbox as seen from the front (Perspex face showing) 35

Figure 3.3: General elevation view from the front (all dimensions in mm) 37

Figure 3.4: Elevation view of the side detail from the front. The left side is shown. The right side has the same geometry. The back face also has the same geometry, and can be seen in the photographs 38

Figure 3.5: Elevation view of the bottom detail from the front (above), and from the back (below) 39

Figure 3.6: Elevation view of the details of the main hole and pilot holes 41

Figure 3.7: Plan view of the box (above) with corner detail (below) 42

Figure 3.8: End view of the box, with detail showing the 6-mm gap 43

Figure 3.9: Clockwise from upper-left: Photograph of the end view of the box; Picture of the end view at the base of the box; typical corner detail of the base 44

Figure 3.10: Photographs of the Perspex cap in plan (above) and of one sawn half with a rubber gasket in elevation view (below) 45

Figure 3.11: Photographs depicting the geometry and location of the strap connectors and connecting rods as seen from the end view (above) and in elevation (below) 46

Figure 3.12: Cross-section of the W-section (left); the position of a steel strap and the position of where the connecting rod was placed through the W-section flange are shown in the dashed circle (right) 47

Figure 3.13: Steel casing and threaded rod (upper-left); detail of steel plates holding the threaded rod (upper-right); detail of the bevelled cutting lip along the leading edge (bottom) 48

Figure 3.14: W-Section stool supporting the steel casing 49

Figure 3.15: Aluminum sleeve with circular section showing (left) and in elevation (right) ... 50

Figure 3.16: Hydraulic jack mounting with pump and connection to the threaded rod (detail) 51

Figure 3.17: Moulds used for cohesive samples (left); sheared samples (right) 52

Figure 3.18: A typical specimen used in coupon testing 55

Figure 3.19: Inner surface of the aluminum cylinder with strain gauge locations (S1, S2, C1, C2, etc.) 56

Figure 3.20: Elevation view of the aluminum cylinder showing the strain gauges aligned with the springlines and crown 57

Figure 3.21: Stages of excavation: (1) Casing outside on front side; (2) Casing inside the box; (3) Casing advancing out of the box at the rear; (4) Lining placed inside of the excavated tunnel 60

Figure 3.22: (clockwise from top left) Conditions for the control test with a uniform medium; Conditions for the test with the presence of a sand layer 1D above the crown of the excavation; Conditions for the test with the presence of a sand layer 2D above the crown of the excavation; Conditions for the test with the presence of a sand layer 3D above the crown of the excavation 62

Figure 4.1: Plan view of the open top depicting the locations of where shear strength readings were taken 64

Figure 4.2: Averaged moisture content values taken from material recovered from each pilot hole. 65

Figure 4.3: Inward uniform radial movement of the lining under an isotropic stress distribution ($\sigma_h = \sigma_v$) 66

Figure 4.4: Inward radial movement of the lining under an anisotropic stress distribution ($\sigma_h > \sigma_v$) 66

Figure 4.5: Inward radial movement of the lining under an anisotropic stress distribution ($\sigma_h < \sigma_v$) 67

Figure 4.6: Micro-strain data from the control test as developed with time 69

Figure 4.7: Photograph showing the deformed shape of the aluminum lining due to full contact with the surrounding soil 70

Figure 4.8: Micro-strain data from the 1D test as developed with time 71

Figure 4.9: Micro-strain data from the 2D test showing a nearly immediate stabilisation of the soil movements 73

Figure 4.10: Micro-strain data from the 3D test 75

Figure 5.1: Hyperbolic stress-strain relation in primary loading for a standard drained triaxial test (Adapted from Plaxis User's Manual, 2004) 80

Figure 5.2: The variation of the modulus of elasticity with confining pressure under CID test condition (Kempfert and Gebreselassie, 2006) 82

Figure 5.3: Finite element mesh depicting the position of the tunnel and the boundary conditions 83

Figure 5.4: Visual comparison of the FE maximum bending moments versus those from the control 1g test and Bobet's solution (2001) 85

Figure 5.5: Finite element mesh illustrating the position of the sand layer for the 2D case ... 86

Figure 5.6: Visual comparison of the FE maximum bending moment versus that from the 1D test. The maximum bending moment from the physical test was located at the crown....86

Figure 5.7: Visual comparison of the FE maximum bending moment versus that from the 2D test. The maximum bending moment from the physical test was located at the crown and was compressive....87

Figure 5.8: Visual comparison of the FE maximum bending moment versus that from the 3D test. The maximum bending moment from the physical test was located at the springline....87

Figure 5.9: Typical distribution of the axial forces arising in the lining for all tests. All forces are compressive....88

Figure 5.10: Vector diagram showing direction and magnitude of soil displacements (1D case) 89

Figure 5.11: Vector diagram showing direction and magnitude of soil displacements (2D case) 89

Figure 5.12: Vector diagram showing direction and magnitude of soil displacements (3D case) 90

Figure 5.13: Vector diagram showing direction and magnitude of soil displacements (control case) 90

Figure 6.1: Summary of the micro-strain data at the crown for all tests....97

Figure 6.2: Summary of the micro-strain data at the springline for all tests....98

Figure 6.3: Summary of the maximum displacements for all cases from the FE analyses....100

Figure 6.4: Summary of the maximum bending moments and axial forces for all cases from the FE analyses 100

LIST OF TABLES

Table 4.1: Summary of the Lining Stresses for All Cases 77
Table 4.2: Summary of the Bending Moments for All Cases 77
Table 5.1: Summary of FE Axial Forces 88
Table 5.2: Summary of FE Maximum FE Displacements 91

CHAPTER 1 – INTRODUCTION

1.1 GENERAL OVERVIEW

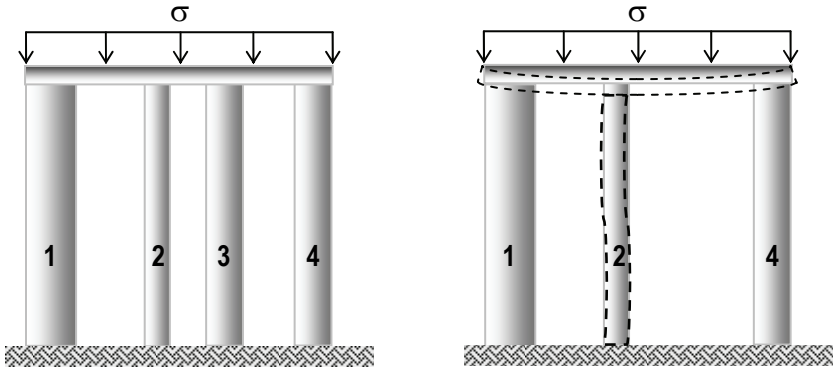
Increasing urban expansion has continued unabated since the beginning of the Industrial Revolution. As such, there is a constant need for matching infrastructure to support and sustain this ongoing growth. The consequential increased intensification of land use within cities has posed challenges that engineers must solve in order to maintain the quality of life that has become associated with contemporary society. Among these is not only the expansion of existing facilities within a densely constructed environment, but also there are the difficulties associated with renewing and maintaining current infrastructure. It is for this reason that the use of underground space is increasingly viewed as a viable option in the modern city. Tunnel construction has facilitated this trend. Working in a subterranean environment reduces service disruptions at the surface, while also minimising damage to existing structures. Therefore it has become imperative for engineers to predict as accurately as possible the response of ground to tunnelling. To this end, a myriad of testing methods have been published in the last 50 years as tools which allow for reasonable and safe estimations of ground behaviour after excavation.

1.1.1 THE ANATOMY OF A TUNNEL

When material is recovered from the ground to create a cavity, there is a re-distribution of stresses within the remaining soil. An analogy can be made with a frame system comprising a continuous beam supported by a number of columns as shown in Figure 1.1. If one column (e.g. column 3 in Figure 1.1) is removed, then the forces in each of the remaining columns will increase in a manner that is proportional to the normal stiffness of each member until static equilibrium is re-established. If the additional loading exceeds the capacity of any of the remaining supports and results in compressive failure, then buckling will be observed in the failed members (e.g. column 2). The overlying continuous beam may then experience a greater deflection as a consequence of an increased unsupported span. A similar phenomenon occurs during tunnelling. Excavation work serves to relieve the in-situ stresses in the soil that comprises the region at or near the wall of the cavity. The loss of ground and support is quickly accompanied by a stress re-distribution

within the remaining soil mass. If the tunnel can be idealised to be perfectly circular, then the re-distribution of stresses is usually associated with an inward, radial movement. Moreover, the increase in stress as a result of tunnelling can produce annular zones of localised plastic failure around the cavity, the extent of which is dependent on the strength of the material. This is akin to the buckling of the column in Figure 1.1.

It is for this reason that a lining may be introduced into the tunnel to support the surrounding material and control the radial displacements. When a Tunnel Boring Machine (TBM) is used, an over-cut which is larger than the proposed tunnel diameter is normally made in order to accommodate the placement of the lining. The result is the creation of a void, or *gap*, between the outer surface of the lining and the wall of the tunnel. Lee et al. (1992) stated that the magnitude of this space is dependent on the construction method, stress release at the face of the tunnel and workmanship. Soil may encroach until it rests in contact with the outer skin of the lining. Figure 1.2 provides illustrated details. As a note of convention, the cardinal points of a tunnel are the *crown* (extreme upper point), the opposing *springlines* (located at points coinciding with a rotation of 90° from the crown along the circumference of the tunnel) and the *invert* (extreme lower point). These terms as defined here will be used extensively throughout this thesis, and can be seen in Figure 1.3.



Columns 1, 2, 3 and 4 are in static equilibrium with the overlying beam and are supporting the imposed stress (σ).

Column 3 has been removed. Slender column 2 has buckled causing a concave deflection of the overlying beam. The stresses in thicker columns 1 and 4 have increased as a result.

Figure 1.1: Analogue of beams depicting the re-distribution of stresses when support is removed.

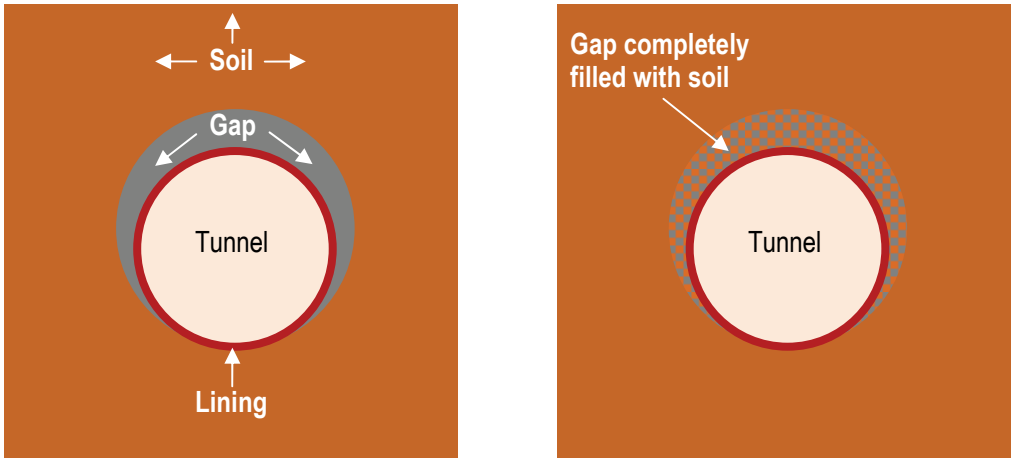


Figure 1.2: Freshly excavated tunnel with gap surrounding the lining (left); after sometime the soil encroaches and rests completely in contact with the lining (right).

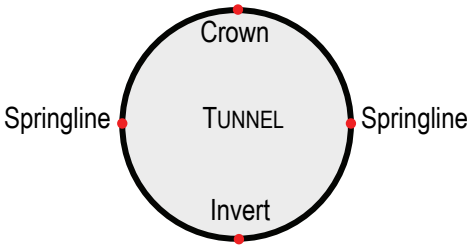


Figure 1.3: Cardinal points of a tunnel.

1.1.2 GROUND-LINING RESPONSE

Peck (1969) outlined a thought experiment to investigate the soil-lining interaction. A circular tunnel lining filled with soil was imagined to exist instantaneously within a semi-infinite soil mass. It was located at an arbitrary depth z_o from the free surface (Figure 1.4). For the purposes of discussion, the at-rest lateral earth pressure coefficient (K_o) was considered to be less than unity, which is generally the case in natural soils. At z_o, the vertical pressure intensity was γz_o, where γ was the unit weight of the overlying material. The lining was assumed to be perfectly flexible, but capable of supporting appreciable ring stresses in compression. Shear stresses were considered to be negligible as well. If the earth contained within the lining was suddenly recovered, then equilibrium will be restored only when radial pressures are equal everywhere along the circumference of the lining. Therefore the horizontal stress due to the soil-lining interaction will have to be increased while simultaneously decreasing the corresponding vertical stress for this to occur. As a result, the

horizontal diameter of the lining would become elongated in order to achieve the necessary increase in horizontal pressure relative to the original circular shape, while the vertical diameter would decrease to facilitate the required relaxation of vertical stress. This is known as ovalisation.

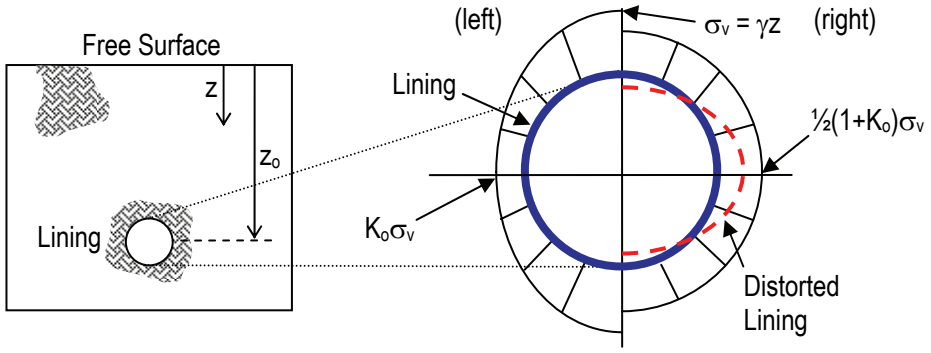


Figure 1.4: Stress distribution before the removal of soil (left-hand half-space); stress distribution after soil removal with distorted lining shape (right-hand half-space) (Peck, 1969).

A second thought experiment as described by Peck involved another imaginary circular lining that was perfectly rigid and infinitely strong. Soil was considered to be present initially within the lining in a manner similar with the first imagined scenario. The earth pressures acting radially against the lining were considered to be as identical as those presented in the left-hand half-space of Figure 1.4. However, once the material was removed to create a cavity, there would be absolutely no deformation of the rigid lining. Instead there would be an internal flexural response across the thickness of the lining. At the crown, there would be tensile reaction forces arising within the fibres of the inner skin housed inside of the lining, and compressive forces acting on the fibres of the outer surface. In terms of flexure, this will correspond with internal negative bending moments with respect to the inner surface. Conversely, at the springlines, compressive and tensile reaction forces along the inner and outer surfaces respectively, will correspond with a positive bending moment relative to the inner surface. The distribution of these bending moments can be seen in Figure 1.5.

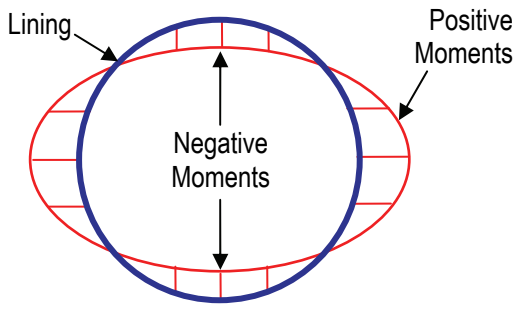


Figure 1.5: Bending moment distribution around an infinitely rigid lining as a response to removing soil from within the lining.

It should be noted that the distributions of stresses and moments shown in Figures 1.4 and 1.5 refer to ground conditions where $K_o < 1$. In the case where $K_o > 1$, the ovalisation pattern shown in Figure 1.4 will have a shape with elongation occurring in line with the vertical axis, and will result with stresses that are greater horizontally than they would be vertically. Similarly, the bending moment distribution will differ accordingly, where the negative moments will arise at the springlines, and positive moments at the crown and invert. This alternate ovalised shape is rarely seen in soils, but has been observed in soft rock (Lo & Lukajic, 1984).

The above thought experiments have provided insight into the response of a lining which is used to support surrounding earth pressures. Linings are neither completely flexible, nor infinitely strong in reality. Instead they have a flexural rigidity that is intermediate between perfect flexibility and rigidity. Therefore the superposition of the two imagined scenarios can be used to describe the basic response of a lining to the re-distribution of soil stresses; that is, the lining will deform while also being able to sustain bending moments. A discussion providing further details about the patterns of deformations and moments will now be presented, beginning with the latter.

Consider a typical planar element that can be found within the tunnel lining. It has a length of $d\ell$ and a thickness of dt, where ℓ is the arc length as measured along the circumference of the lining, and t is the thickness of the lining. If the element can be considered to be infinitesimally small, then $d\ell$ can be regarded as a straight, non-curved segment (therefore not an arc length) since the angle that describes this length approaches

zero. Please refer to Figure 1.6 for an illustration. An element located at the crown will experience negative bending moments with reference to the inner skin of the lining when the there is a vertical squeezing action as shown in Figure 1.4. Accordingly, if a similar element is located at the springline, then this same distortion will result in positive bending moments about the element with respect to the inner surface of the lining. Hence the inner surface of the lining can be said to be in tension at the crown, and in compression at the springline.

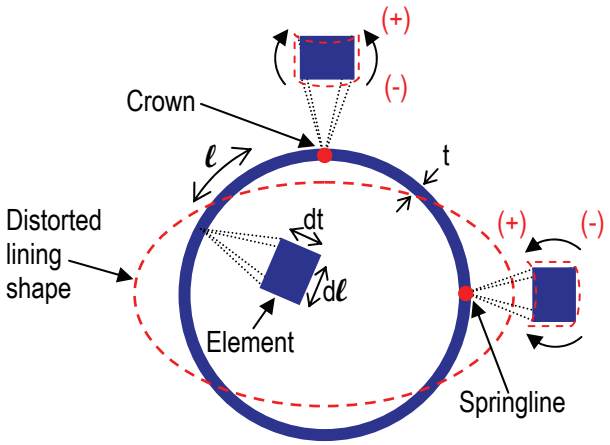


Figure 1.6: Elements at the crown and springline experiencing tensile and compressive action, respectively.

The deformation of a tunnel can be the result of mechanisms other than that shown in Figure 1.4. In general, the movement of the tunnel wall (which influences the reaction behaviour of a lining) is non-uniform, and can be considered to be the sum of the following ground responses (González and Sagaseta, 2001):

- a uniform radial inward displacement normally associated with ground loss, or a filling of the gap; this is also known as a radial contraction,
- ovalisation without a change of section (i.e. no ground loss), and
- a vertical uniform translation, with no distortion.

These modes are summarised graphically in Figure 1.7.

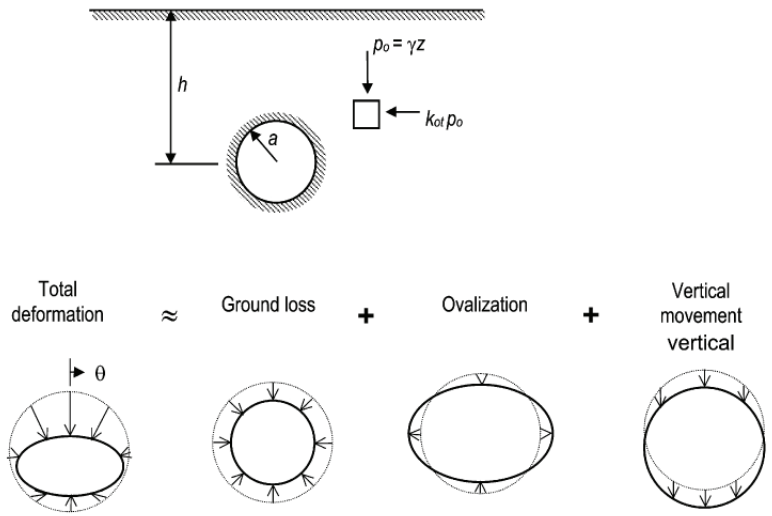


Figure 1.7: Superposition of various modes which contribute to total deformation patterns of a tunnel. (after González and Sagaseta, 2001)

1.1.3 THE PLANE-STRAIN CONDITION

The focus of discussion thus far has been on a generalised soil response to tunnelling. The phenomena outlined in the preceding sections can be observed at any cross-section along the alignment of the tunnel. However it should be stated that the behaviour of earth surrounding sections near to the excavated face of the tunnel differs from those which are further away. Consider cross-section A-A in Figure 1.8, which is adjacent to the tunnel face. It has been noticed that the magnitudes of the radial displacements eventually converge as the face of the tunnel advances with excavation; as work progresses and as the face moves further away from A-A, soil movements become fully developed. A'-A' represents this region, where activity at the face does not influence the radial contraction of the cavity. This unaffected zone can be considered to be the *plane-strain* region. Soil movements are at a maximum (u_{max}) here, and are co-planar with the cross-section under study (x-y plane).

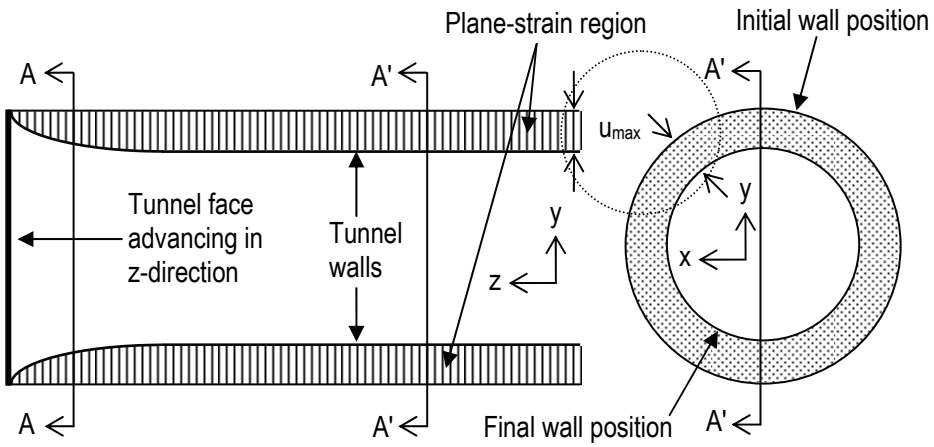


Figure 1.8: Displacement profile showing the development of the plane-strain region where movements converge to a maximum value, u_{max} (left); two-dimensional movement in A'-A' (right).

1.1.4 PREDICTING RESPONSE

The purpose of understanding the ground response to tunnelling is to facilitate the modelling of observed phenomena in order that future behaviour of excavated works may be predicted. Analytical closed-form solutions, empirical relationships and numerical computer-based analyses are examples of attempts to estimate observed activity in the field. Peck (1969) famously compiled empirical data from various worldwide tunnelling projects in order to formulate a unifying model for displacements at the surface due to ground loss. It was noticed that the profile of the subsidence could be approximated by the normal distribution curve as described by statisticians.

Mindlin (1940) studied the effect of a boundary (i.e. the ground surface) under differing biaxial stress distributions acting on a circular opening in an elastic medium. Most work before this considered the same problem, but in infinite media. Ensuing similar work was done using these results, leading to more refined closed-form analytical solutions for predicting displacements and stresses. Chief among these are the works done by Morgan (1961), Muir Wood (1975), Einstein and Schwarz (1978), Sagaseta (1987), Verruijt and Booker (1996), and Loganathan and Poulos (1998). Hefny and Lo (1999) presented solutions for the displacements and stresses along the circumference of unlined tunnels driven in an elastic, anisotropic rock medium.

Bobet (2001) investigated the soil-lining interaction in terms of stresses, moments and thrusts under fully saturated and dry ground conditions. The following assumptions were made:

- a circular cross-section (radius, r_o),
- plane-strain conditions in a direction normal to the plane of the tunnel cross-section,
- the existence of a gap (w) which accounted for ground losses ($loss$) as outlined by Lee et al. (1992), where $w = \frac{loss(\%)}{200} \cdot r_o$, and $loss$ was the difference in the cross-sectional area of the cavity before soil moved into the gap, and after the gap is filled,
- no mobilised shear stresses (τ) at the interface between the soil and lining,
- the elevation of the springline was at a depth of at least 1.5 equivalent radii beneath the free surface in order that boundary effects were negligible, and
- the ground was homogeneous and isotropic.

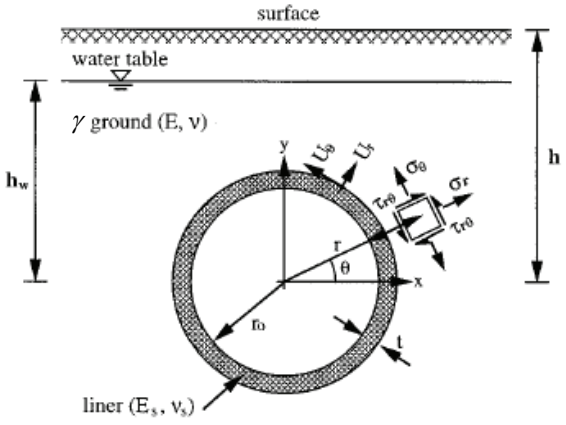


Figure 1.9: Circular tunnel considered by Bobet (2001).

Figure 1.9 depicts the idealised opening upon which Bobet's analysis was based. U referred to displacements, σ to stresses, τ to shear stresses, E to the elastic modulus, ν to the Poisson's ratio and h to a height above the springline. Subscripts 'r' and 'θ' denoted modes of action in radial and tangential directions, respectively. Angles were measured by rotating a terminal arm fixed at the centre of the opening of length r_o through a counterclockwise orientation. Rotation was done relative to an initial position which coincided with the positive abscissa.

The following cases were considered:

1. a shallow tunnel in dry ground,
2. a shallow tunnel in saturated ground, and
3. a shallow tunnel in saturated ground with air pressure to support the excavation.

The solutions for the simplest case (1) will be presented hereafter, as the others are not within the scope of this thesis. The flexibility ratio (F) relating the liner and ground properties (E, ν) is normally very large. Therefore a return to the thought experiments of Peck aids in obtaining an approximate analytical solution for stresses (σ), moments (M) and thrust forces (T) that arise in a lining placed within a soil cavity. A perfectly flexible liner ($F = \infty$) that was also perfectly incompressible ($C = 0$) was considered. The radial stresses were seen to be constant along the circumference of the tunnel at the interface between the soil and lining under this assumption. They had a magnitude of:

$$\sigma_{r=r_o} = \frac{E}{1+\nu}\cdot\frac{w}{r_o} - \frac{1}{2}\gamma h(1+K_o) \quad \text{.....} (1.1)$$ (Bobet, 2001)

Bobet's (2001) general solutions for thrusts and moments were found to be:

$$T = \frac{1}{2}\frac{\left[2E\frac{w}{r_o} - \gamma h(1+K_o)(1+\nu)\right](C+F)}{(C+F)(1+\nu)+(1-\nu^2)CF} r_o - \frac{3}{2}\frac{3-4\nu}{(1-\nu)F+3(5-6\nu)}\gamma h(1-K_o)r_o\cos 2\theta + \ldots$$

$$+\frac{3-4\nu}{(1-\nu)F+8(7-8\nu)}\gamma(1-K_o)r_o^2\sin 3\theta \quad \text{.....} (1.2)$$

$$M = -\frac{3}{2}\frac{3-4\nu}{(1-\nu)F+3(5-6\nu)}\gamma h(1-K_o)r_o^2\cos 2\theta + \ldots$$

$$+\frac{3-4\nu}{(1-\nu)F+8(7-8\nu)}\gamma(1-K_o)r_o^3\sin 3\theta \quad \text{.....} (1.3).$$

1.2 TUNNELLING METHODS

There is a variety of methods that can be employed to perform excavation work. However emphasis will be placed on those techniques which are applicable to tunnelling in soils only. These will be presented below. Other methods are not within the scope of this thesis.

1.2.1 CUT AND COVER

This is the simplest method, where a trench is dug from the surface to the desired elevation of the invert. A structural element such as a concrete culvert that is to act as a lining is placed at the base of the excavation, and material is back-filled and compacted to specification until the desired free-surface elevation is reached. This technique is usually used for infrastructure renewal works. Solutions for buried elements are applicable, while the solutions presented above are not, as boring action is not employed. Cut and cover is invasive in terms of disrupting activity at the surface, however simplicity is the main advantage. Figure 1.10 is a photograph of a section of highway in Britain that was buried in the ground; a concrete box-section was used to act as the lining to support earth pressures.



Figure 1.10: An example of cut and cover construction (http://www.iht.org/motorway/hatfield.htm).

1.2.2 TUNNEL BORING MACHINE

A tunnel boring machine (TBM) is an automated excavating system. As the name implies, it is a mechanised means of creating a tunnel, and is usually used for large-scale projects. Rotating cutting heads remove soil at the face of the excavation. The machines are manned by workers inside of it, who are responsible for maintaining the alignment of the

tunnel, as well as for removing cuttings and performing maintenance. A TBM can be used in soft rock, or in soft, water-bearing soil. Earth-pressure balance or a bentonite slurry is used to support the face from moving significantly into the excavation. This is especially important when working beneath the water table. A cylindrical shield supports the surrounding cavity wall near the face. Lining segments are put into place immediately behind the edge of the shield. An overcut is necessary to accommodate this work, thereby creating a gap between the soil and the lining. TBMs are costly and slow, and are normally customised for each project. However minimal disruption at the surface is an advantage. Figure 1.11 is a photograph of a typical TBM, while Figure 1.12 is a photograph of a TBM and the end of a freshly created tunnel. Soil cuttings can be seen in this photograph.

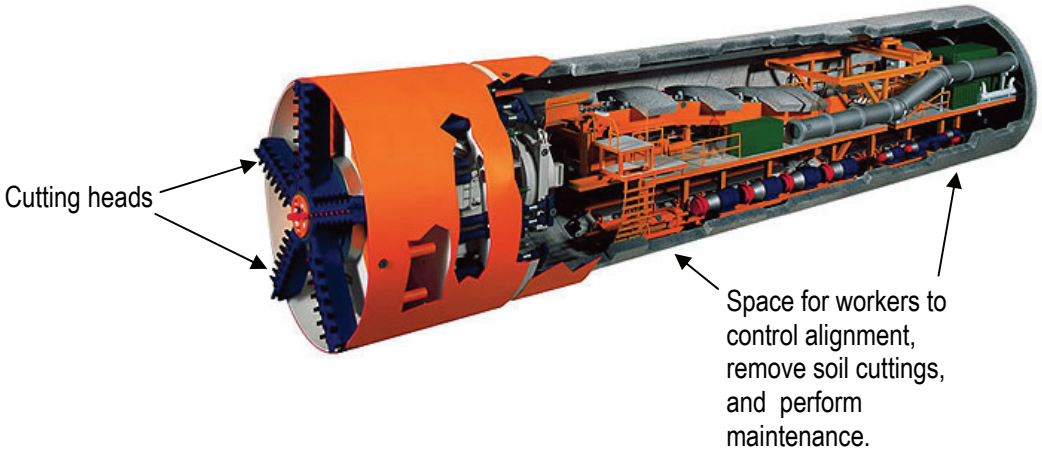


Figure 1.11: A typical TBM
(http://www.urbantransport-technology.com/projects/amsterdam/amsterdam3.html).



Figure 1.12: A TBM at the end of the tunnel alignment (http://www.soundtransit.org/x5590.xml).

1.2.3 PIPE-JACKING

Pipe-jacking is also known as *microtunnelling*. It is used in smaller scale infrastructure projects, such as retrofitting conduits or for creating new sewers. It involves the use of hydraulic or pneumatic jacks which thrust segments of pipe or tunnel into the ground, and into place along the proposed alignment. Excavation work is done either by hand under the protection of a shield, or by using a small-scale TBM. As the tunnel advances, segments are pushed into place at the rate of excavation. The jack is situated in a jacking station. This is a pit which is dug to accommodate the proposed elevation of the tunnel. A receiving pit at the end of the alignment is also required for completing the project. When far reaches of work are required, access pits are necessary, as long segments of tunnel mobilise shear stresses that will eventually match the driving force of the jack. Pipe-jacking causes a minimal disturbance at the surface, and is cost-effective when compared with older and more conventional methods. Figure 1.13 is a photograph of a typical jack. Figure 1.14 is a schematic of the process.



Figure 1.13: A typical jack (http://www.sanwakizai.co.jp/kouhou/pje-e.html).

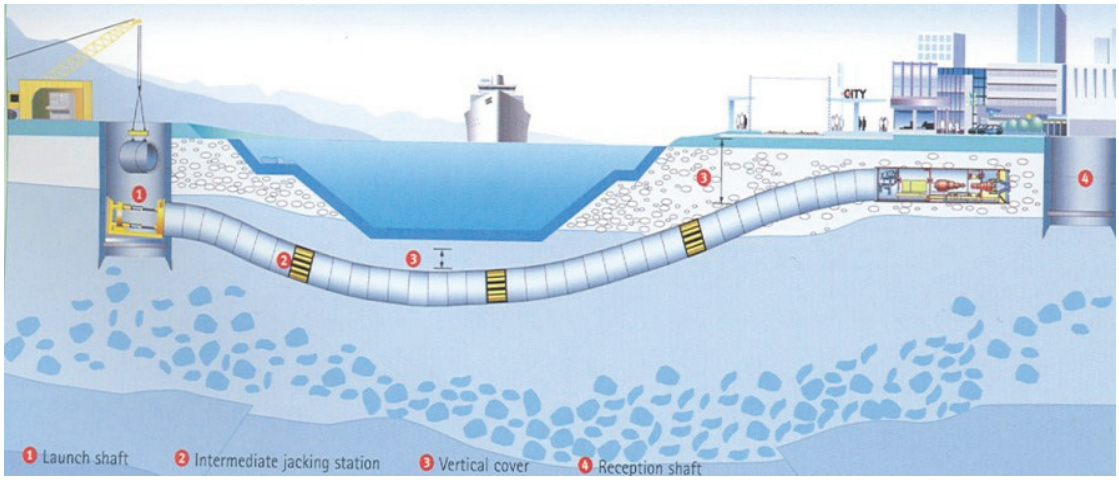


Figure 1.1: A schematic of the procedure of pipe-jacking (http://www.iem.bham.ac.uk/infrastructure/cable.htm).

1.2.4 New Austrian Tunnelling Method

The New Austrian Tunnelling Method (NATM) was developed in Austria. It is used for larger projects and has the following characteristics (Romero, 2002):

- the strength of the surrounding ground is deliberately mobilised to the maximum possible extent,
- strength mobilisation is achieved by controlling the contraction of the cavity walls,
- and initial primary support is installed with deformation qualities that are appropriate to the ground conditions, and installation is timed with respect to ground movements.

The tunnel can be excavated and supported in stages, with varying sequences of work. Shotcrete can be used in combination with appropriate reinforcement to provide initial, primary support. A lining is eventually put in place in order to provide permanent support for the excavation. The NATM is used extensively in soft rock; however it is also

appropriate for stiff soils provided that support is installed immediately after excavation. Dewatering and grouting can be used as methods for improving the stability of soils as well.

1.3 RESEARCH OBJECTIVES

Research involving tunnelling in uniform ground has been extensive to date. However, work focusing on the heterogeneous nature of soil as found in the field is surprisingly scant. Therefore it is the purpose of this investigation to research the effects of tunnelling under multi-layer ground conditions. This will be accomplished by varying the elevation of a single layer of granular material above a tunnel within a physical model. The granular material will be confined by two cohesive strata, the lower of which will be underlain by a rigid boundary which will simulate bedrock. All excavation work will be conducted only in the lower cohesive layer, at a fixed elevation above the rigid boundary. Primary attention will be placed on observing the response of a lining in terms of stresses, bending moments and thrusts which arise when tunnelling in stratified soil. The objectives of this project are explicitly itemised as follows:

1. Summarise the available pertinent information concerning the various testing methods used for studying ground response due to tunnelling,
2. Construct an apparatus specially designed for observing activity in non-uniform ground,
3. Design a cohesive material that does not require consolidation and will act as a tunnelling medium,
4. Monitor and observe patterns of stresses and moments within the lining as the location of the granular layer varies within the physical model by electronic instrumentation,
5. Construct and calibrate a numerical model based on the Hardening Soil Model to investigate further the effects of multi-layer ground on soil displacements and axial forces as a result of tunnelling, while identifying any trends resulting from this activity.

The work of accomplishing these objectives is presented in the remainder of this thesis. A comprehensive review of the literature is presented in Chapter 2 in order to fulfil the first objective. The experimental programme implemented to achieve the objectives 2

through 4 is detailed extensively in Chapter 3; all designs, construction, initial testing, procedures and methods of analysis will be presented there. Chapter 4 will be a summary of the qualitative and quantitative results obtained from the experimental programme. The numerical analysis that was used to fulfil the fifth objective will be discussed in Chapter 5. Finally, a summary and the recommendations for future work will be given in Chapter 6. All pertinent supporting information can be found in the appendices at the end of this thesis. ■

CHAPTER 2 – LITERATURE REVIEW

2.1 INTRODUCTION

Increased urbanisation has resulted in the use of tunnelling as the preferred method of construction in major urban centres. However, the complex ground conditions normally associated with the modern city provide challenges that need to be studied. To wit, modelling has aided in compiling a base of knowledge to address these issues. Among these are the induced displacements and stress re-distribution that arise when removing material beneath the ground surface, and how these might impact existing structures above. The empirical methods of Peck (1969), Schmidt (1974), Attwell (1978), O'Reilly & New (1982) have provided tools based on limited field data that enable the engineer to make predictions of surface subsidence and lining stresses. However, these methods are based on plane-strain conditions and do not account for three-dimensional behaviour normally encountered with tunnelling activity.

Numerical modelling has proven useful in solving this problem. Work by Mair et al. (1981), Panet and Guenot (1982), Rowe and Lee (1989), Swoboda et al. (1989), Corbetta et al. (1991) and Chen and Baldauf (1994) allows the engineer to analyse realistic scenarios which account for the three-dimensional aspect of tunnelling, more specifically, the construction sequence as well as the advancement of the tunnel face, along with the soil-lining interaction. In addition to this, data from instrumented projects (Attwell and Farmer, 1974; Rowe and Kack, 1983; Lo et al., 1984; Harris et al., 1994) have enriched the knowledge base; yet these works are limited by cost, scale, and are difficult to repeat.

Investigations of tunnelling activity are therefore best done by using reduced physical models in the laboratory. Models can either be run under the influence of gravity, or in a centrifuge. Ground response to tunnelling has been investigated using a variety of techniques, including the trap-door method, a dissolvable polystyrene foam core, or a miniature tunnel boring machine, among others. Most of the work cited so far has considered only the case of tunnelling in a homogeneous medium. However physical and numerical tests can also be applied to the cases where homogeneity is non-existent.

This literature review seeks to present the relevant studies that have been used to investigate tunnelling in soft ground as can be applied to stratified media. A brief review of each work will be presented in the following sections as described by the original authors,

and will comprise all testing techniques, along with the applicable and corresponding numerical studies.

2.2 PHYSICAL MODELLING

Researchers have in the past depended on physical modelling to understand the phenomena resulting from tunnelling activity. These include the patterns arising from soil movements as well as failure mechanisms. Testing can be done under the influence of gravity (so-called *1g* conditions) or in a centrifuge. 1g models allow the researcher to examine and refine complex systems in a controlled environment at scaled magnitudes. It should be noted that testing of this nature does not accurately simulate in-situ stresses as might be encountered in the field. Centrifuge testing by contrast, while more expensive than 1g modelling, can overcome this limitation by reproducing more realistic gravitational stresses in a small model. It also allows for greater control until failure. This was done for the first time by Bucky (1931) and Pokrovsky and Fedorov (1936). Studies of this nature were continued extensively by Cairncross (1973), Orr (1976), Potts (1977), Mair (1979), Senevitratne (1979), Bolton et al. (1994), Yoshimura et al., (1994) and Nomoto et al. (1999). Nevertheless, limitations do exist; grain size effects in smaller models and the inconsistency of scaling factors for different measured quantities such as length, inertia, force and creep. Additionally the radial forces induced by centrifugal motion are not uniform throughout the model.

2.2.1 TECHNIQUES

Most, if not all physical models have the same basic characteristics. First, they are usually conducted in containers of fixed, rigid boundaries, into which the medium that is to host the tunnel is placed. Second, the inner surfaces of these containers are lubricated to minimise the friction that arises from the presence of the medium (e.g. the friction between sandy soil and the inside of a steel container). Third, one face of the container is usually transparent to facilitate a visual record of whatever interests the researcher (e.g. displacements and failure mechanisms).

2.2.1.1 Trap-Door Models

Terzaghi (1936, 1943) explained the arching theory based on the translation of a trap-door into the soil (passive case) or away from it (active case). This can be seen in Figure 2.1.

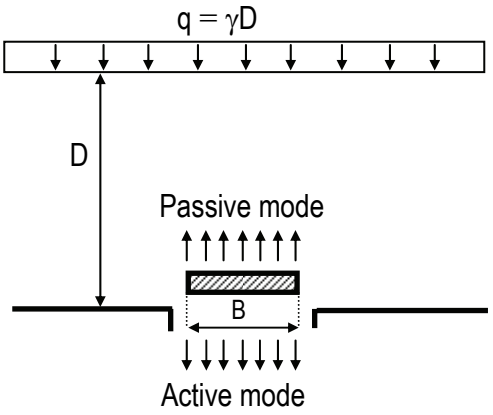


Figure 2.1: The classical Trap-Door Problem (after Meguid et al., 2008).

The active mode can be used to simulate the earth pressure on a tunnel lining. Several researchers followed Terzaghi's work and conducted 1g trap-door tests using either aluminum rods (Ladanyi and Hoyaux, 1969), dry sand (Vardoulakis et al., 1981) or glass beads (Sakai, 1996) to model the response of granular material under plane-strain conditions. Typical failure patterns can be seen in Figure 2.2.

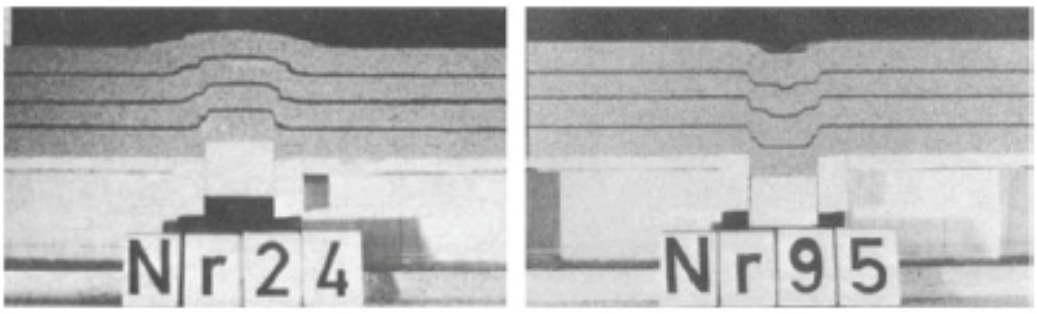


Figure 2.2: The classical Trap-Door Problem, left: passive mode; right: active mode. (Vardoulakis et al., 1981)

Trap-door methods are used mainly to study earth pressure distribution on buried structures, such as anchor plates, culverts and tunnels. They also aid in understanding the surface subsidence above tunnels excavated in soft ground.

Tanaka and Sakai (1993) and Park et al. (1999) conducted a series of 1g experiments to investigate tunnelling in an inclined layered medium. Aluminum rods (γ = 21.1 kN/m^3, ϕ = 30°) and aluminum blocks (γ = 26.4 kN/m^3, ϕ = 20°) are arranged in layers inclined at 30°, 60° and 90° with the horizontal plane (See Figure 2.3).

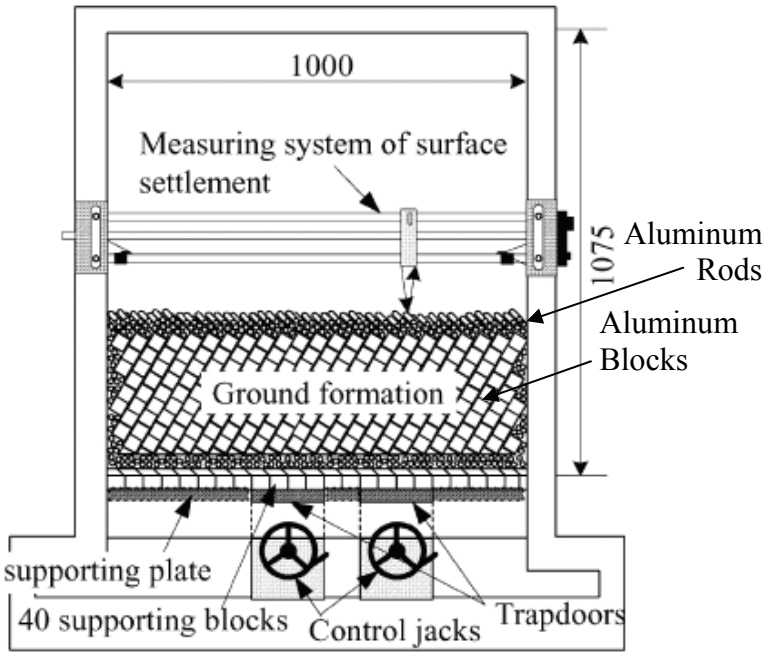


Figure 2.3: Schematic of trap-door apparatus used by Park et al. (1999). Dimensions are in mm.

Forty blocks over a supporting plate were installed along the base of the container. Forty load cells were installed between each supporting block and the supporting plate in order for the distribution of the earth pressure on the trap-door to be measured. The blocks are spaced evenly at 0.05 mm to avoid inter-block interactions. The trap-door is lowered by using a control jack through distances of 1 to 4 mm. The angle of inclination was found to have a significant effect on the subsidence trough. Results can be seen in Figure 2.4 below.

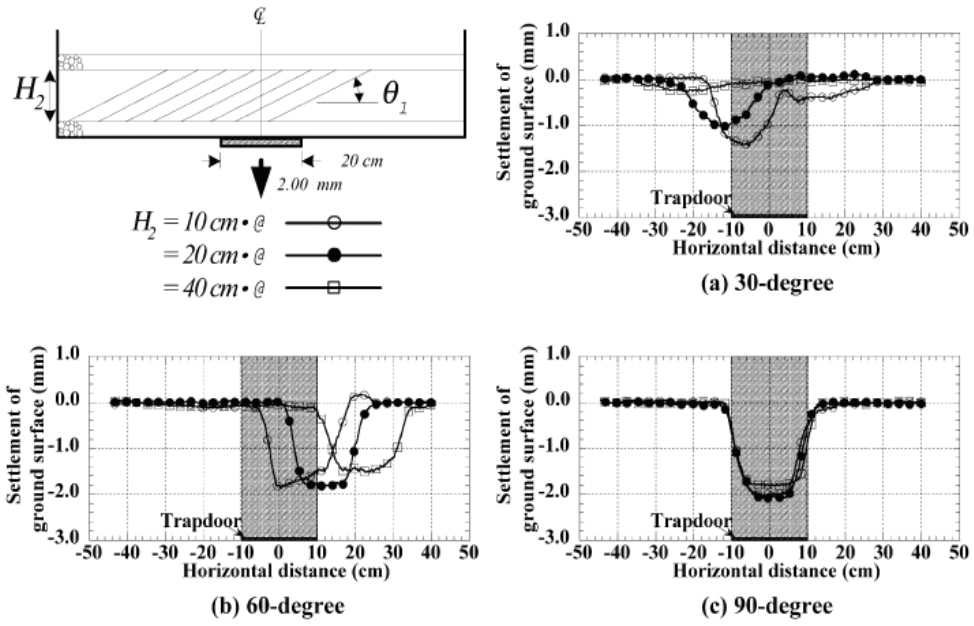


Figure 2.4: Settlement troughs for displacements of 1 to 4 mm. (Park et al., 1999)

Nakai et al. (2000) conducted a two-dimensional trapdoor test and validated their experimental results using finite-element modelling. Ten blocks comprised the apparatus (A to J in Figure 2.5), each eight cm wide, placed along on the centreline of an iron table. Block F is lowered using the handle to a prescribed elevation to simulate the excavation. A load is then applied to the top of the free surface close to the lowered trapdoor. This load is maintained until the test is completed. Subsidence is measured using a laser type displacement transducer and earth pressures are measured using load cells.

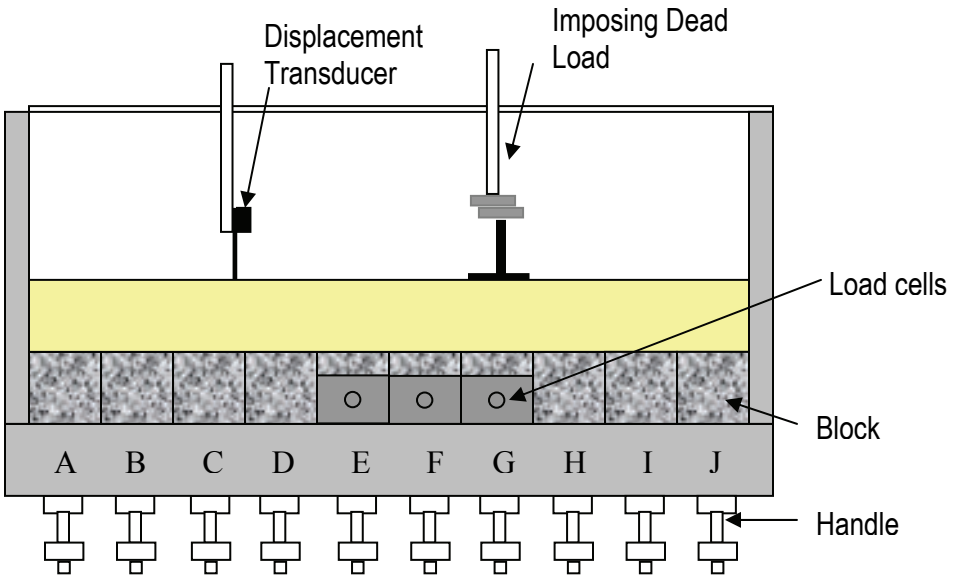


Figure 2.5: Trap-door apparatus with loading plate. (After Nakai et al., 2000)

Axi-symmetric trap-door experiments such as those conducted by Adachi et al. (1995) were done under both 1g and centrifugal conditions. The apparatus was a hollow drum made of stainless steel, having a radius of 380 mm and a height of 300 mm. At the centre of the drum is a circular trap-door of diameter five cm, which can be lowered via a screw jack powered by an electric motor. Silica sand was used as the tunnelling medium. Displacements and earth pressures at and near the trap-door are measured, with surface movements being recorded by a laser displacement gauge when the trap-door is lowered by five mm. Displacement patterns for dry sand and saturated clays are shown in Figure 2.6, along with a schematic of the apparatus.

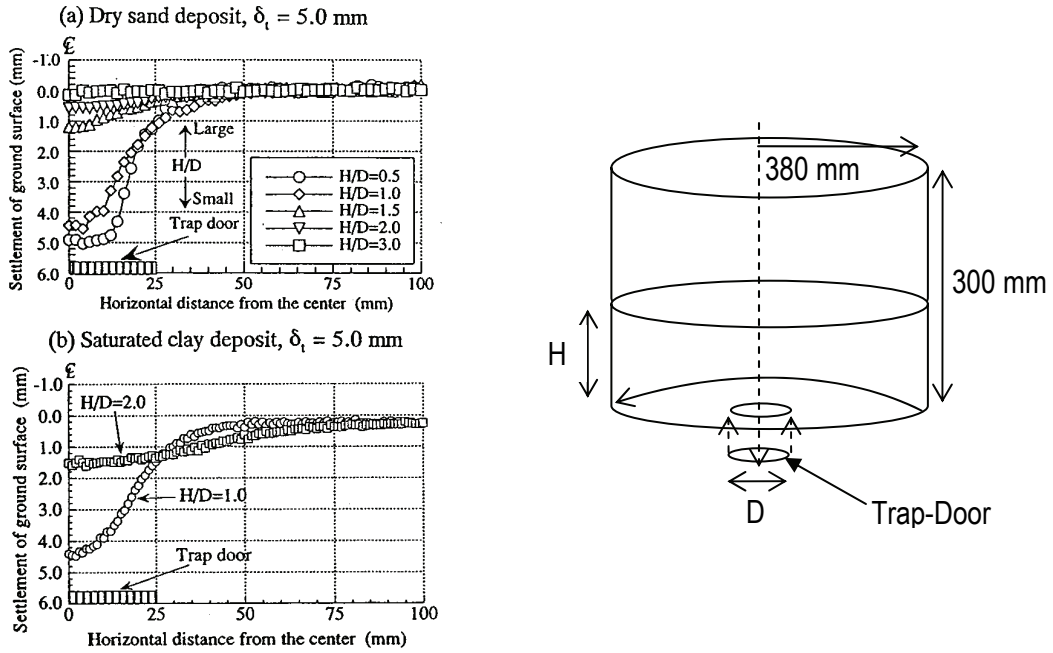


Figure 2.6: Displacement patterns from the axi-symmetric trap-door test. (Adachi et al., 1995)

A similar apparatus was used by Adachi et al. (2003) to investigate the three-dimensional effect of the trap-door system on induced surface settlements and earth pressures under the 1g condition. The medium was once again No. 6 silica sand. It was found that for any given overburden pressure and trap-door displacement, both the surface settlement and the earth pressure measured in the two-dimensional cases were found to be greater than those of the three-dimensional tests.

2.2.1.2 Rigid Tubes

Rigid tubes, as used by Chambon et al. (1991), Sterpi et al. (1996), and Kamata and Masimo (2003), has have been employed to examine the near-face stability of shallow tunnels and to evaluate the stresses transferred to the lining. This technique involves resting a tube on top of soil material that has already been placed, then burying the tube by adding more material to the desired elevation. It should be noted that this method is limited to granular materials, as the presence of the tube prohibits the proper and uniform consolidation that would be required for cohesive soils. In order to focus on the near-face effects, a diaphragm that is either rigid or flexible can be used to observe the response of the soil in this region. Representative apparati with flexible faces will be discussed first.

Chambon et al. (1991) have used flexible-face devices to examine the face stability of a shallow tunnel in soft ground. The model consists of a metal tube of 100 mm diameter which has a latex membrane affixed to the far end, representing the face of the tunnel. The membrane is not left in a taut condition so as to avoid influencing the displacement of the face mechanically. The movements at the face are tracked by using a displacement transducer. Fine homogeneous sand is then poured evenly into a rigid container to the proposed elevation above the tunnel crown. The tube and membrane element are then put into position, and more sand is poured, thereby burying the pipe. The whole set-up is subjected to centrifugal forces at revolutions simulating 50g, 100g, and 130g. Internal pressure created by fluid within the tunnel is gradually reduced until failure. Tests were done with differing cover to diameter ratios (C/D). A schematic of this test can be seen in Figure 2.7.

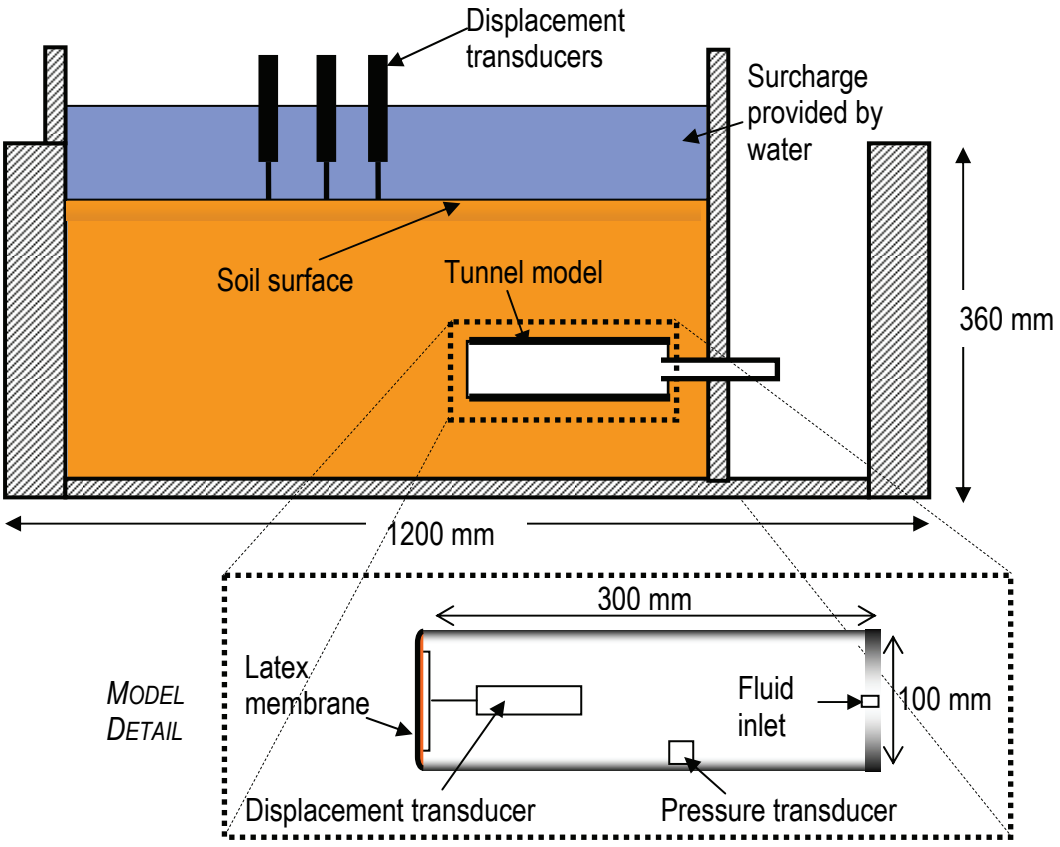


Figure 2.7: Model used by Chambon et al. (1991)

Sterpi et al. (1996) created a large-scale tunnel heading that is used for studying three-dimensional effects under 1g conditions. The model consists primarily of a "D-shaped"

steel structure which is 1.1 m in length, is 1.145 m wide and 1.32 m high. A vinyl bag is used to support the tunnel face when it is inflated to a prescribed pressure. The pluvial deposition technique was used to fill the container with medium uniform sand having a friction angle of 32° levelled in layers of an approximate constant thickness (300 mm). Figure 2.8 shows a three-dimensional schematic of this model, the positions of instruments, along with the recorded failure pattern induced by reducing the air pressure support at the tunnel face.

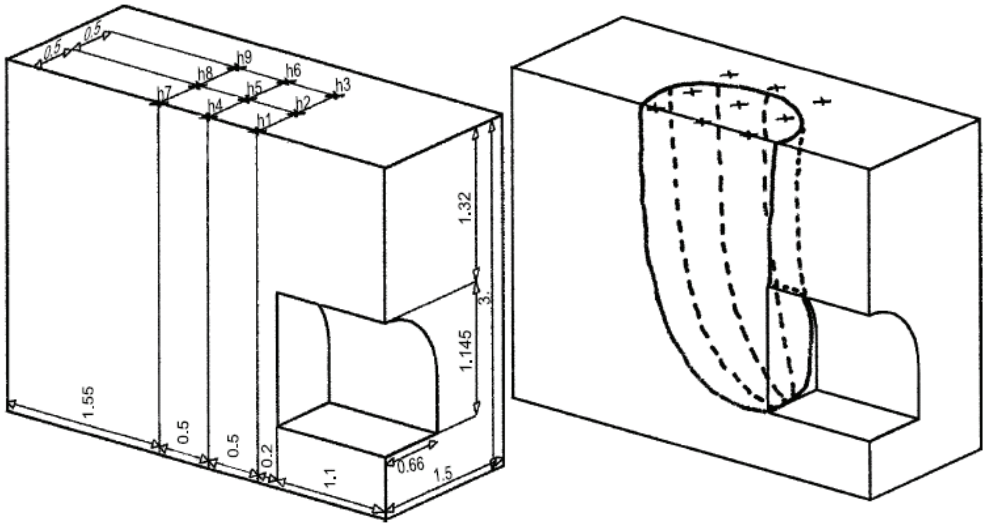


Figure 2.8: Left: model used by Sterpi et al., and right: observerd failure mechanism (1996)

Similar work with rigid faces was done by Kamata and Masimo (2003) to investigate the face stability of shallow tunnels. Their work consisted of a semi-circular acrylic shell which is 80 mm in diameter. Toyura sand (γ_{bulk} = 15.1 kN/m^3, w = 6.5%, c = 4.6 kPa, ϕ = 34.5°) is poured and compacted in layers that are two cm in thickness. The face of the simulated tunnel is supported by an aluminum plate which is 25 mm thick. The C/D ratio was kept at 1.0 for all tests. The apparatus is then placed into a centrifuge, and the stability of the tunnel face is evaluated by moving the aluminum plate. Complete failure is seen at 30g. Refer to Figure 2.9 for more details.

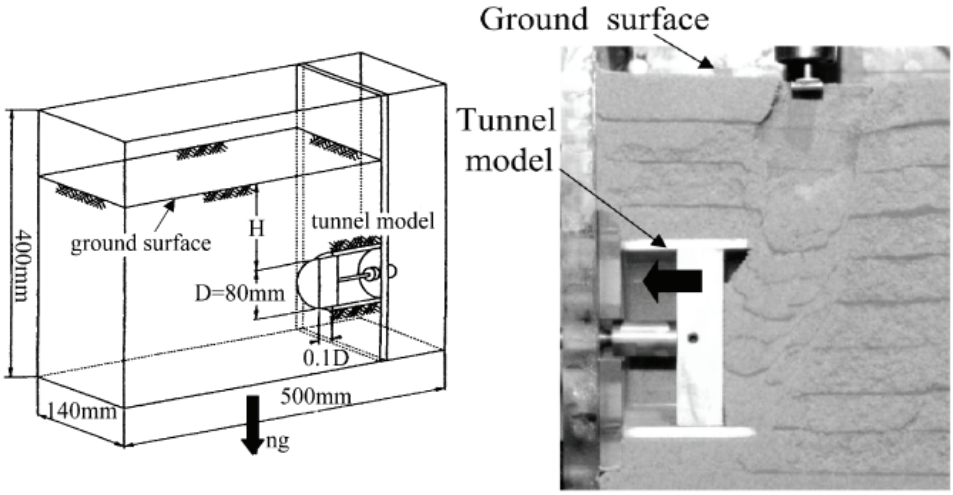


Figure 2.9: Left: schematic of the apparatus by Kamata and Masimo, and right: observerd complete failure pattern (2003)

2.2.1.3 Pressurised Air Bags

Another common means of simulating tunnelling activity is by using pressurised air bags of negligible strength to support the surrounding soil. Atkinson et al. (1975), Hagiwara et al. (1999), Wu and Lee (2003) and Lee et al. (2006) have done extensive research using this technique. Normally a tube is pushed through a medium (most commonly soil) or is buried beneath a chosen material. A series of inflatable membranes or one large membrane is then inserted within the tube and inflated to a predetermined pressure, normally to a value that matches the overburden stress to create a condition of equilibrium. The pressure is then reduced incrementally to simulate the removal of in-situ stresses from within the opening until failure is induced. This method is best suited for evaluating ground response to tunnelling under plane-strain condition.

The problem of tunnelling in a multi-layer ground was investigated by Hagiwara et al (1999). They conducted a series of centrifugal tests by simulating the construction of a tunnel in a clay stratum which was overlain by a sand layer. The soil sample was prepared by first consolidating kaolin clay under a vertical stress of 500 kPa inside of a plain-strain box. A tunnel cavity was then excavated and lined with a latex rubber bag connected to a regulating air-pressure valve. Surface subsidence measurements were taken by two arrays of LVDTs at the free surface of the overlying sand layer. It was found that the type and

stiffness of the upper sand stratum has a significant effect on the movement of the underlying clay. Schematic of the apparatus is shown in Figure 2.10.

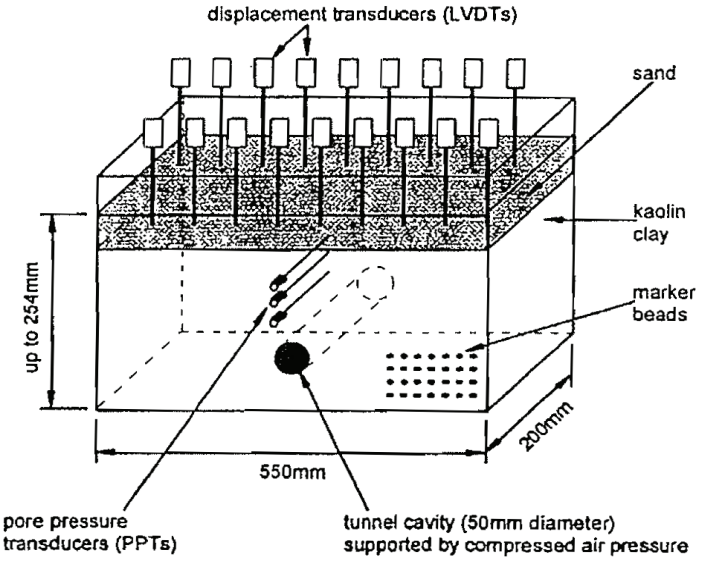


Figure 2.10: Schematic of the apparatus used by Hagiwara et al (1999)

2.2.1.4 Polystyrene Foam & Organic Solvent

This method was developed by Sharma at al. (2001) to simulate the process of tunnel in a centrifuge. A stiff cylinder of polystyrene foam is placed within a medium, and is exposed to an organic solvent. The deterioration of the polystyrene simulates the unloading that occurs during the removal of material to create a tunnel. The model that was used consisted of a cylinder measuring 70 mm in depth and 35 mm in diameter. The elastic modulus of this material was found to be 1500 kPa. Sand was used to surround the polystyrene (see Figure 2.11 for details) which was also wrapped in a hard brass foil which simulated a tunnel lining. A silicone rubber sealant was used to fill any gaps to ensure full contact between the lining and the polystyrene. The inflow of organic solvent was regulated in order to control the dissolution of the foam. This simulated the progressive advance of the excavation. Instrumentation was used to measure the subsidence profile.

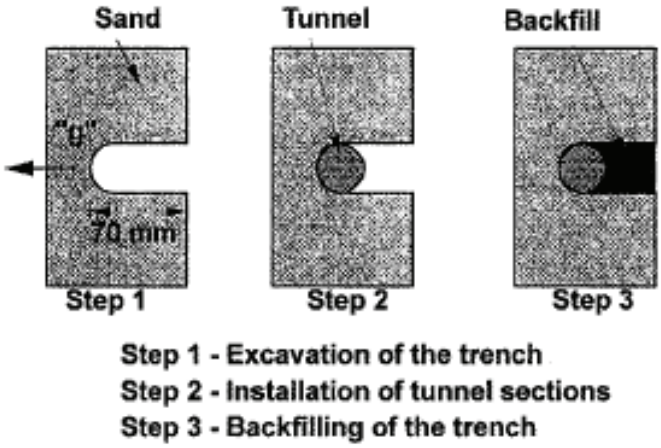


Figure 2.11: The steps of placing a polystyrene cylinder within a sand medium as described by Sharma et al. (2001)

2.2.1.5 Soil Augering

Soil augering involves cutting through soil using an auger-type device. Love (1984), Kim (1996), and Chapman et al. (2006) all employed this technique in their work. This method is best suited for testing cohesive materials. Clay is usually placed into a rigid container and consolidated to a desired strength. An auger is then used to bore a hole through the sample at a prescribed elevation, with a lining following the path of the auger. This requires an over-cut in order to accommodate the lining, which is of a lesser diameter than that of the original excavation. This also results in a gap between the lining and the crown of the excavation, which then facilitates a surface settlement profile if the C/D ratio is appropriate.

Chapman et al. (2006) conducted such tests under 1g conditions. Kaolin clay was mixed at a water content of 126% and over-consolidated (OCR = 2.7). A large water bag was used for the consolidation process. An auger-shield device was used in the excavation of two parallel tunnels at the same elevation. Surface settlement was monitored and recorded with the focus of the study being placed on settlement patterns due to the influence of a nearby tunnel. Figure 2.12 depicts the equipment used in this investigation.

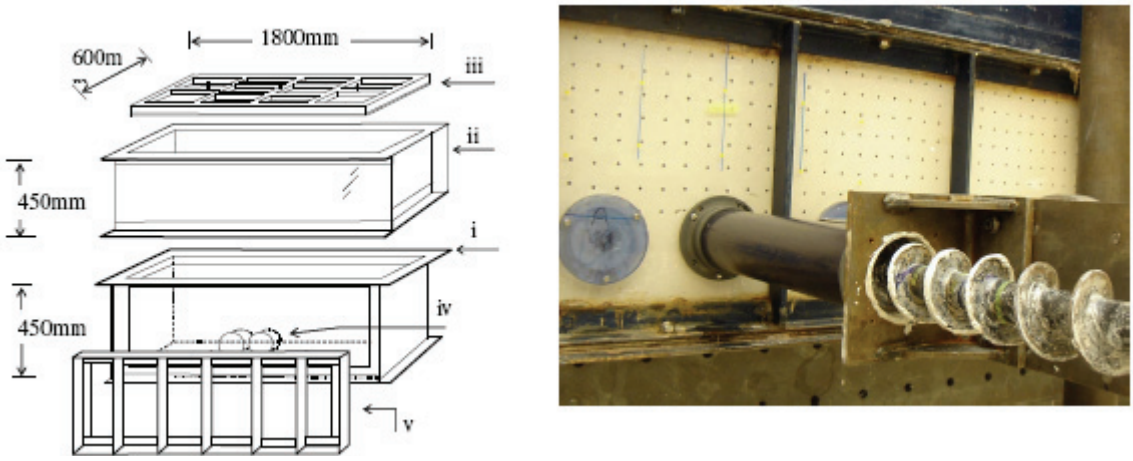


Figure 2.12: The equipment used by Chapman et al. (2006)

2.2.1.6 Miniature TBM

Nomoto et al. (1999) developed a miniature tunnel boring machine (TBM) to simulate the excavation process as realistically as possible, but on a scale suited to the laboratory. The machine consists of a shield comprised of three tubes. A stainless steel tube that is 100 mm in diameter contains a spiral conveyor with a cutting head to excavate the soil. A middle tube of 96 mm diameter is the lining, while another 100 mm-diameter stainless steel tube simulates the tail void formation. Two motors drive the machine: one for forward motion and the other for driving the cutting mechanism. The machine has been tested in a tunnel of 100 mm in diameter under a maximum centrifugal acceleration of 25g which represents a tunnel of 2.5 m in diameter. Figure 2.13 illustrates the miniature TBM.

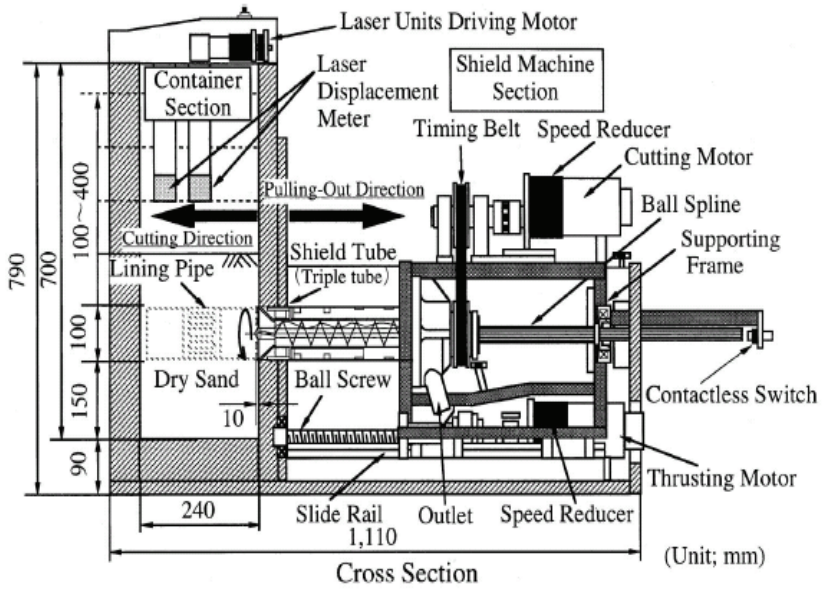


Figure 2.13: The schematic of the miniature TBM. (Nomoto et al. 1999)

2.2.1.7 Other Methods

A device that can be adjusted to provide a desired volume loss was created by Lee and Yoo (2006). It was used to investigate tunnelling near to a row of loaded piles under 1g conditions. The tests were two-dimensional in nature. Six segments or shims comprised the device and were formed into a cylindrical formation as shown in Figure 2.14. They are arranged such that the turn of a mechanical knob in one direction can increase the diameter of the formed cylinder, and reduce it by turning it in the other direction.

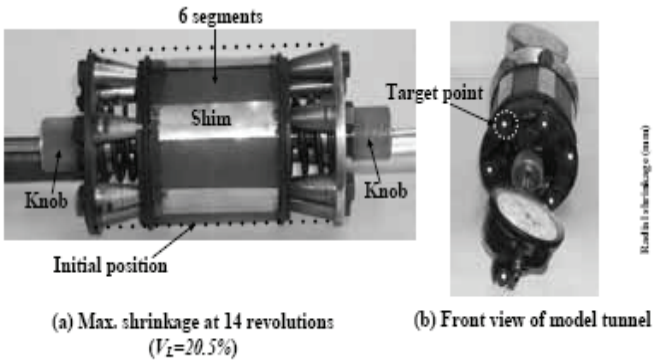


Figure 2.14: Mechanically adjustable device. (Lee and Yoo, 2006)

Other methods have been developed to simulate the ground response to tunnelling. One such method is the Base Friction method. It has been used to reproduce the effect of gravity and to visualise displacements in two-dimensional models, primarily soft rock tunnels. A belt moving along the base of the model is used to simulate gravity. Solid brick-like elements are stacked in either a flat orientation or they can be inclined with respect to the horizontal plane (see Figure 2.15). This method has been used by researchers such as Hoek (1971), Goodman (1972), Whyte (1973), Egger and Gindroz (1979) and Bray and Goodman (1981). This technique facilitates a visual record of ground movement as well as the failure mechanisms resulting from tunnel excavation.

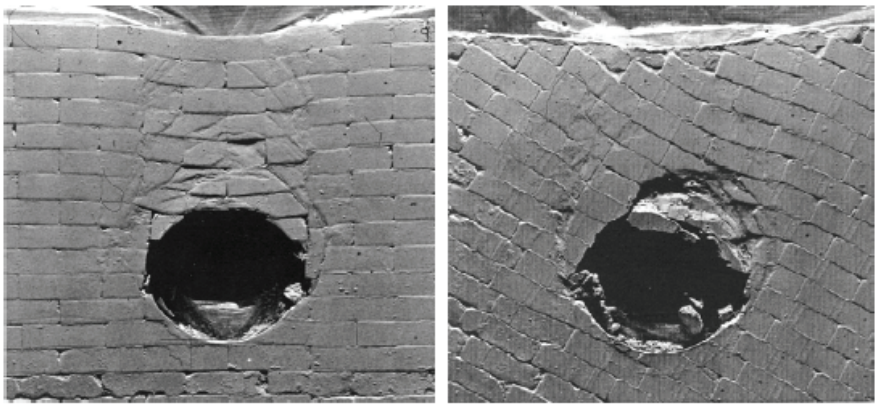


Figure 2.15: Failure mechanism as a result of the Base Friction Method (Egger and Gindroz, 1979)

2.3 LAYERED GROUND

As it is evident in most of the work presented above, the current practice of investigating the effects of tunnelling activity is based on the assumption of homogenous ground conditions. Relatively very little research has been done with non-homogenous ground to date. However Naik (1977), Selby (1988), Grant and Taylor (1996), Grant (1998) and Grant and Taylor (2000) have all approached the problem of tunnelling in layered ground extensively. Naik (1977) employed finite-element methods (FEM) to address the scenario of tunnelling through a stratified medium. He assumed perfect contact between the liner and the medium and conducted a parametric study by varying the moduli of the strata as well as the position and orientation of the interface between the strata. Results indicated that stresses at the springline were minimum when the interface of the differing media was about half of one radius below the horizontal centreline, and that the moduli of elasticity of

the liner and lower stratum are nearly equal. The thrusts, moments and circumferential movements are a maximum when the interface is inclined at 45°.

Grant and Taylor (2000) performed a series of centrifuge model tests to study the stability of a tunnel in clay overlain by coarse grained material. Kaolin clay was consolidated by first being subjected to a vertical effective stress (σ_v') of 500 kPa before allowing the clay to swell to a σ_v' of 250 kPa. Sand was rained from above onto the clay surface until the desired upper layer of sand was formed (Figure 2.16). A latex lining was placed inside of a cylindrical cavity that was made through the clay layer. Air was fed into the lining in order to support the cavity whilst being subjected to centrifugal forces. Results validated previous work regarding the stability of unlined excavations. They also showed that the upper stratum has no bearing on the tunnel stability when loose sand comprises the upper layer, except that it acts as extra surcharge weight. Finally, when the clay cover over the crown of the tunnel was less than a C/D ratio of two, it was found that a relatively dense sand enhanced the stability of the tunnel.

Little else has been done in terms of investigating tunnelling in multi-layer ground to the knowledge of the author. The following chapters will present a study of tunnelling in a two-layer medium under 1g conditions. Stresses that arise in the tunnel lining, as well as the moments and thrust forces that resulted were of special interest. ■

CHAPTER 3 – EXPERIMENTAL PROGRAMME

3.1 INTRODUCTION

Physical modelling under 1g conditions is an economic and accurate means of investigating the tunnelling. However this normally requires first, the use of a large quantity of material for simulating excavation work. This is to ensure that in-situ stresses are sufficient to mobilise adequate soil movement and stress re-distribution once an opening has been created. Second, the design and construction of any apparatus which is to host a tunnelling medium is such that it should withstand the immense pressures that arise when material accumulates inside of it. It should also be dimensioned appropriately to minimise or eliminate as much as possible any boundary effects as well. This can be accomplished even further by using a lubricant on the inner surfaces.

The next aspect of experimental testing is sample design and preparation. It is imperative to standardise as much as possible the materials that will be used in the study. Therefore preliminary tests are necessary before undertaking any large-scale work. The third module to any experimental scheme is that of recording data. First, suitable instrumentation must be selected, which is important to the data acquisition throughout the test. The position of any instruments will also be critical. Next is the calibration of the overall system to ensure that all recorded data reflect accurately the observed physical results.

It should be emphasised that testing in the laboratory under 1g conditions does not simulate truly the in-situ conditions that may be found in the field, but it does allow for insight into any patterns or trends that may exist in a large-scale prototype. The following sections of this chapter will detail the design of the model that was used for this project, a description of the sample preparation, an overview of the data acquisition scheme, and a summary of the testing procedure.

3.2 STRONGBOX

As discussed in Chapter 2, a strong container that can endure the rigours of holding large volumes of heavy material was required for this project. Hence an open box made primarily of steel was chosen to meet this requirement. The following sections will provide

more details about the strongbox that was used in this project. The ensuing sketches are for illustrative purposes only; actual blueprints are provided in Appendix A.

3.2.1 OVERVIEW

It was decided that one side of the box was to be made of transparent Perspex, 12 mm in thickness, while the remaining four faces were made of steel, each six mm thick. Once assembled, the inner edges and corners of the steel panels were sealed with water-proof calking. The inner dimensions of the box were 1410 mm wide by 305 mm deep by 1175 mm high. These dimensions were chosen to minimise boundary effects, as outlined by Mair (1979), who specified a width of at least four model tunnel diameters on either side of the excavated model opening. Three 100 × 100 mm HSS beams, each 1550 mm in length were hung horizontally on threaded rods along the two wide faces to act as stiffeners and prevent any bulging that would occur once material was placed inside. The box rested on two footings 850 mm in length, cut from 100 × 100 mm HSS members. These footings were then supported atop four levelling screws, one at each end of the length of each footing. They were used to keep the box in a level horizontal position with respect to the grade. Two holes 152 mm in diameter were cut each in the Perspex and the opposing steel faces. The centres of the holes coincided with the point located along the vertical centreline of the box as seen in the elevation view, and 178 mm from the inner base surface of the box. The holes were sealed using caps made of Perspex, affixed to the box by threaded rods which were fixed permanently to the Perspex and steel panels. The photographs in Figure 3.1 and 3.2 offer a graphical summary. Each component of the box will be discussed in further detail in the following sections.

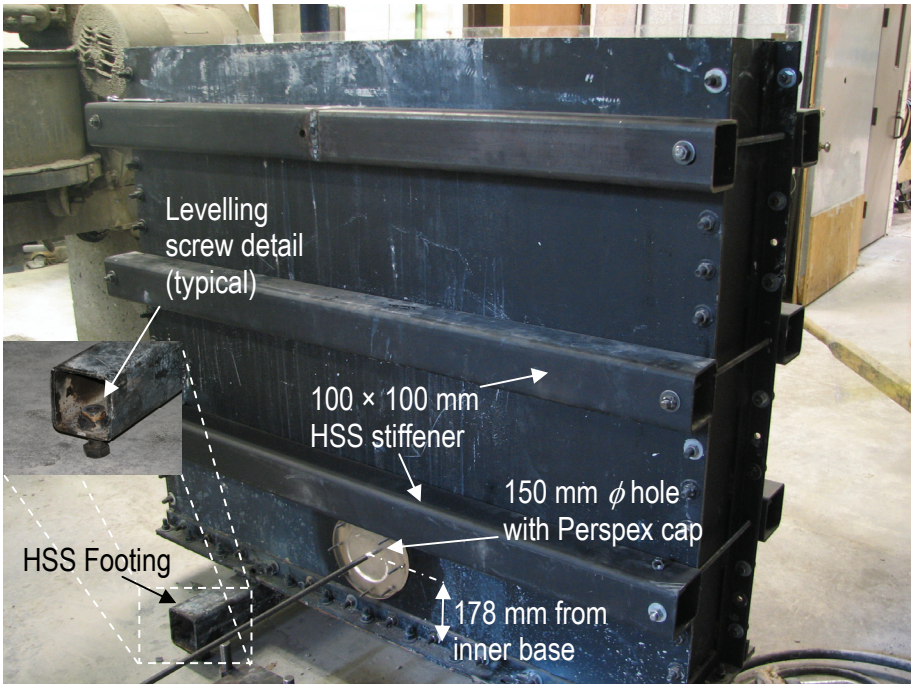


Figure 3.1: Strongbox as seen from the rear (back steel face showing)

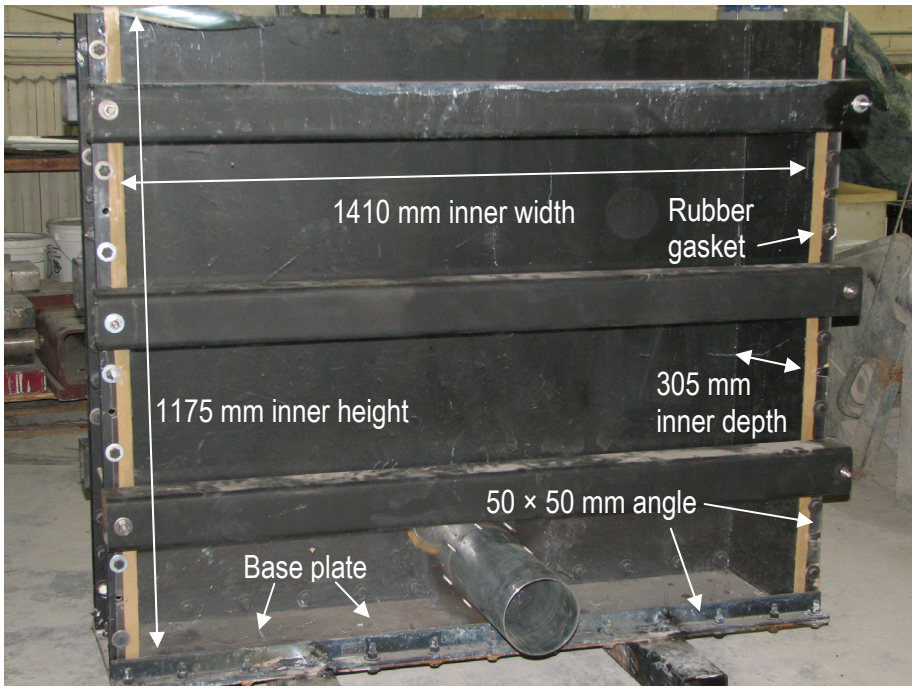


Figure 3.2: Strongbox as seen from the front (Perspex face showing)

3.2.2 ELEVATION VIEW

The three steel side panels, each six mm in thickness along with the 12-mm Perspex face were all mounted on a steel base plate, also six mm in thickness. 50 × 50 mm angles were used to facilitate adjoining each face of the box in a mutually perpendicular orientation. An example can be seen in Figure 3.2. Each steel face was connected to the angle sections with steel nuts and bolts or welds. All bolts were 57 mm long, with a threaded length that was 11 mm in diameter. Each bolt-head was hexagonal in shape measuring 19 mm across. The nuts that were used on each bolt had the same geometry as the bolt-heads. All welds were about 25 to 50 mm long, and about seven mm thick. The total height of the box was 1180 mm as taken from the underside of the face plate. The total width was 1524 mm.

Three pairs of 100 × 100 mm HSS stiffeners were hung, with each paired member abutting against either the back steel panel or the Perspex face. They were hung on threaded rods 11 mm in diameter, which passed through each stiffener and secured with nuts. When hung, the centreline of the lower-most stiffeners was aligned at a height of 356 mm as taken from the underside of the base plate. The upper stiffeners were placed at 330 mm, centre-to-centre. Five pilot holes, each 44 mm in diameter were made in the Perspex face. Please refer to Figure 3.3 for an illustrated summary. Two beige rubber gaskets (Figure 3.2), two mm thick and 40 mm wide were placed along the two vertical 50 × 50 mm angle sections 1175 mm in height (Figure 3.2) which served to seal the contact with the Perspex face. Specific details concerning each component of the strongbox as seen from the elevation view will be given in the following sub-sections. It should be noted that the elevation view presented in Figure 3.3 is that of the front of the box. The elevation view of the back gives the same geometry, with a steel panel replacing the Perspex face, and only a 152-mm diameter hole without any pilot holes.

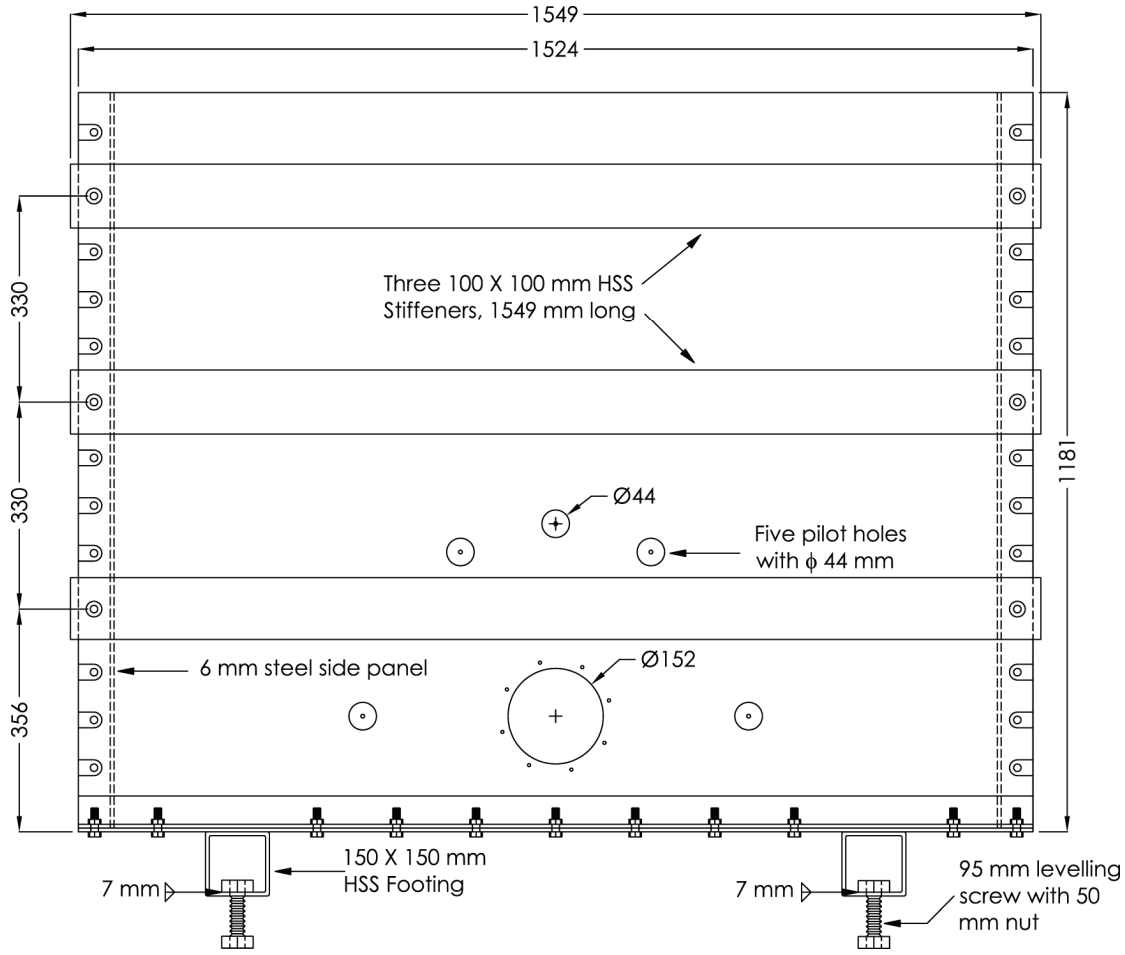


Figure 3.3: General elevation view from the front (all dimensions in mm).

3.2.2.1 Details – Side

The centre of the first bolt along the side was placed at a height of 102 mm as taken from the lower edge of the base plate (Figure 3.4). The second and third bolts in this series were inserted at 178 and 254 mm, respectively, as taken from the same reference point. The second and third series of three bolts each began at a distance of 89 mm from the centre of the HSS stiffeners. The second and third bolts in each series were then located at 165 and 241 mm, respectively, as taken from the same reference point. 25-mm wide slots were cut out of the Perspex to accommodate the insertion of the bolts. This allowed for free movement horizontally, which aided in centring the front panel, while restraining any movements vertically and in the direction normal to the Perspex face.

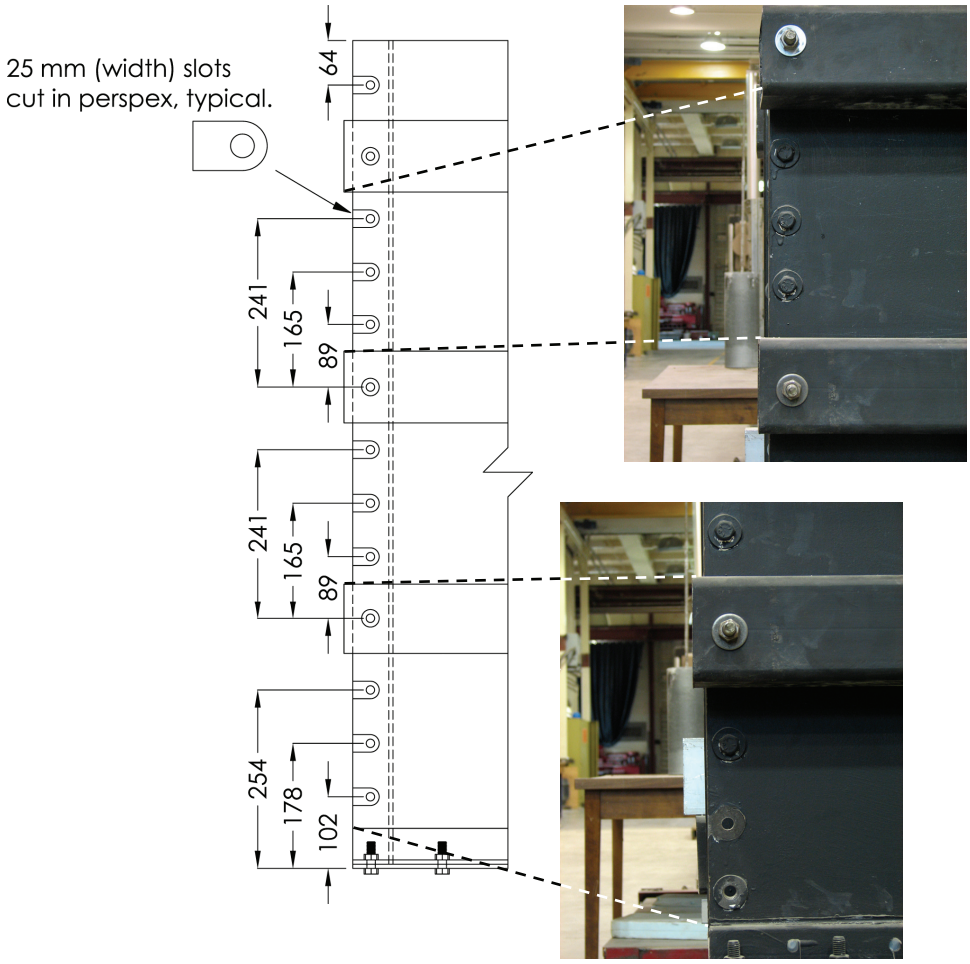


Figure 3.4: Elevation view of the side detail from the front. The left side is shown. The right side has the same geometry. The back face also has the same geometry, and can be seen in the photographs.

3.2.2.2 Details – Base

Two 50 × 50 mm angle sections, 1524 mm in length were attached the base plate with 11 bolts, of which the spacing and placement can be seen in Figure 3.5. The back steel sheet was connected to the upper leg of the angle section by 12 bolts (Figure 3.5). The Perspex face was not connected in the same manner, as it was never meant to be fixed permanently. The centres of the 100 × 100 mm HSS footings were welded at 254 mm from the side edge of the base plate.

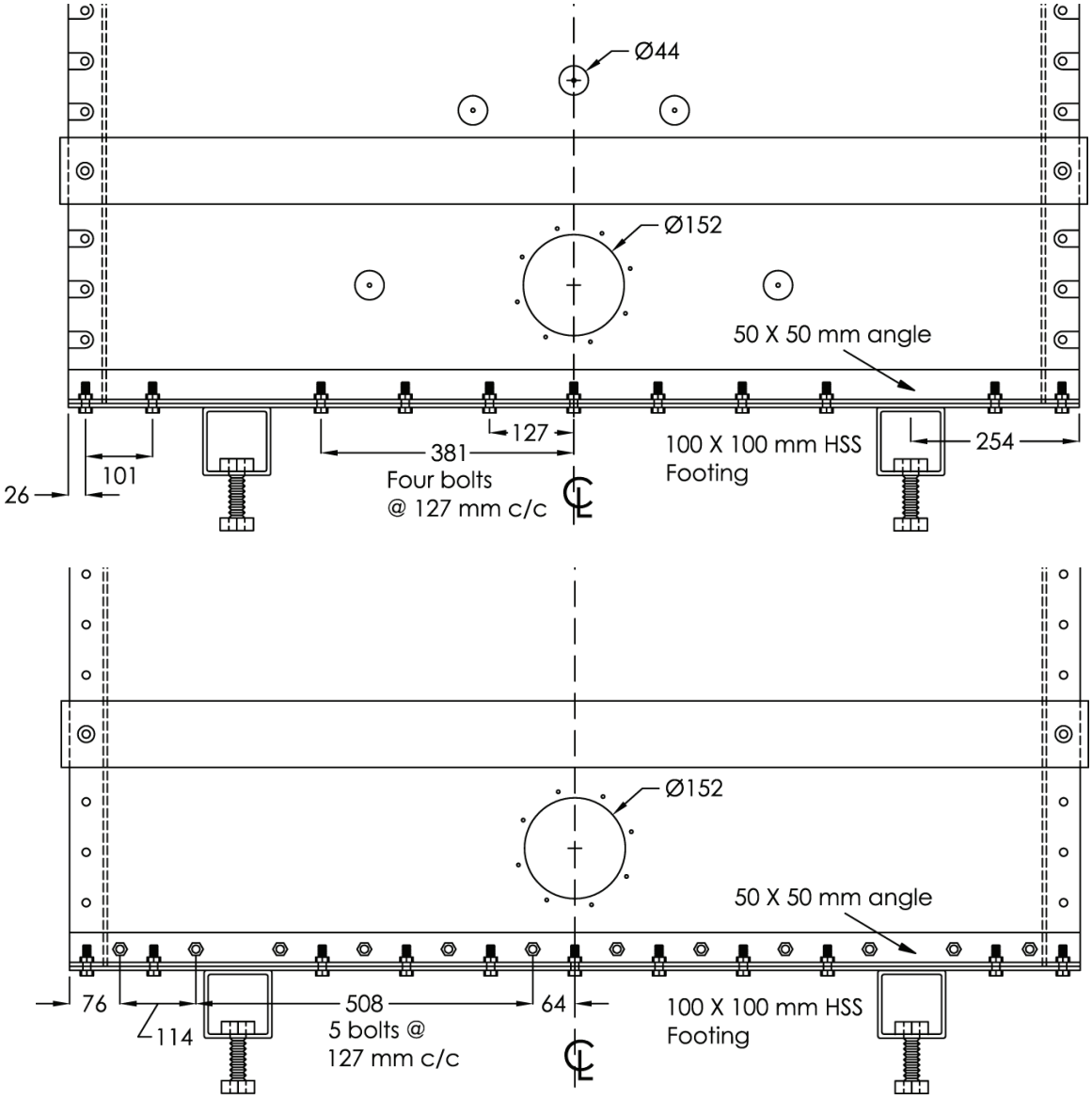


Figure 3.5: Elevation view of the bottom detail from the front (above), and from the back (below).

3.2.2.3 Details – Perspex Face

Six holes were cut into the Perspex front panel, five pilot holes and one hole to accommodate the tunnel. The centres of the two pilot holes in line with the springline were cut at 308 mm away from the centreline. The upper-most pilot hole was similarly placed at 308 mm above the centre of the main hole (152 ϕ mm), but directly above the crown. The two remaining pilot holes were also located at a distance of 308 mm from the centre of the main hole, but were oriented at 30° away from the centreline, on either side. The original plan was that there would be an array of pilot holes with centres coinciding on the line which

can be described by a semi-circle with a radius of 308 mm from the centre of the main hole. However the pattern presented in Figure 3.6 was chosen instead, since it was decided that the HSS stiffener should not be removed in order to maintain the structural integrity of the box. Work on other holes was not completed as a result. The distance of 308 mm was chosen because it represented a distance of two equivalent excavated diameters away from the centre of the opening. This was deemed an appropriate length for taking soil samples that would be undisturbed by tunnelling activity. 30° was chosen as a reasonable angle of turn with respect to the upper-most pilot hole, for the same reason.

Eight threaded rods (Figure 3.6), each 5 mm in diameter and 44 mm in length, were evenly spaced at 45° and centred on a circle described by a radius of 89 mm placed at the centre of the main hole. The rods were offset by 16° rotated counter-clockwise from the centreline instead of being in a plum position with respect to the centreline. The same arrangement was used around the 152 ϕ mm hole cut out of the back steel panel as well. These rods were used to secure Perspex caps that sealed the box before any material was placed into it. More details on these caps will be presented in another section.

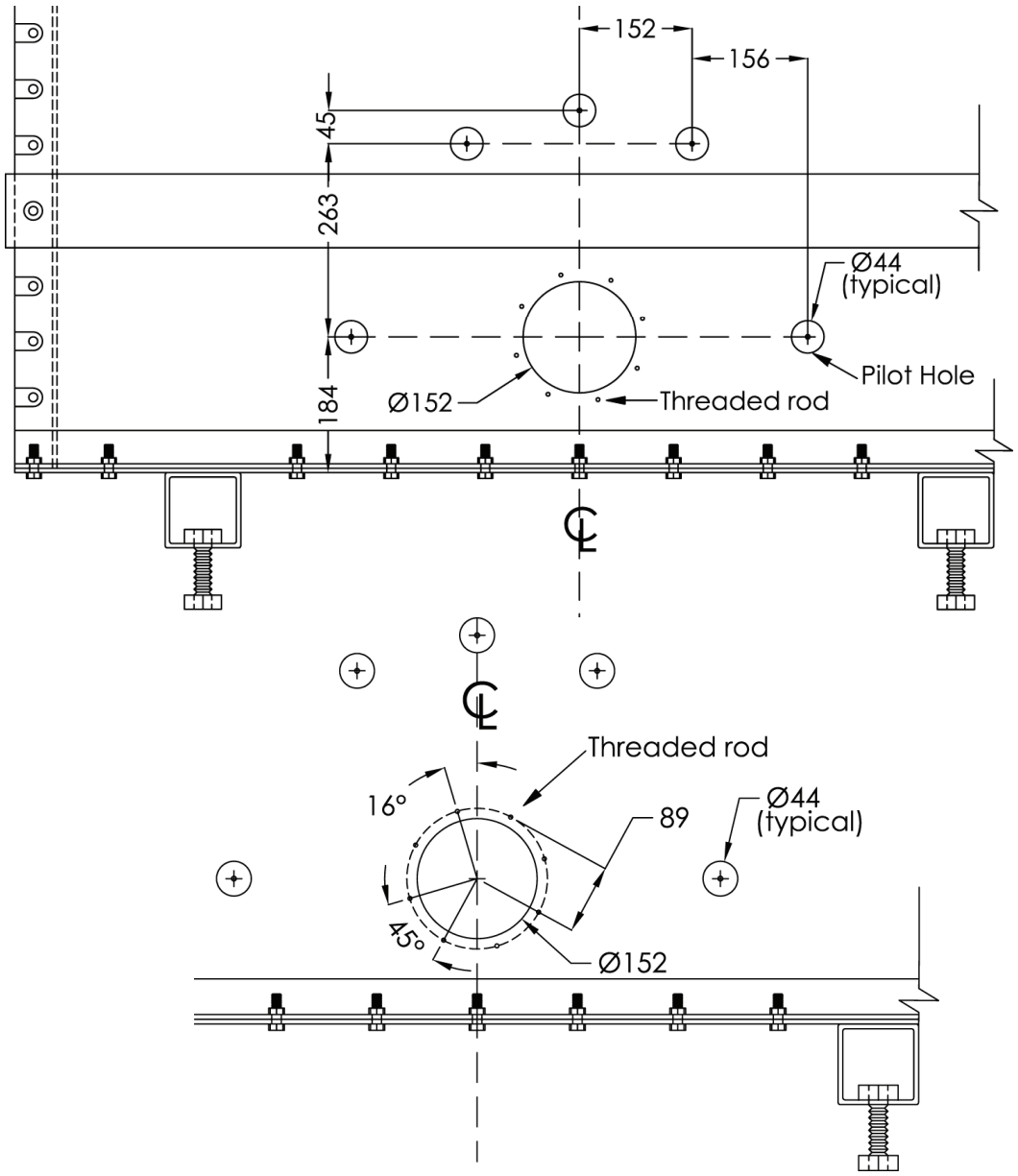


Figure 3.6: Elevation view of the details of the main hole and pilot holes.

3.2.3 PLAN VIEW

Figure 3.7 is a sketch of the box in plan view along with the detail of the typical corners in plan. The 584-mm long threaded rods that were used to hang the HSS stiffeners are more easily visible. Also visible is the footprint of the base plate, which measured 438 mm by 1524 mm. The specifications of the seven-mm welds used to connect the HSS footings to the base plate are also depicted. They were each approximately 25 mm long.

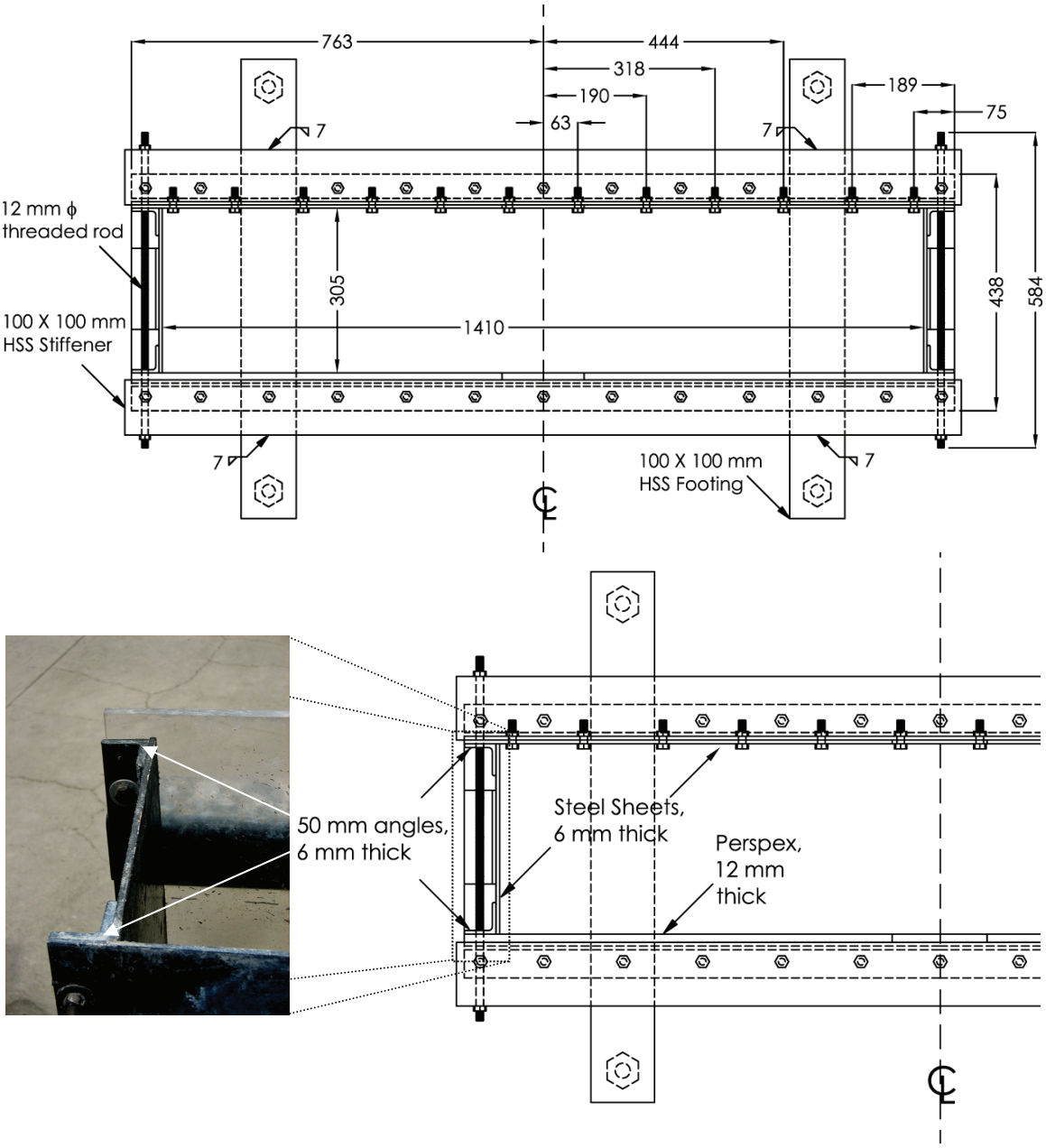


Figure 3.7: Plan view of the box (above) with corner detail (below).

3.2.4 END VIEW

The end view as seen in Figure 3.8 offers a final depiction of the box. The levelling screws that supported the HSS footings were located at 51 mm recessed from the edge of each end of each footing. Three bolts spaced at 62 mm centre-to-centre attached two 50 × 50 mm angle sections. The centre of the first bolt was located at 363 mm from rear edge of the HSS footings. These angles were used to buttress the base of the six-mm thick side steel

panel. The lengths of both of these angle sections differed as they were merely scrap pieces and were not cut to any particular dimension. Of particular note is the gap that is six mm wide between the base of the Perspex panel and the leading 50 × 50 mm angle section located along the front edge of the base plate. This is a remnant of a previous design which was supposed to accommodate a steel panel six mm in thickness. This panel was to aid in stiffening the Perspex, as the original plan called for a clay slurry to be consolidated within the box. However this space enabled the Perspex to be manoeuvred with ease during assembly and disassembly, and was a useful feature. The gap was shimmed with scrap plywood sections of the same thickness, and wedged into place with a hammer. Figure 3.9 contains some photographs detailing important features of the sketch in Figure 3.8.

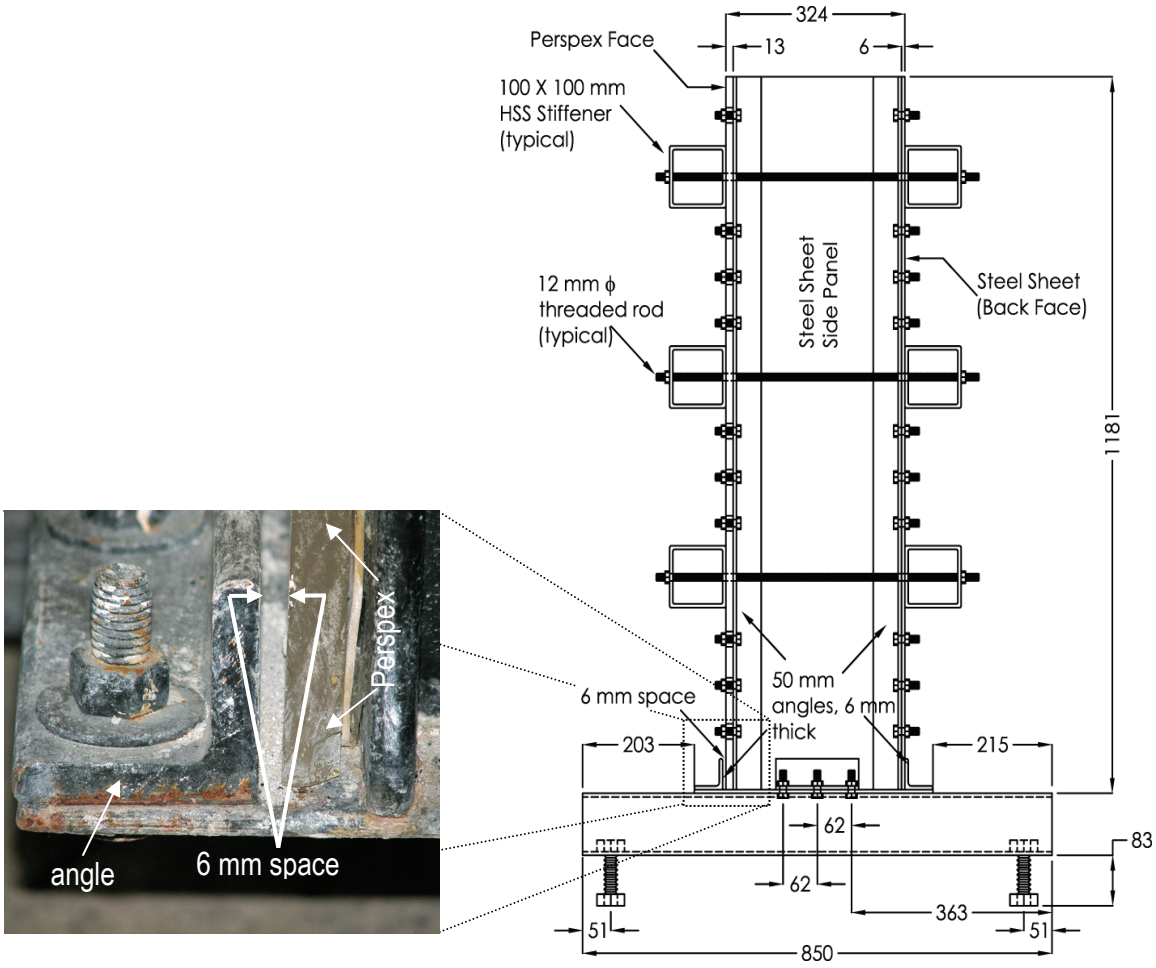


Figure 3.8: End view of the box, with detail showing the 6-mm gap.

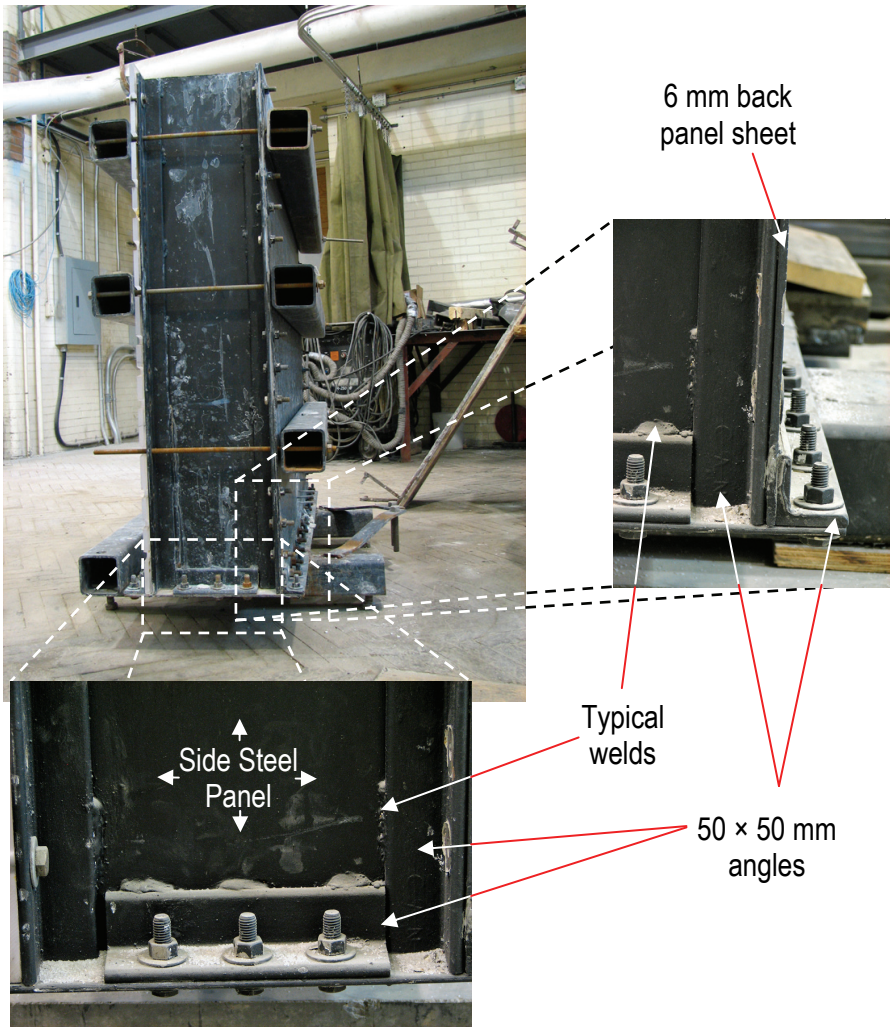


Figure 3.9: Clockwise from upper-left: Photograph of the end view of the box; Picture of the end view at the base of the box; typical corner detail of the base.

3.2.5 Supporting Components

There were additional components that were added to the box in order to facilitate a successful testing programme. They were of two differing types; those that were attached directly to the strongbox, and those which did not. A discussion about the former will be presented first, with a transition to the latter in the subsequent sections.

3.2.5.1 Perspex Caps

Perspex caps were used to seal the 152 ϕ mm holes in both the Perspex and steel panels in order that the box would be sealed completely before any material was poured inside. They were attached to the box by using the 5 ϕ mm threaded rods found near the

edge of the main holes. Essentially each disc was composed of two discs of Perspex; a 127 ϕ mm disc, 25 mm thick was mounted concentrically on top of another 203 ϕ mm disc, 12 mm in thickness, and glued. A hole 12 ϕ mm was drilled through the centres of both discs. Four 5 ϕ mm holes were made at a distance of 12 mm from the edge of the 203 ϕ mm disc at right angles from each other as measured from the centre of the disc. The caps were secured with the inner discs inside of the model. The cap that was used on the Perspex panel was sawn in half. A rubber gasket was glued to one sawn face to ensure a properly sealed joint. Circular rubber gaskets were also put between the caps and the abutting faces of the box to achieve the same purpose. Nuts were used on the threaded rods once the caps were in place to secure them tightly. Figure 3.10 shows the cap used on the Perspex face, however it is entirely representative of the cap used on the back steel face, despite the fact that it was not sawn in two.

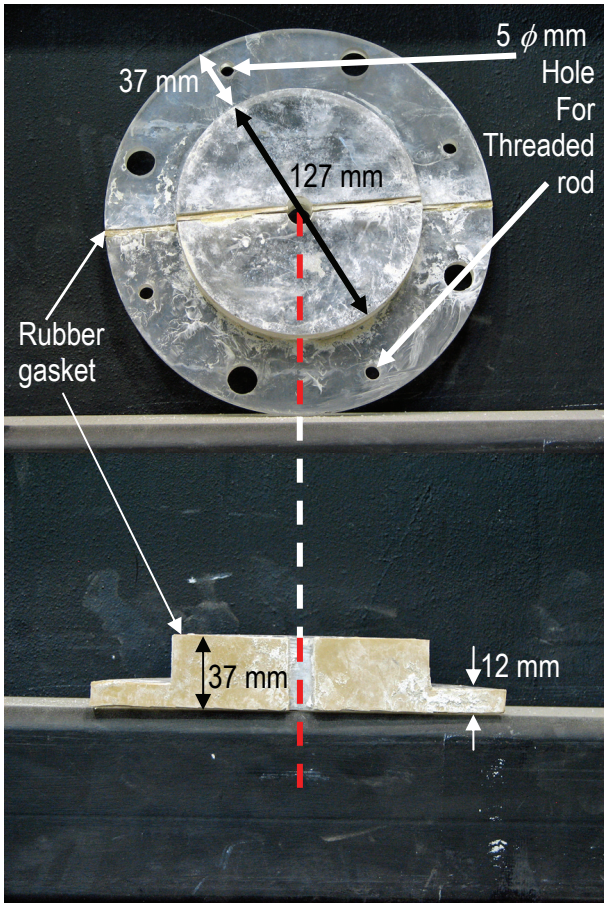


Figure 3.10: Photographs of the Perspex cap in plan (above) and of one sawn half with a rubber gasket in elevation view (below).

3.2.5.2 Steel Strap Connectors

The entire strongbox arrangement had to be anchored to ensure that it remained in place during the experiment. This was accomplished by welding steel straps to the footings behind the back steel face, which then facilitated a connection of the strongbox with a W-section 3100 mm in length. The W-section acted as an anchor. The straps had to be bent to the dimensions shown in Figure 3.11 in order that a flush connection with the W-section be made. 19 ϕ mm holes were drilled at the ends of the straps, through which 19 ϕ mm threaded rods 150 mm in length and capped with 29 mm nuts were used to connect the straps to the W-section. They are located 325 mm from the back panel and 50 mm from the centreline.

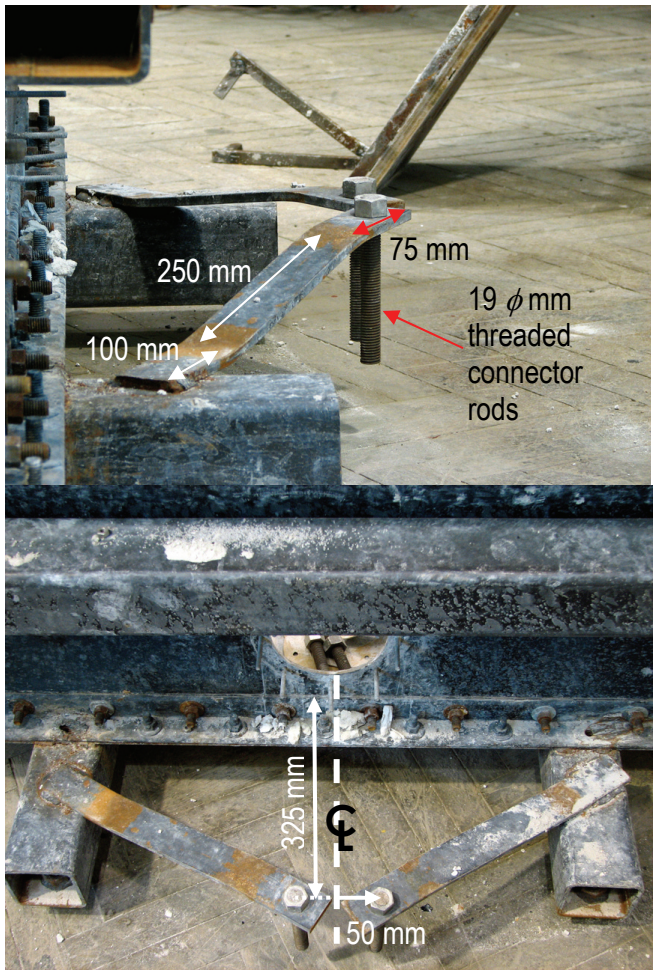


Figure 3.11: Photographs depicting the geometry and location of the strap connectors and connecting rods as seen from the end view (above) and in elevation (below).

3.2.5.3 Anchoring W-Section

As mentioned in the previous section, the connecting rods were passed through the steel straps and into holes cut into the flange of a W-section. They were located 25 mm from the leading edge and 50 mm from the centreline passing along the length of the section. 29-mm nuts were welded to the flanges at about 25 mm from each leading edge of the flanges so that 19 ϕ mm threaded rods 250 mm long could act as levelling screws, which served to keep the top flange of the W-section flush the adjoining steel straps. Figure 3.12 shows a cross-section of the W-section and how it was used to anchor the strongbox.

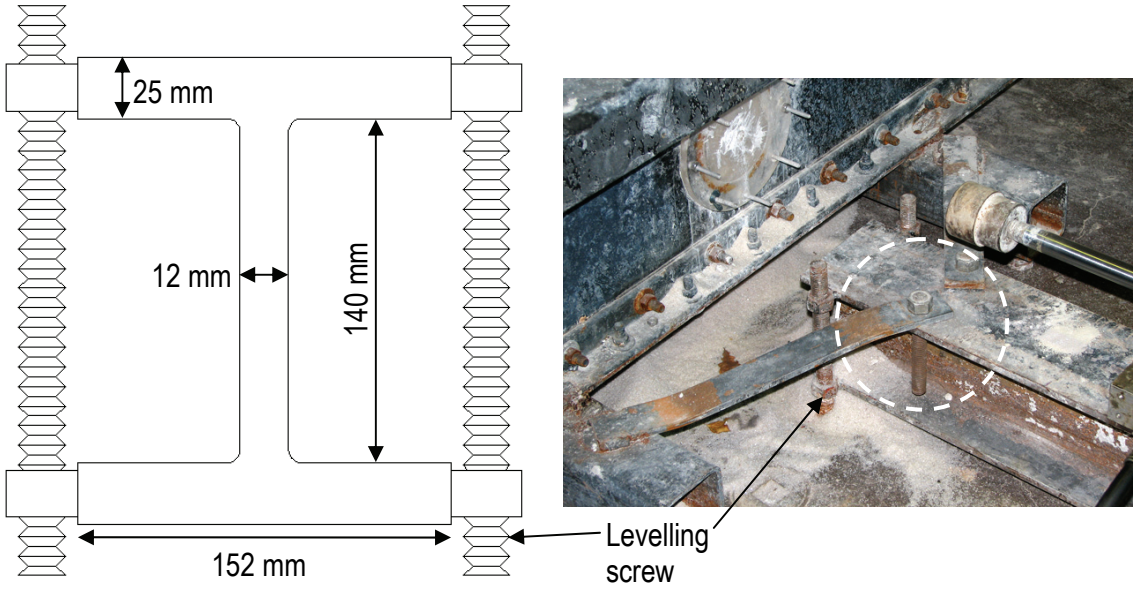


Figure 3.12: Cross-section of the W-section (left); the position of a steel strap and the position of where the connecting rod was placed through the W-section flange are shown in the dashed circle (right).

3.2.5.4 Casing

A galvanised steel pipe with an outer diameter of 152 mm, and an inner diameter of 150 mm (I = 1.35 × 10^6 mm^4) was chosen to perform excavation work within the model. The casing pipe was approximately 405 mm in length, which was longer than the inner depth of the steel tank. This was to ensure that there would always be an extra section of pipe protruding from one or both sides of the box that was available in the event that the pipe became lodged or otherwise immobile during excavation. The leading edge of the casing was bevelled by using an angle grinder to create a sharper cutting lip which would disturb the unexcavated material less than it would have had it remained blunt.

Four four-mm thick steel plates approximately 25 mm deep were welded in a cruciform on the inside of the pipe, at a recessed depth of 25 mm from the leading edge. The plates were placed in an orientation such that strong-axis properties would prevail. A 19-mm hexagonal nut was secured at the centre of the cross-form via welding. A threaded rod 12 mm in diameter and 915 mm in length was secured to the bolt. Please refer to Figure 3.13 for more details.

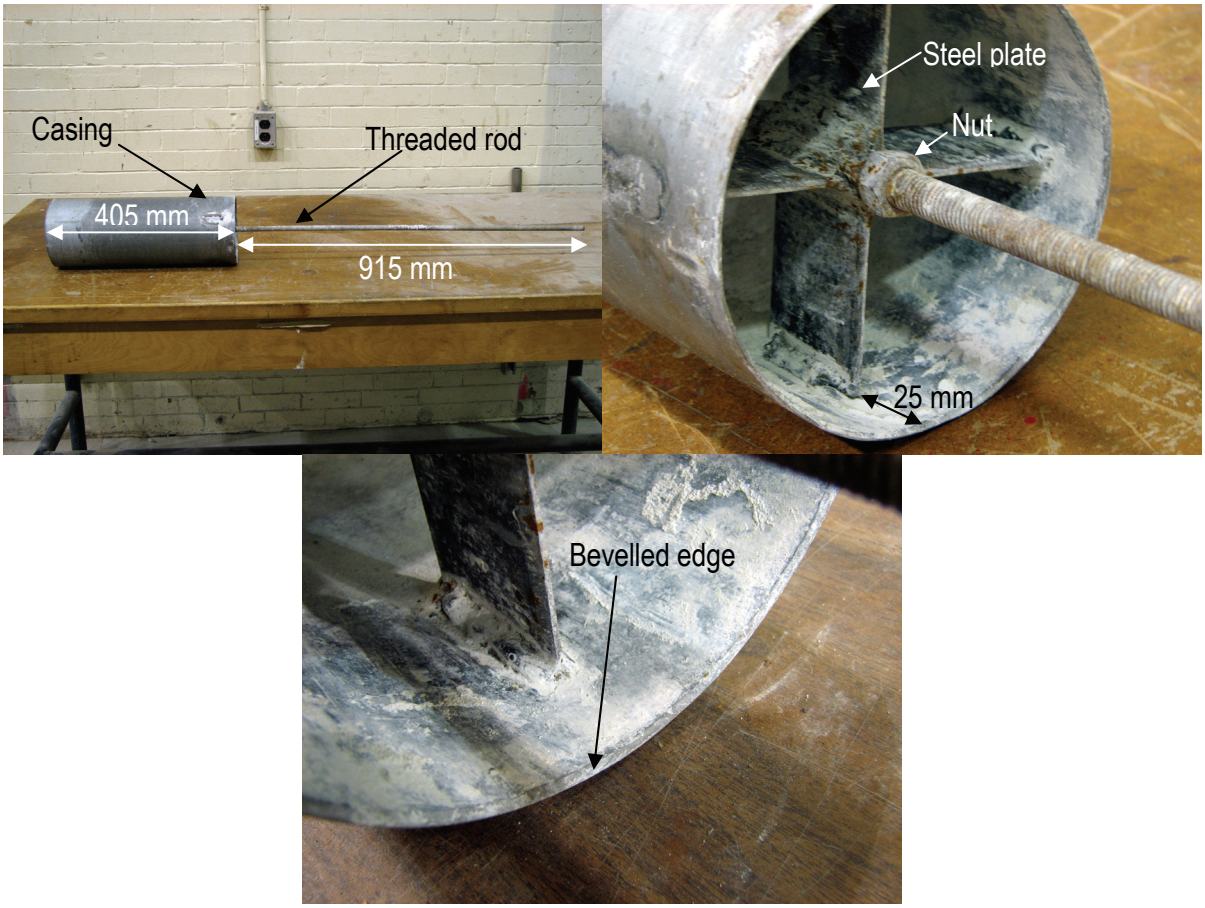


Figure 3.13: Steel casing and threaded rod (upper-left); detail of steel plates holding the threaded rod (upper-right); detail of the bevelled cutting lip along the leading edge (bottom).

3.2.5.5 Stool

The pipe section of the casing was allowed to rest on a stool whenever the casing was not completely inside of the model. It comprised four levelling screws and a W-section 330 mm long by 150 mm wide, in plan. This enabled the casing to remain in perfect alignment for excavation at all times. A picture of this can be seen in Figure 3.14.

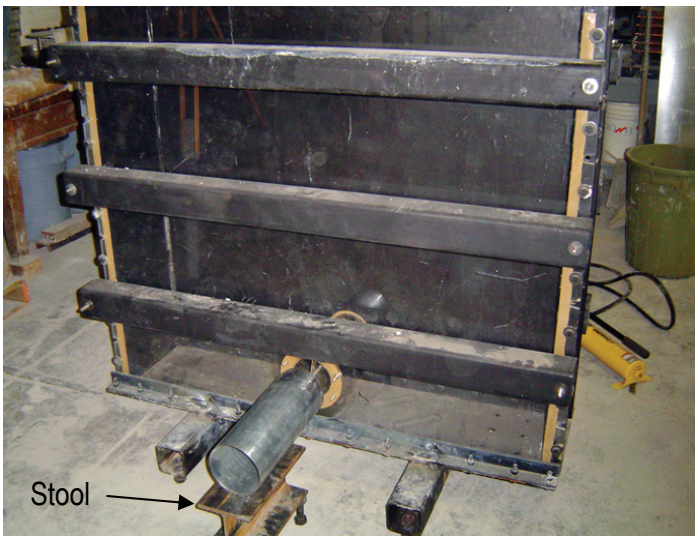


Figure 3.14: W-Section stool supporting the steel casing.

3.2.5.6 Lining

An aluminum foil sheet which was 0.25 mm thick ($I = 1.30 \times 10^{-3}$ mm^4/mm, based on the cross-sectional thickness of the thin sheet) and 305 mm wide was worked mechanically through rollers in order to form a thin-walled cylinder which was approximately 125 mm of outer diameter. The sheet was held in a cylindrical shape by five small screws. The outer screws were set 25 mm in from the outer circular edges. The middle screw was at 150 mm from the outer edges. The two remaining intermediary screws were halfway between the middle and outer screws. This kind of foil was chosen because of the malleable elastic properties it exhibited which visibly and mechanically enhanced the soil-lining interaction. Figure 3.15 contains photographs of the lining.

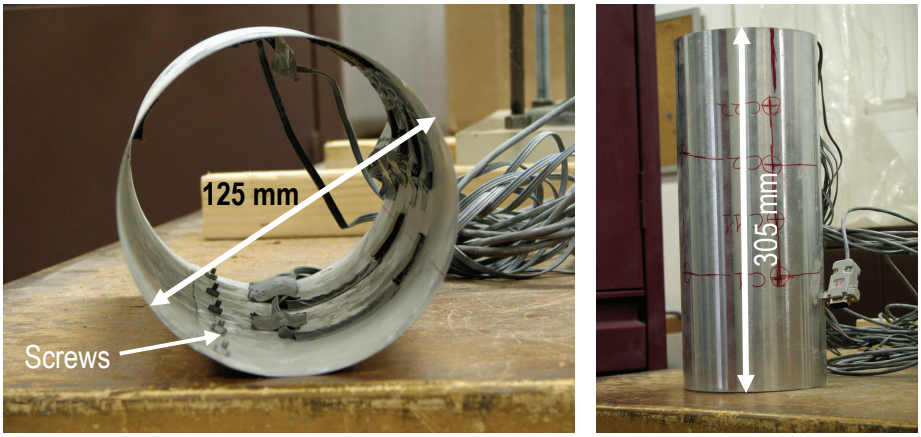


Figure 3.15: Aluminum sleeve with circular section showing (left) and in elevation (right).

3.2.5.7 Hydraulic Jack

A hydraulic jack was used to excavate the opening within the model. A piston head with a 12 ϕ mm threaded bored hole was mounted on the end of the driving shaft of the jack. The shaft could move only in a horizontal direction along the length-wise axis, parallel with grade. A hydraulic pump was connected to the jack, and the jack was actuated by lifting and pushing downwards on the lever arm. The pump also allowed for bi-directional movement of the piston. The entire piston mounting rested on the W-section anchor, and was secured in place with nuts and bolts. The levelling screws attached to the flanges of the W-section anchor ensured that the piston and shaft were always in perfect alignment with the threaded rod attached to the casing, which was aligned with the 152 ϕ mm hole in the box. Each depression of the lever arm advanced or withdrew the piston through 25 mm. Refer to Figure 3.16 for a graphical summary.

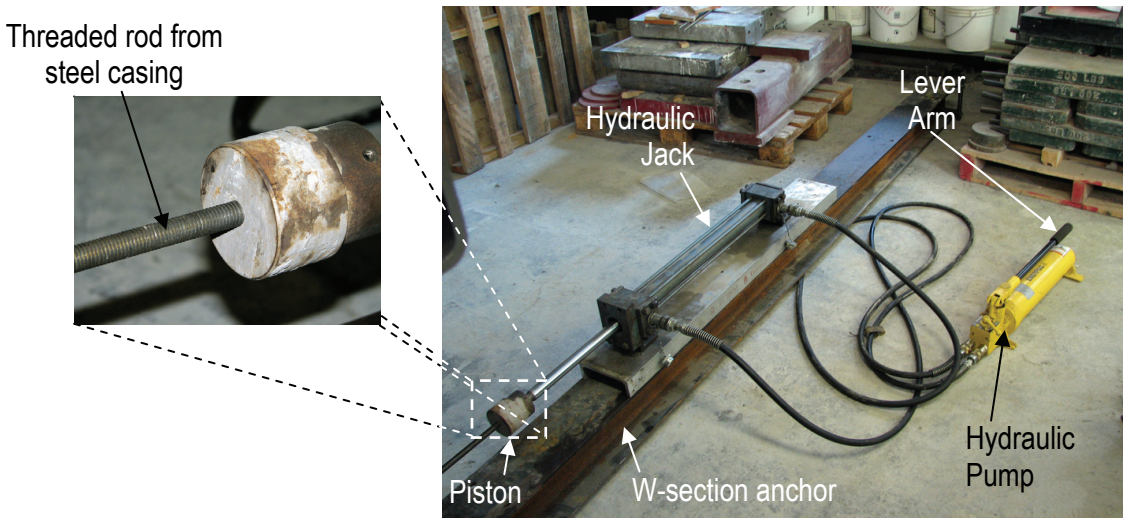


Figure 3.16: Hydraulic jack mounting with pump and connection to the threaded rod (detail).

3.3 A Cohesive Medium

As outlined in Chapter 2, consolidation was usually – if not always – required when preparing cohesive soil samples such as clay. This would not only involve great overburden pressures for large-scale soil samples, but also periods of time on the order of days or weeks between each successive test. These constraints were less of a concern when tests were conducted in a centrifuge, as the physical scales were relatively much smaller than 1g-models. It was preferred to prepare a cohesive material that would attain an adequate strength over a much shortened period of time for this project, since time did not permit for the usual consolidation process. This section will outline the sample preparation scheme that met the constraints mentioned above.

3.3.1 Rationale

Stimpson (1970) summarised the use of various materials that can be employed in the laboratory for simulating the properties of other materials in the field. Dykeman and Valsangkar (1996) and Dunham et al. (2004) adapted Stimpson's work to simulate a soft ground medium which was to be subjected to piling activity in centrifuge testing. Dykeman and Valsangkar (1996) in particular used three different mix proportions of bentonite clay, cement, sand and water to mimic a stiff clay or soft rock. The inclusion of cement increased greatly the rate at which the sample strengthened, normally on the order of a day or two. Shear strength values were taken from Dykeman and Valsangkar's samples and then

compared with known values of other media in order to relate analogous material from the field. Their work provided an appropriate context for this project for investigating the design of a mixture that would simulate the basic behaviour and properties of a soft, cohesive material, within hours of mixing.

3.3.2 Mix Design

Rounds of initial, *ad-hoc* testing were done by varying the proportions of clay, cement, sand and water, starting from the mix design proposed by Dykeman and Valsangkar (1996). However the cement content was reduced to produce weaker samples. Kaolin, bentonite and reconstituted illite were used in these tests. All samples were judged based on qualitative cohesion and monitored every hour after mixing, for a total period of six hours. The mix that yielded the best initial results was that which comprised (by mass) 10% bentonite clay, 4% cement, 36% water, and 50% sand. More rigorous testing involving a hand-held shear vane device was done on refined mix designs, varying slightly only the sand and water mass fractions. For these trials, samples with 2.6 kg of total mass were placed into moulds 100 × 100 mm in plan with an inner depth of 250 mm (Figure 3.17). These samples reached an average height of 200 mm in each mould. A shear vane with a blade diameter of 19 mm was used to obtain the undrained shear strength of each sample. One other important quality that was evaluated was that of workability. The mix not only had to be sufficiently viscous so that it would fill the strongbox with minimal void spaces, but it also could not have too large a water content as this would retard the rate of strengthening. The mix design that best fulfilled all the criteria was that which comprised 10% bentonite clay, 4% cement, 42% water and 44% sand.



Figure 3.17: Moulds used for cohesive samples (left); sheared samples (right).

Repeated vane testing for undrained shear strength was done on samples of this finalised mix after 120 minutes had elapsed. Timing commenced once water was added to the dry material. This yielded an average shear strength range of about 2 to 3 kPa. It should be noted that this range underestimated the actual shear strength that would develop in the model at locations in line with the proposed tunnel elevation; this was a consequence of an effective self-consolidation process that resulted from the self-weight of the overlying material, and would serve to increase the shear strength appreciably.

3.3.3 MATERIAL PROPERTIES

Further testing was done on each material chosen for the mix to determine all relevant properties. The following sections will present the results of the work done on each constituent of the mix. In addition to this, one section will detail the valid characteristics of the sand that was used to form a granular layer between surrounding strata of cohesive material within the model. The aluminium used to form the tunnel lining sleeve is also discussed.

3.3.3.1 Fine Sand

A fine sand was used as a constituent of the cohesive mix. This sand was chosen because it was observed during the initial *ad-hoc* testing that it contributed to a smoother, more workable mix. The vendor labelled this grade of sand as *Quartz Industrial 7030*, as it was claimed that 30% of material would be retained on a No. 70 mesh. A sieve analysis was performed on several randomly selected samples of this sand according to the standards prescribed by ASTM D6913-04e1, and a particle-size distribution was generated. From this the coefficient of uniformity (C_u) of the sand was estimated to be 1.90. Please refer to Appendix B for more details. The coefficient of curvature (C_c) was found to be about 0.89. The specific gravity (G_s) of the sand was determined according to ASTM D854-06. G_s was found to be 2.66. Appendix C provides more details about this test.

3.3.3.2 Coarse Sand

The coarse sand was not a constituent of the cohesive mix, but instead was used to form a granular stratum placed within overlying and underlying layers of the cohesive mix. The vendor labelled this grade of sand as *Quartz Industrial 2075*, as it was claimed that 75%

of material would be retained on a No. 20 mesh. A sieve analysis was performed on several randomly selected samples of this sand according to the standards prescribed by ASTM D6913-04e1, and a particle-size distribution was generated. From this the coefficient of uniformity (C_u) of the sand was estimated to be 1.88. Please refer to Appendix B for more details. The coefficient of curvature (C_c) was found to be about 0.91. The specific gravity of the sand was determined according to ASTM D854-06. G_s was found to be 2.65. Appendix C contains further details about this test.

3.3.3.3 Bentonite Clay

Bentonite clay was one of the constituents of the cohesive mix. Tests were done according to the standards prescribed by ASTM D4318-05 to determine the plasticity index (*PI*) of the clay. After several trials, the plastic limit (*PL*) of this clay was found to be about 31% moisture content by mass. The liquid limit (*LL*) was found to be approximately 85%, thereby yielding a $PI = 54$. More information on these results can be found in Appendix D.

3.3.3.4 Cement

Type GU (formerly *Type 10*) Portland cement (CSA A3001) was chosen as the agent for accelerating the strength of the mix. It was used because it was the most basic and most common type of cement available.

3.3.3.5 Aluminum

The elastic modulus (*E*) of the aluminum sheet was obtained by testing 'dog-bone' shaped coupon specimens, approximately 225 mm in length. The coupons were cut from the same roll of aluminum used to create the lining sleeve. They were also cut in an orientation that matched that of the sleeve with respect to the bending axis. The two wider flange sections of the specimens were about 19 mm across, while the thinner middle section of each coupon was on average 12.54 mm, as read from a digital calliper (Figure 3.18). The thickness was 0.25 mm, as previously mentioned in the description of the aluminum sleeve. Each coupon was subjected to tensile forces until complete failure. This was accomplished by firmly securing the wide flange sections within grips that were separated at a rate of 0.1 mm/min. Forces arising from this action were recorded at a sampling rate of 10 Hz, which

enabled the generation of a stress-strain relation for each coupon. The average elastic modulus for the aluminum was found to be 64 GPa. More details are provided in Appendix E.

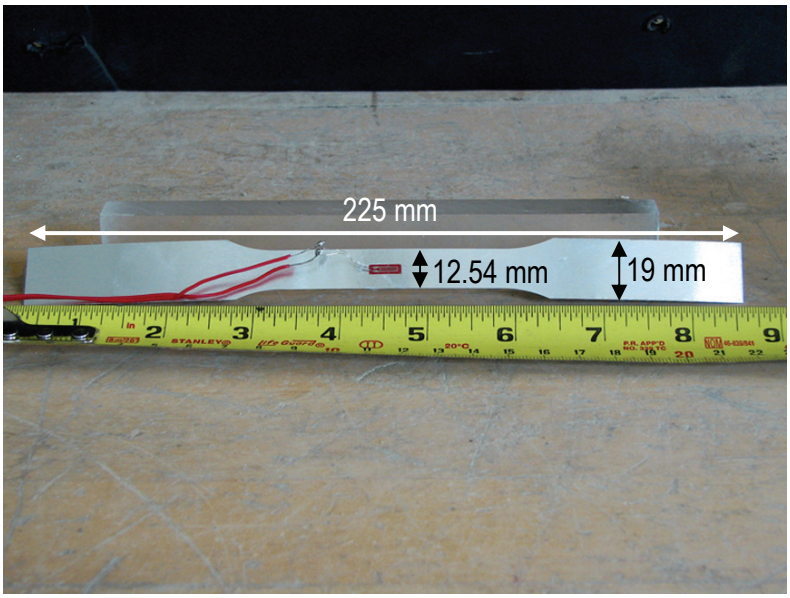


Figure 3.18: A typical specimen used in coupon testing.

3.3.4 Mix Density

The density of the mix was determined in order to calculate as accurately as possible the forces and stresses that would arise inside of the medium. This was achieved first by calibrating the inner volume of a vessel, into which samples would be poured and weighed. A cylinder was used for this purpose, having a volume of 223.13 mL. Sample batches with a total mass of 500 g each were prepared using the same proportions that were used in the model. The cylinder was filled completely with mix, and the resulting net increase in mass was recorded for each trial. The average density was then calculated to be 1.83 g/cm^3, or a unit weight of 17.9 kN/m^3. Further details regarding these tests can be found in Appendix F.

3.4 Data Acquisition

All electronic data for this project were acquired via strain gauges, read and filtered by an Ethernet acquisition system, which was controlled by a desktop computer. Each of these components will be discussed briefly in the following sections.

3.4.1 STRAIN GAUGES

The strain gauges chosen for the project had a gauge length of 5 mm and a resistance of 120 ± 0.3 Ω. The gauge factor was 2.11 ± 1%. Please refer to Appendix G for further details. A total of eight gauges were affixed to the inner surface of the aluminum sleeve along lines coinciding with the proposed crown and springline axes (Figures 3.19 and 3.20). Four gauges along the crown were spaced evenly by 50 mm, centre-to-centre, with the first gauge situated at a recessed distance of 50 mm from the leading edge of the cylinder. Two pairs of gauges were placed along each springline. They were spaced by 100 mm, with each gauge situated at a recessed distance of 100 mm from the leading edge of the sleeve. All gauges were bonded such that they would measure strains in line with the axis of bending. Figure 3.19 shows the strain gauge alignment, as well, it denotes the nomenclature that will be used hereafter.

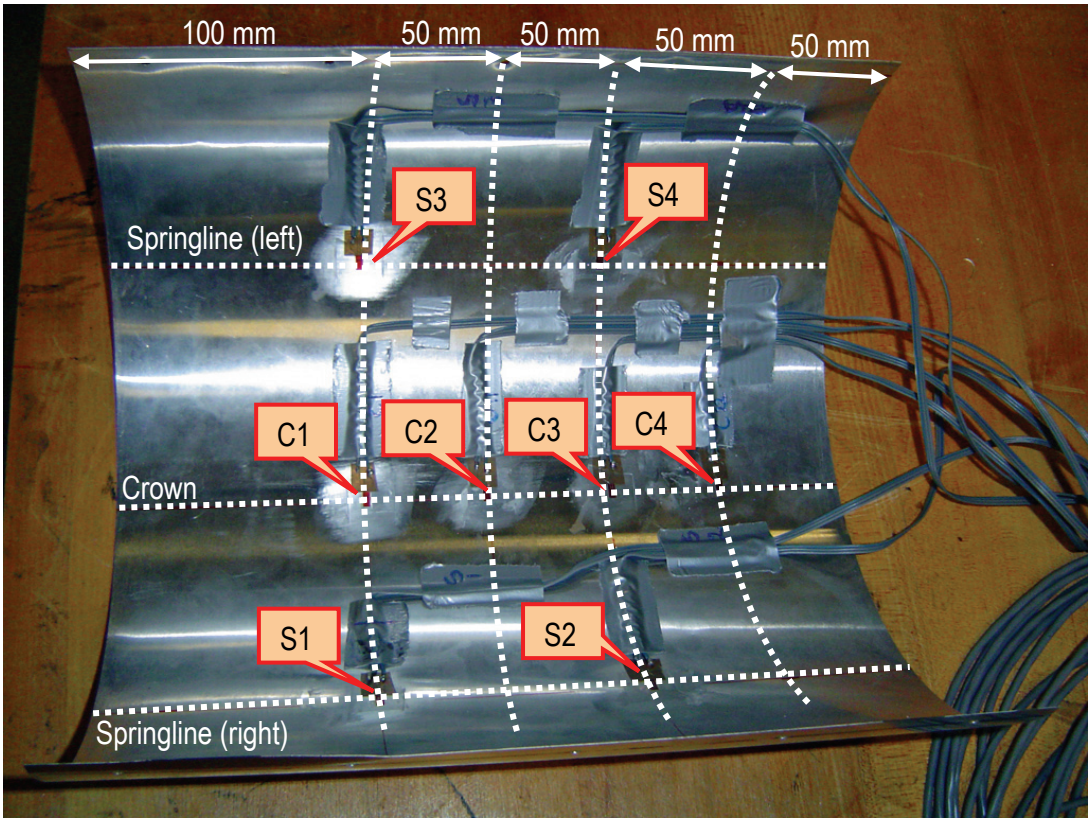


Figure 3.19: Inner surface of the aluminum cylinder with strain gauge locations (S1, S2, C1, C2, etc.).

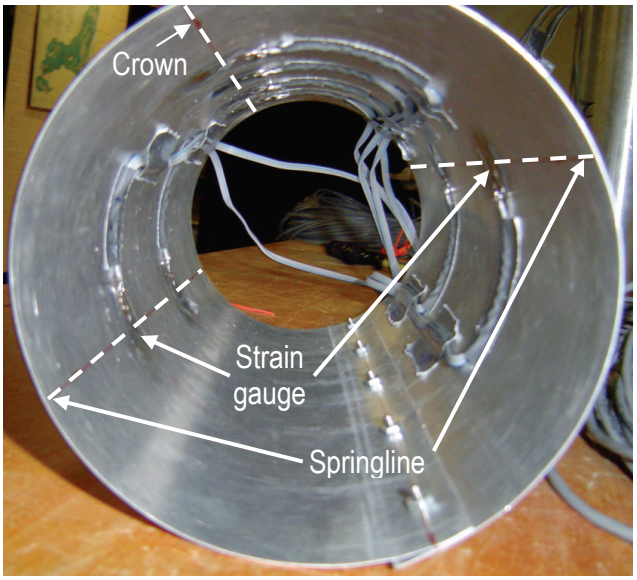


Figure 3.20: Elevation view of the aluminum cylinder showing the strain gauges aligned with the springlines and crown.

3.4.2 DATA ACQUISITION SYSTEM

Data was acquired and filtered by *Strainbook/616*, which is an Ethernet-based strain gauge measurement system. It contained eight channels, each with one gauge connected to it via a lead wire and nine-pin connector. All channels were configured for a quarter-bridge circuit, with respect to the wheat-stone bridge arrangement for resistors. All constituent resistors on each port were 120 Ω.

3.4.3 SOFTWARE

The data acquisition system was actuated using the WaveView 7.0 software package installed on a Pentium IV 2.7 GHz processing platform. The excitation voltage was always ± 2.0 V for all channels. All output was read in engineering units (i.e. the so-called '$mx + b$' readings), which converted instantly all raw data to actual strains based on the excitation voltage and the nominal gauge factor of the strain gauges. Further details regarding this of conversion are provided in Appendix G.

3.5 METHODOLOGY

The first part of this section will contain the objectives of the experimental programme of this project. Details concerning sample preparation will be presented next, followed by the procedures used in all tests.

3.5.1 OBJECTIVES

Four tests were proposed for this project to study the strains, stresses and bending moments arising from tunnelling in multi-layer ground. The first was a control test, in which the tunnelling medium was that of a homogeneous ground (i.e. only the cohesive mix). The other three tests involved the presence of a coarsely grained sand layer located at distances equivalent to one, two and three excavated diameters (i.e. 150 mm ϕ) above the crown of the excavation. The thickness of this sand layer was also equivalent to one excavated diameter. An investigation into the resulting strains of the tunnel lining placed within a layered medium was done by contrasting them against the values recorded from the test involving uniform ground conditions. Moreover similar comparisons of bending stresses and moments were done using these data.

3.5.2 PROCEDURE

Before any work could be done, the strongbox was inspected to ensure that it was dry and clean. Once this had been confirmed, the inner surfaces were lubricated liberally by applying a generous coating of clear, silicone-based grease. It had the primary function of minimising friction at the interfaces between the medium and the surfaces of the box. This particular kind of lubricant was chosen because it was water-proof and inert with respect to the constituents of the cohesive mix.

Next, both the Perspex face and the Perspex caps were bolted in place. The outer exposed surface of the steel casing was then greased liberally with the same silicone-based grease used inside the model. The threaded rod attached to the casing was then fed through the 12 ϕ mm holes in the middle of the Perspex caps, and into the 12 ϕ mm threaded hole in the piston of the hydraulic jack. The casing was left to rest on the stool, and was covered to prevent debris from becoming attached to the greased surface. Material was placed into the box, until the proposed elevation of the model was reached. More details on sample

preparation and placement will be given in the next section. It should be noted that the 19 ϕ mm threaded rod that connected the casing to the piston was exposed across the inner extent of the box, at an elevation of 178 mm from the inner base. It was submerged fully once material was poured.

Excavation work always started after 150 minutes had elapsed, commencing at the time at which the mixing of the first batch began; after this period, the strength of the mix had evolved sufficiently. First, the casing was advanced by the hydraulic jack until the cutting edge was about 25 mm from the outer face of the front Perspex cap. At this time, the two halves comprising this cap were removed quickly and the cutting edge of the casing was advanced into the exposed hole as swiftly as possible in order to avoid any loss of material. The casing was advanced at a rate of about 25 mm every two seconds, which corresponded to one complete cycle of lowering and re-arming the lever arm of the hydraulic pump. When the cutting edge of the casing was approximately six mm from the inner surface of the rear Perspex cap, the nuts holding this cap in place were removed hurriedly, along with the cap itself, and the casing was advanced until the leading edge had passed out of the hole by about 50 mm. The cuttings inside of the casing were removed by hand continually as the casing was advanced. This was to minimise any unnecessary increase in pressure against the inner face of the rear Perspex cap.

At this point, the casing was then advanced through the soil until the rear edge was almost flush with the outer surface of the Perspex front panel. Then the aluminum cylinder was placed inside of the larger casing, and the data acquisition system was armed. The bolts comprising the invert of the aluminum sleeve were used to align this cylinder with the centreline of the box in order that the crown and springline locations were true and consistent for each test. Finally, the casing was then advanced further, allowing the aluminum sleeve to become exposed to the walls of the soil cavity. It was at this point that the aluminum cylinder simulated a tunnel lining. As the casing passed through the model, the surrounding soil moved into contact with the lining in a progressive manner, until the casing was completely out of the box. At the instant that the surrounding soil came into contact with the lining and it was observed to begin deforming as a result. The data acquisition system was triggered once the lining was exposed to contact with the surrounding soil, and recorded data for a period of 15 minutes. Nothing else was done to the model during this time. The software stopped acquiring and recording data upon

completion of these 15 minutes. It was at this point that the experiment was terminated. Please refer to Figure 3.21 for an illustration for different stages of construction.

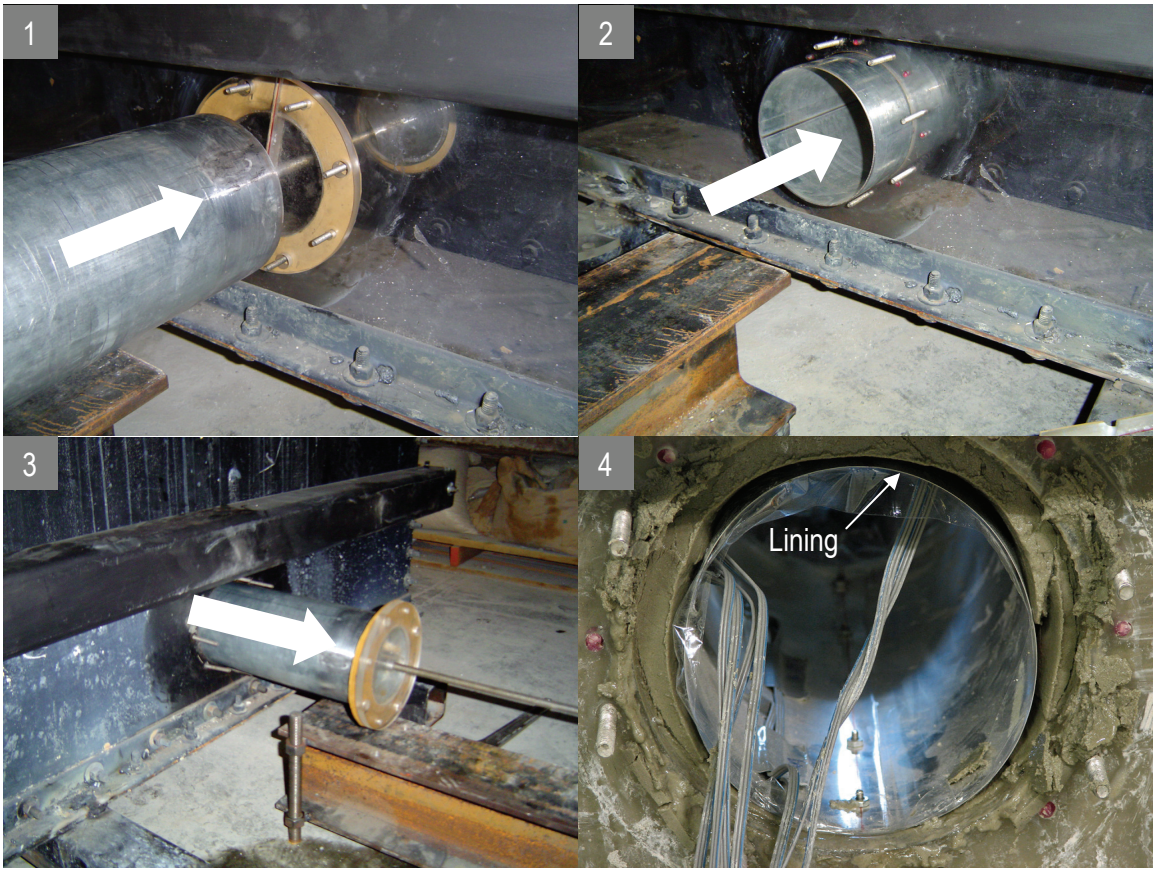


Figure 3.21: Stages of excavation: (1) Casing outside on front side; (2) Casing inside the box; (3) Casing advancing out of the box at the rear; (4) Lining placed inside of the excavated tunnel.

3.5.3 SAMPLE PREPARATION

All of the constituents necessary for the cohesive mix were mixed in a concrete mixer. However, the volume of the mixer (approximately 0.01 m^3) was such that it limited the amount of mix that could be prepared at any given time. Therefore it was necessary to divide the work into separate batches, each with a total mass of about 164 kg. Separate measures of bentonite clay (16.380 kg), cement (6.550 kg), 7030 silica sand (72.1 kg) and water (68.7 kg) were weighed to create batches of the previously outlined proportions of 10%, 4%, 44%, and 42%, respectively. The control test with homogeneous ground conditions was the least complicated of all the tests in terms of sample preparation. This was because the tunnelling medium would be uniform across the entire model. It is for this reason that the preparation for this test will be described first.

Five individual batches were weighed and prepared for the control test as described above. First, only the dry material were loaded into the concrete mixer. Second, water was added in a controlled manner in order to avoid unnecessary spills. The slurry was mixed for 15 minutes, commencing from the time at which the water was added. It was found based on experience that this was an adequate period of time to allow the batch to attain a smooth, workable consistency. Once the mixing period had elapsed, the batch was evacuated via a trap-door at the base of the mixer into a hopper that was placed directly beneath. Finally, the slurry was poured into the open top of the box in a controlled manner in order to avoid a violent rush of material into the model.

Each batch, on average, reached an effective depth of about 200 mm in the box. All batches were prepared and placed in this manner. The mean elevation of the free surface of the entire sample was found to be approximately 1070 mm, or about seven equivalent excavation diameters ($\sim 7 \times 150\ \phi$ mm). Vibration using an industrial concrete vibrator was performed after every second batch was placed. This was done to minimise as much as possible the existence of air voids that became entrapped during the pouring. It also served to keep the consistency of the slurry as uniform as possible across successive batches.

The procedure outlined above was similar as that for the tests involving the presence of a sand layer between cohesive strata, however with a few notable differences. These will now be described. The total masses of the batches either preceding or following the placement of the sand layer needed to be adjusted, as the presence of the granular material meant that less cohesive material was required for each test. This also served to avoid wasting material. Once the elevation of the underlying cohesive layer was achieved, a geotextile which was cut to have a surface area just slightly less than that of the inner surface area of the box, was placed atop the free surface of the slurry in a fully saturated condition. 2075 silica sand, which had been soaked before sample preparation had begun, was placed by hand in a loosely packed and moist condition until the appropriate elevation was achieved. A geotextile was placed atop the free surface of the sand in the exact manner as mentioned for the slurry. Finally, cohesive mix was poured gently on top of the sandy layer in order that the jet of slurry passing through the mouth of the hopper would not scour or punch through the underlying sandy layer. This was done until the mean free surface elevation of about 1070 mm was achieved. It should be noted that the geotextile was placed at the interfaces between the strata because previous experience had shown that the 2075

silica sand would become absorbed into the surrounding slurry, thereby significantly reducing the depth of the granular layer in an uncontrolled manner, and changing the local properties of the surrounding slurry as well. Figure 3.22 depicts the dimensions of the samples prepared for this study. ■

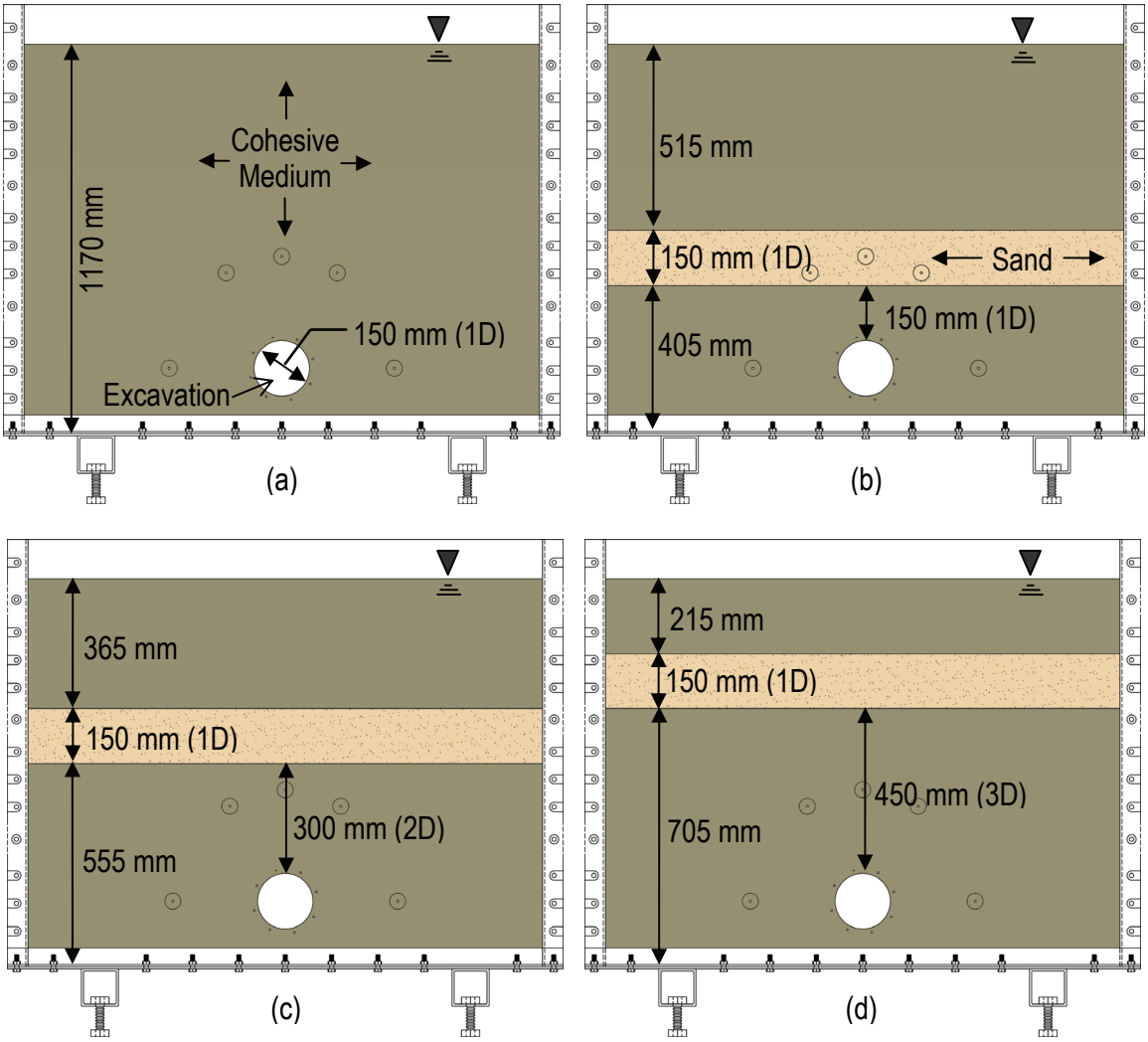


Figure 3.22: (a) Conditions for the control test with a uniform medium; (b) Conditions for the test with the presence of a sand layer 1D above the crown of the excavation; (c) Conditions for the test with the presence of a sand layer 2D above the crown of the excavation; (d) Conditions for the test with the presence of a sand layer 3D above the crown of the excavation.

CHAPTER 4 – EXPERIMENTAL RESULTS

4.1 INTRODUCTION

This chapter will present the results from the work that was outlined in the previous chapter. First, there will be an overview of qualitative observations, as well as secondary data such as in-situ moisture contents and shear strength readings taken from the sample. This will be followed by a presentation of the strain gauge readings of each test. Stresses and bending moments were calculated based on each set of data, and these values will be presented in the ensuing sections.

4.2 OBSERVATIONS

The strongbox was constructed to minimise leaks of any kind due to the fluid nature of the mixture that was to be placed inside. However it was noticed that clear water seeped through the interface between the Perspex and the rubber gasket once the free surface of the material reached about 800 to 900 mm. All leaks would occur only at the base at the front face of the box. It was concluded to be the result of a self-consolidating phenomenon due to sufficient overburden pressures, which was enhanced further by the presence of sand as a constituent of the mixture. It was estimated that the volume loss of water was on the order of tens of mL over the first two hours, after the first batch was placed. This led to the conclusion that the tests were not done under fully saturated conditions. Furthermore, the observed seepage near the base of the box was also a consequence of the dissipation of pore-water pressures, which increased the vertical effective stresses (σ') in this area.

4.2.1 SHEAR STRENGTH

A hand-held shear vane device was used to investigate the in-situ, localised undrained shear strength of the sample. An extension rod 300 mm in length was used so that the vane could penetrate as deeply into the model as possible. The vane was driven to a depth of about 400 mm into the sample, as measured from the free surface. The diameter of the shear vane was 35 mm. All testing was done in accordance with ASTM D2573-01(2007) (*Standard Test Method for Field Vane Shear Test in Cohesive Soil*). Readings were taken at five locations as outlined in Figure 4.1, which shows the plan view of the box. The locations

were chosen in order to minimise boundary effects as much as possible. Shear-vane testing was conducted upon the termination of all electronic data acquisition. The trials were done first in a control sample that was used for refining the methodology and one that was not an actual test. They were also repeated in the live control test. No further trials were possible in other tests because of the presence of the layer of coarse sand. It was found that the local shear strength was on average 3 – 4 kPa, which was higher than the initial testing done with the moulds as outlined in Chapter 3. This discrepancy was expected and can be explained as a consequence of consolidation and slight drainage.

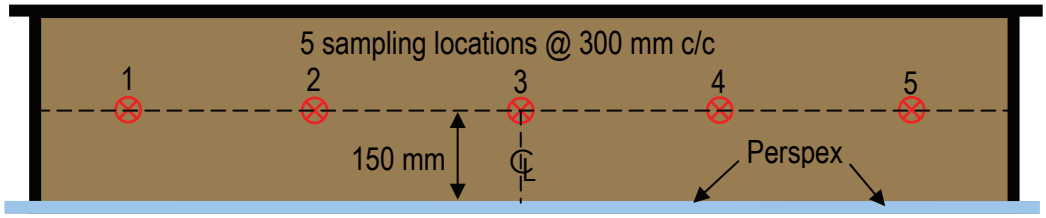


Figure 4.1: Plan view of the open top depicting the locations of where shear strength readings were taken.

4.2.2 Moisture Content

Moisture content values were taken from samples recovered from the pilot access holes in the Perspex face. They were done for all four live tests. Each cap was removed first by turning an O-ring screw into the threaded hole of the cap, and then by pulling the cap out of position. The caps were sealed with duct tape on the outer face of the Perspex during testing to prevent against leaks and against undesired displacement. A knife was pushed into the hole to a depth of approximately 150 mm in a direction normal to the Perspex face immediately after each cap was removed. Samples recovered from this penetrated depth were taken from the blade of the knife, weighed, and then placed in an oven set to a temperature just over 100 °C for a period of at least 24 hours. Each tested yielded one set of readings, for a total of four sets. The averaged moisture contents from all four tests are presented in Figure 4.2. It was noticed that a very slight gradient in the moisture content of the sample was present, with slightly higher values at higher elevations. This also seemed to validate the self-consolidation action as mentioned previously. It was also confirmation of the water loss at the lower elevations of the sample.

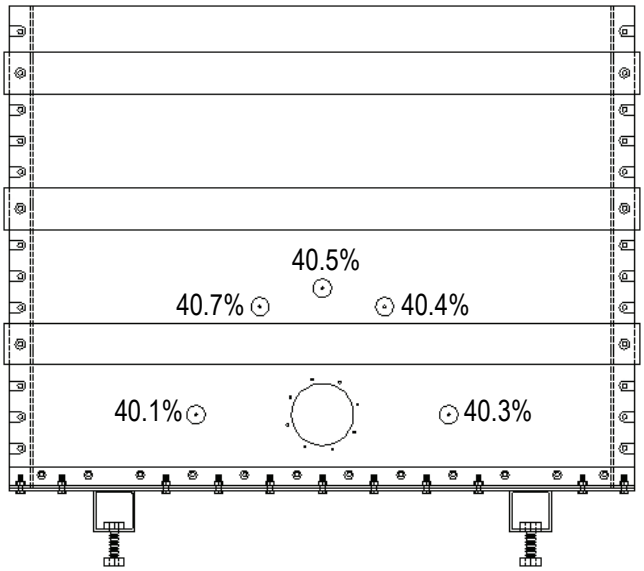


Figure 4.2: Averaged moisture content values taken from material recovered from each pilot hole.

4.3 DATA

The data that was acquired during each test will be presented in this section. Each set of raw strain data had to be treated before it could be analysed, and this process will be described first. The processed data were then used to calculate stresses, as well as the subsequent bending moments.

4.3.1 TREATMENT

The convention that will be used throughout this thesis is that compressive strains will be taken as negative and tensile strains, positive. Figures 4.3 to 4.5 depict the idealised ovalisation patterns of a lining due to the soil-lining interaction under different stress distributions, and also serve to illustrate how the convention was determined for this work.

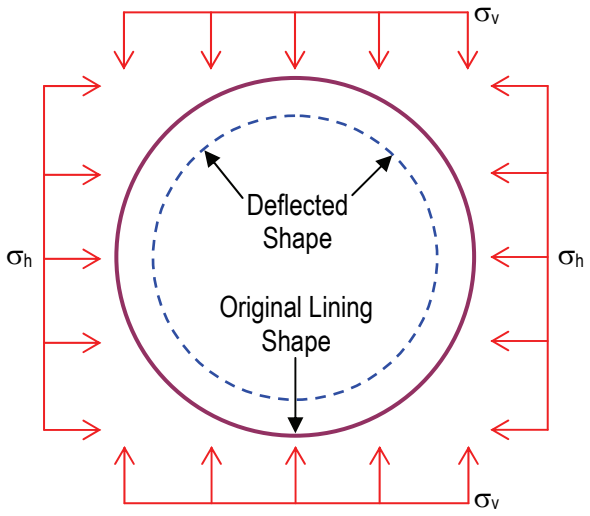


Figure 4.3: Inward uniform radial movement of the lining under an isotropic stress distribution ($\sigma_h = \sigma_v$).

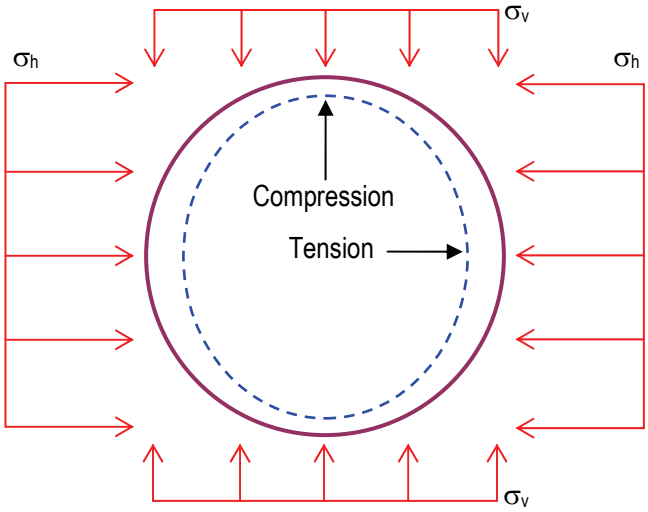


Figure 4.4: Inward radial movement of the lining under an anisotropic stress distribution ($\sigma_h > \sigma_v$).

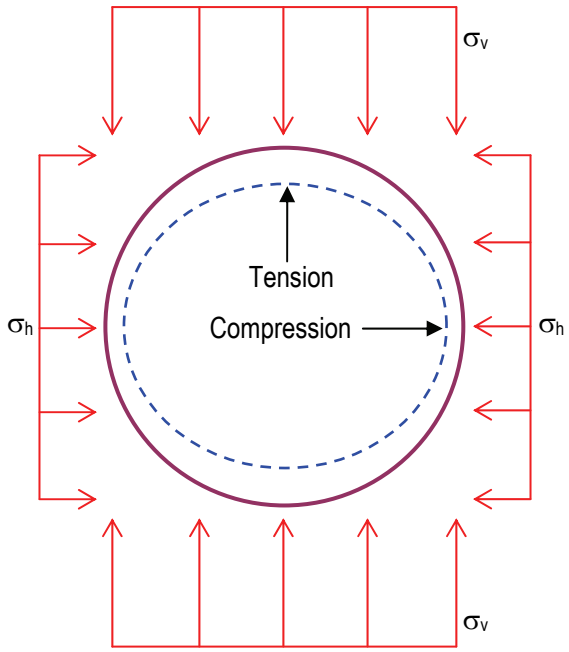


Figure 4.5: Inward radial movement of the lining under an anisotropic stress distribution ($\sigma_h < \sigma_v$).

Under a uniform, or isotropic stress distribution, the inward radial displacement of the lining will also be uniform. If the stresses are anisotropically distributed, then an oval-shaped displacement pattern will develop. The orientation of the distorted shape will depend on if either the horizontal stresses (σ_h) or the vertical stresses (σ_v) are greater. The strain gauges were bonded to the inner surface of the aluminum lining. As such, if bending were to occur as shown in Figure 4.4, then the gauges located at the crown will experience compressive action, while those at the springline will experience tensile action, relative to the initial, undistorted shape (i.e. before the lining is subjected to external stresses). Conversely, if bending were to occur as shown in Figure 4.5, then the response of the gauges will be reversed.

Inspection of the first plots of raw data revealed offset strain values for each gauge when there should have been negligible strains at the time of initialisation, not accounting for noise. This was the result of the manner in which the aluminum sleeve was placed inside of the rigid casing once each test was begun. These offsets were corrected by locating the value that most closely matched the true start-time of the test, or when the gauges began to react to the bending of the aluminum pipe. Once this value was determined, it was subtracted from all other values, resulting with a corrected initial strain of zero at the time of initialisation.

Another observed trend was that of the strains along the crown. The aluminum sleeve was exposed progressively to the soil as the rigid casing was pulled through the model. This meant that a portion of the sleeve was inside of the casing while soil began to move into contact with the naked, expoed portion of the lining. Consequently, bending of the sleeve was unrestrained wherever the lining was shielded by the casing. This was especially appreciable at the crown when viewing the raw data. The values would only stabilise once the overlying soil moved into contact with the crown, thus restricting it from further movement. It is for this reason that the portion of the lining that came into contact with the soil last (C1) yielded the highest strains; whereas the portion that came into contact first yielded the lowest (C4). Refer to the inset in Figure 4.6 for an illustration.

All test results revealed the same chronological pattern. First, there was a range of values that corresponded to the initial movements of the soil. Then there was an intermediate range that corresponded to the gap closure. The final range represented a state of static equilibrium between the lining and the surrounding soil. All three phases are denoted as regions I, II, and III, respectively, in all of the ensuing plots presented in this chapter. It should be noted that on occasion, some gauges registered extraneous data. These values were excluded from all analyses. Those values which showed agreement were included and averaged. A regression analysis was performed based on these averaged numbers in order to present a visual comparison between the averaged and the actual data. A dark curve with short dashes was used to depict the average crown strains in all plots, while a dark curve with long dashes was used to illustrate the average springline strains. Refer to Figure 4.6 for more details.

4.3.2 CASE 1: CONTROL TEST

The first test performed was the control test, which did not involve the presence of a layer of coarse sand. Figure 4.6 presents the results from this test.

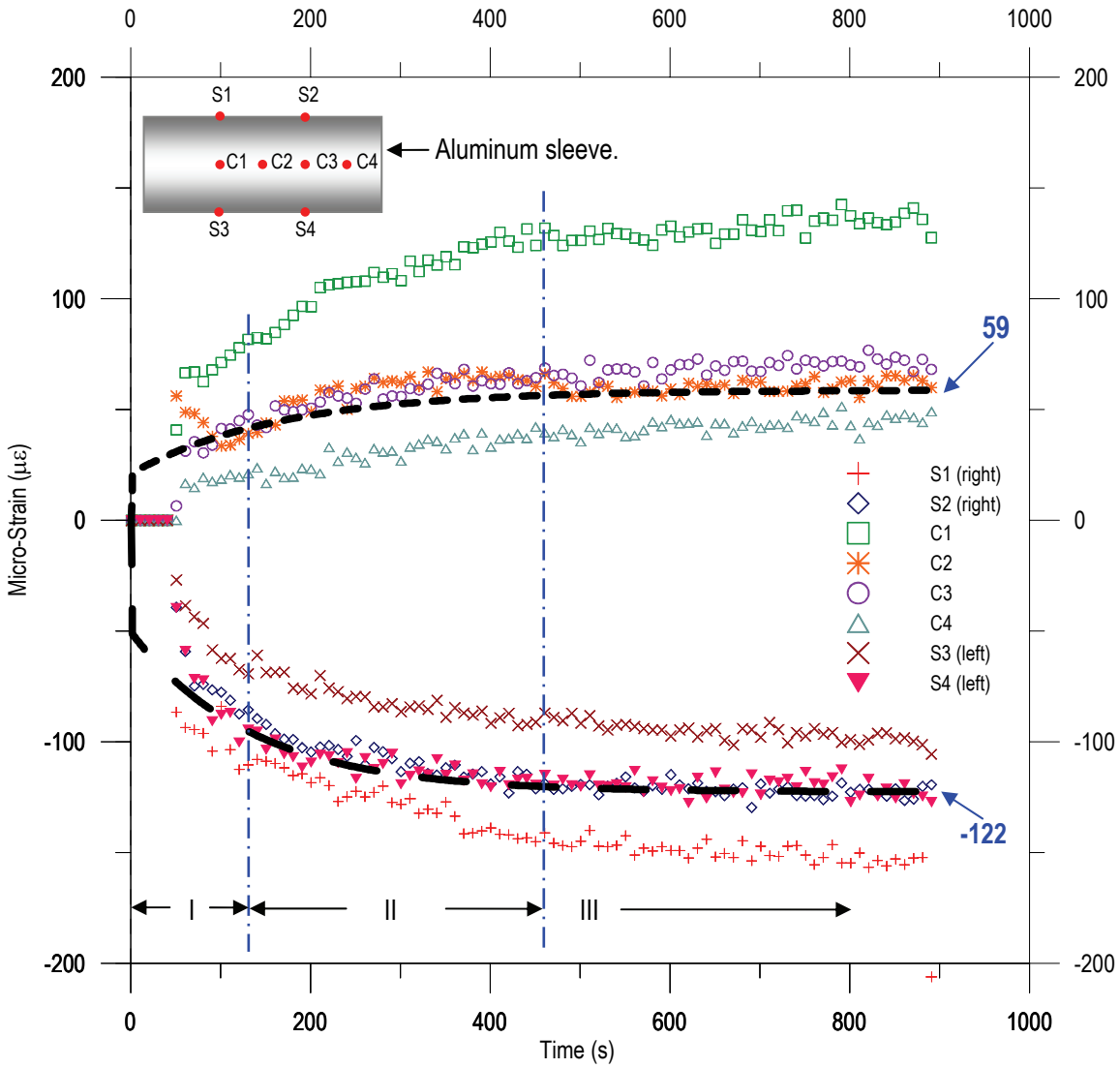


Figure 4.6: Micro-strain data from the control test as developed with time.

The tensile strains at the crown along with the compressive strains at the springlines indicate a deformed lining shape as depicted in Figure 4.5. Readings from gauges C2, C3 and C4 were averaged to yield strains of 59 $\mu\varepsilon$ at the crown. Data from C1 were not included as they did not agree with the other gauges at the crown. Readings from all gauges at the springlines yielded an average strain of 122 $\mu\varepsilon$. This value accounted for the spread of values between S1 and S3, and the regression curve can be seen to approximate well the average strains of these two gauges. Figure 4.7 contains a photograph of the soil in contact with the aluminum lining which was taken near the end of this test. Full contact is visible at

the springline, whereas contact at the crown, while not as extensive near the edge of the lining, is complete further inside, away from the edge.

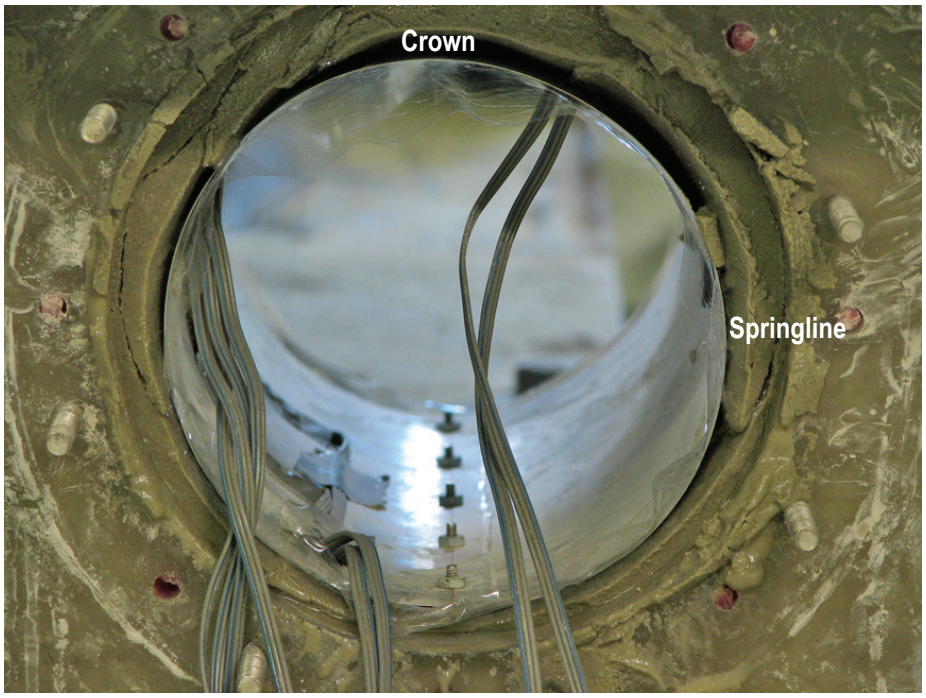


Figure 4.7: Photograph showing the deformed shape of the aluminum lining due to full contact with the surrounding soil.

4.3.3 Case 2: Sand Layer 1 Diameter Above the Tunnel (1D Test)

The 1D test was the first test involving the presence of a layer of coarse sand. It was located at a distance of 150 mm above the crown of the excavation. Figure 4.8 presents the measured data for this test. The strains at the crown and springline were significantly less than those read from the control test, registering at 21 and 11 $\mu\varepsilon$, respectively. Only the values from the left springline were used in this analysis, as those from the right springline indicated tension there, which is not in agreement with the lining reactions depicted in Figures 4.3 to 4.5. These small values were considered to be negligible; however they did represent an appropriate response to the observed slight movements of the soil.

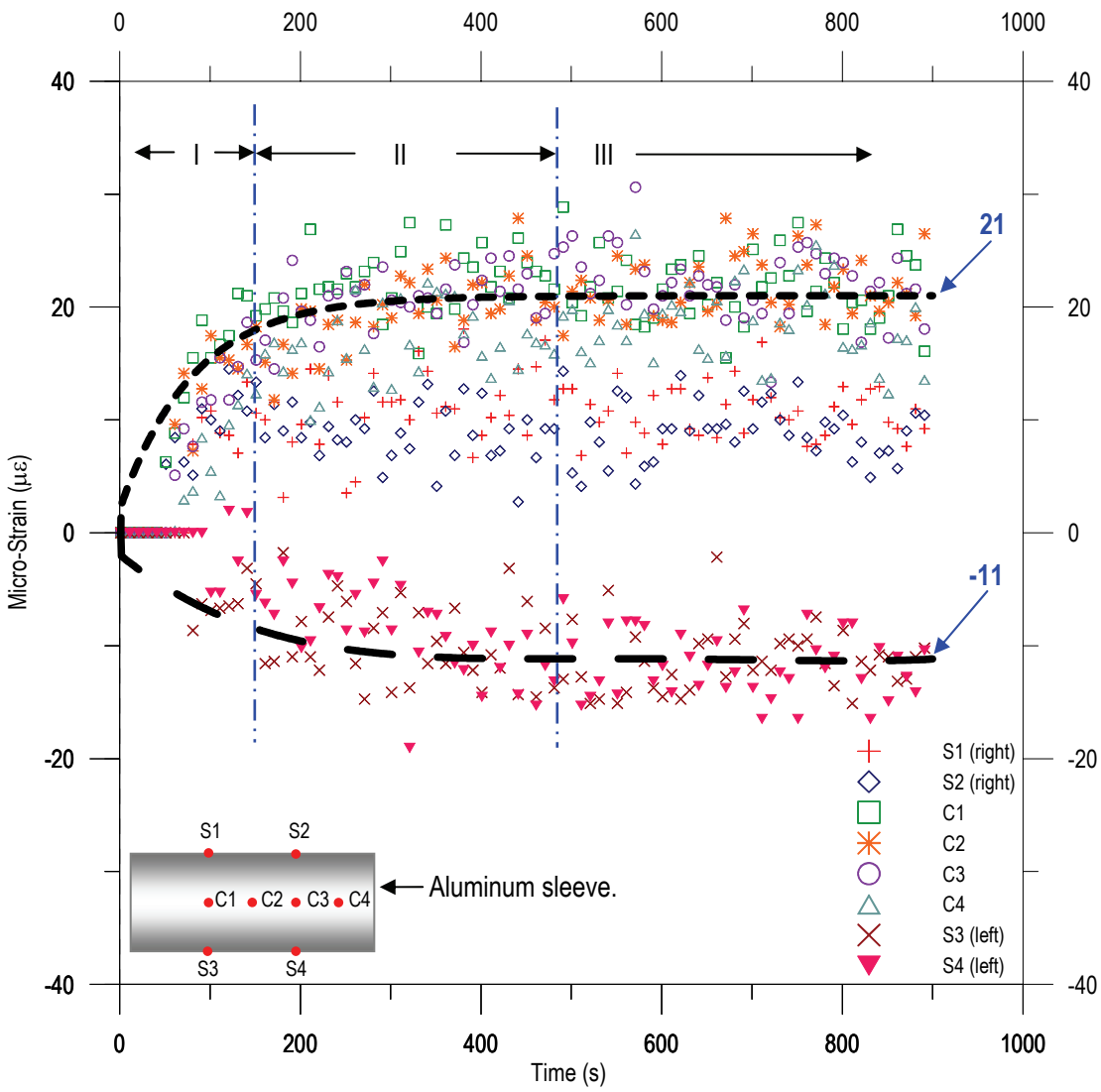


Figure 4.8: Micro-strain data from the 1D test as developed with time.

4.3.4 CASE 3: SAND LAYER 2 DIAMATERS ABOVE THE TUNNEL (2D TEST)

The 2D test involved placing the sand layer at a distance of 300 mm above the crown of the excavation. Figure 4.9 summarises the data from this trial. This case presented behaviour that differed from the previous two tests. First, the strains at the springline were found to be tensile, stabilising around 21 $\mu\varepsilon$. The data from S4 were excluded from this value because of the agreement of the other three readings. Second, this indicated compressive action at the crown. The averaged strains of 29 $\mu\varepsilon$ at the crown confirmed this. The deflected lining pattern was similar to that shown in Figure 4.4. However the magnitudes of these strains were much smaller when compared with those from the control case, yet still, they were larger than the 1D case. Tensile strains from C3 and C4 were excluded from this value because of the tensile action indicated by the readings at the springline. Third, static equilibrium (region III) was established almost immediately after the soil began moving towards the lining (region I).

4.3.5 CASE 4: SAND LAYER 3 DIAMETERS ABOVE THE TUNNEL (3D TEST)

The final test was the 3D test which involved placing the sand layer 450 mm above the crown of the excavation. The average compressive strain at the springline was 194 $\mu\varepsilon$ (Figure 4.10). This excluded the readings from the gauges along the left springline, as they were considered to coincide while the data from the other pair of readings did not. The average tensile strain at the crown was 47 $\mu\varepsilon$. Measurements from C2 were excluded because of the relatively much closer agreement among the remaining three gauges. The data would indicate an ovalisation displacement that matches with the pattern shown in Figure 4.5.

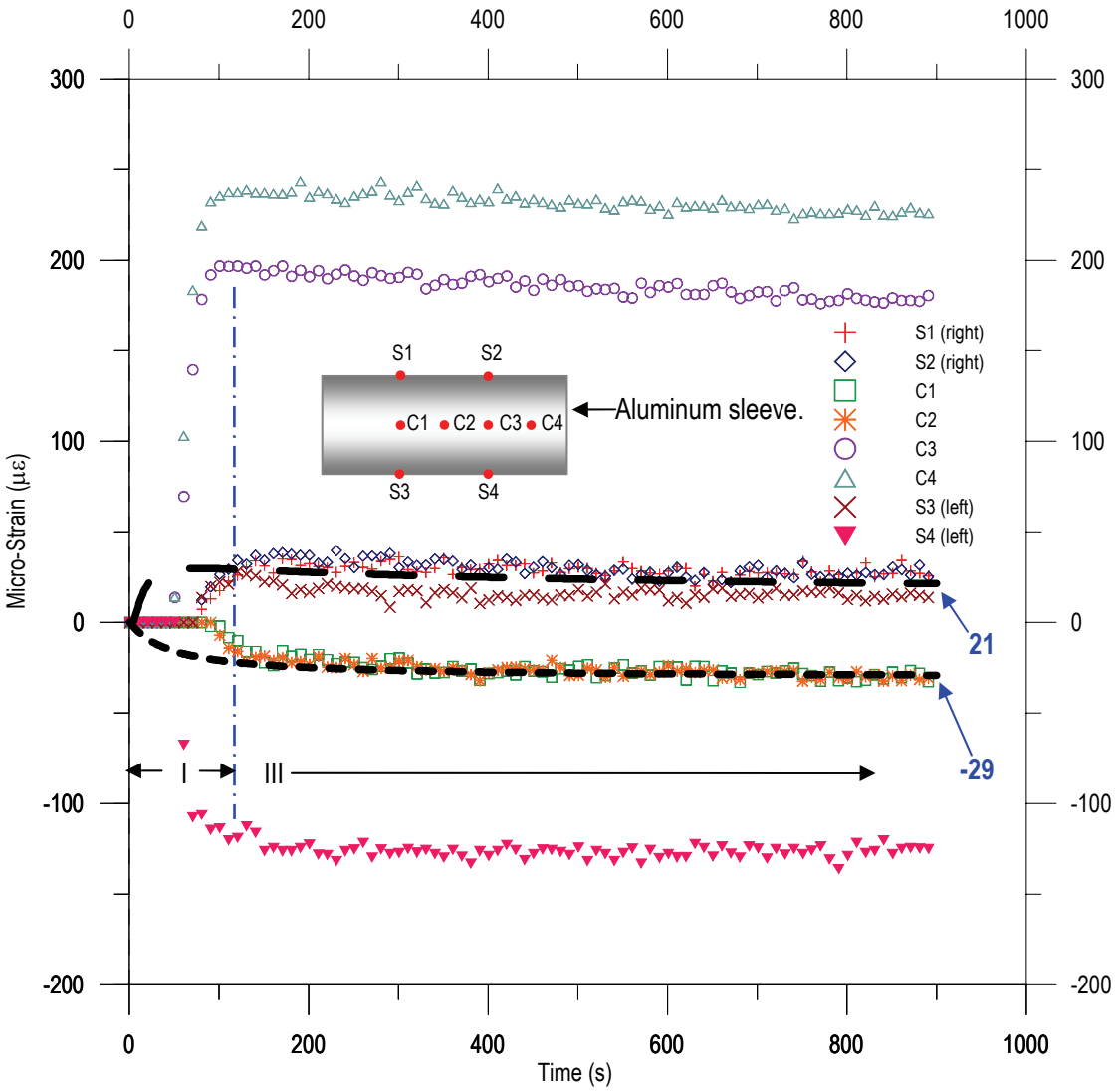


Figure 4.9: Micro-strain data from the 2D test showing a nearly immediate stabilisation of the soil movements.

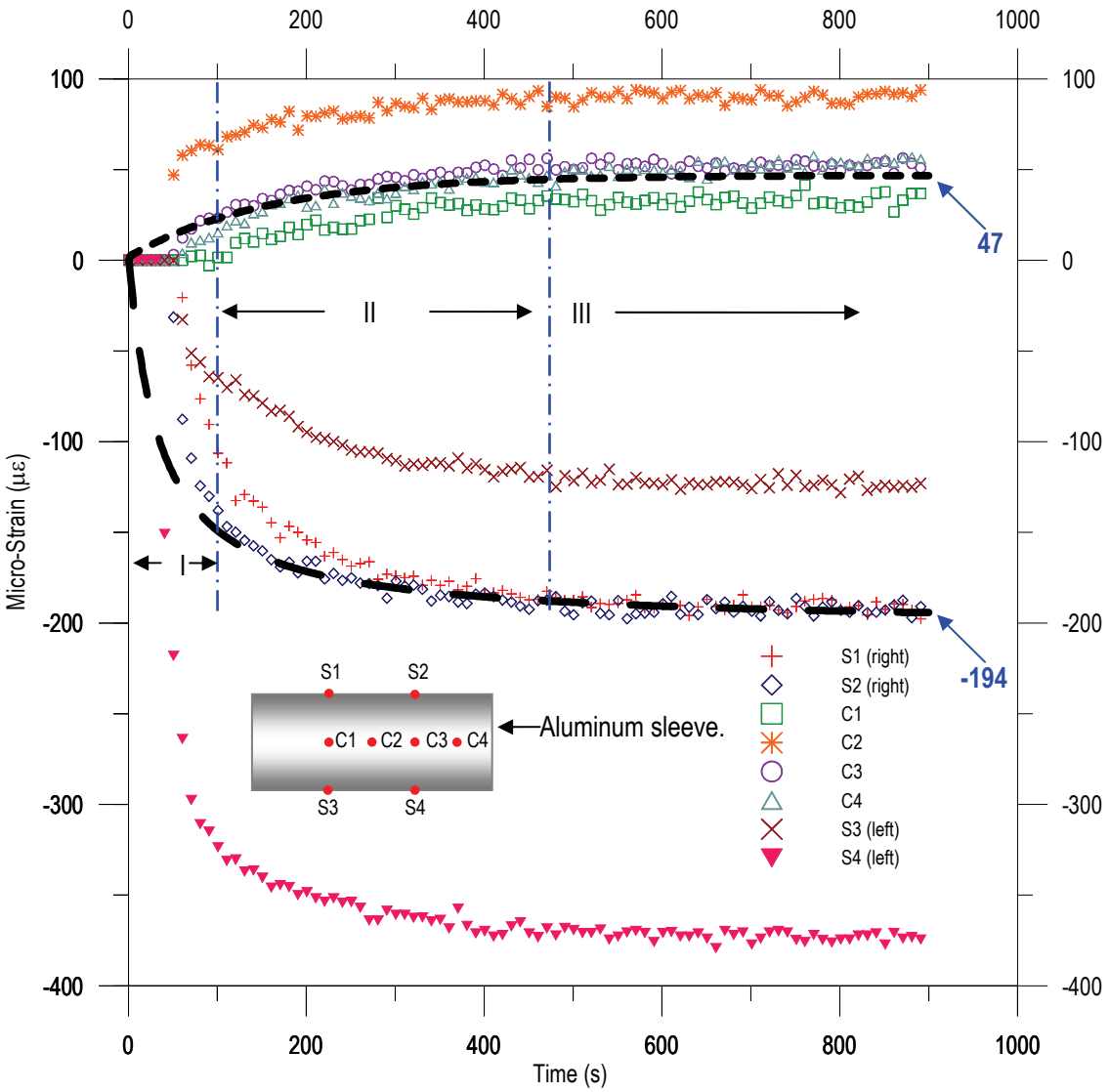


Figure 4.10: Micro-strain data from the 3D test.

4.4 CALCULATED RESULTS

The following sections will detail the processes by which the stresses and bending moments were found based on the data acquired from the four tests as outlined above.

4.4.1 STRESSES

The elastic modulus (E) of the aluminum as determined in Appendix E (64 GPa) was used in the calculation of the stresses (σ) at the crown and at the springline for all four scenarios. In no case did the strains exceed the value which corresponded with the elastic limit (about 350 MPa). Hooke's Law (equation 4.1) was used to calculate the stresses based on the averaged converged strain values.

$$\sigma = E\varepsilon \quad \text{.....(4.1)}$$

Table 4.1 presents a summary of the results. The same sign convention applies; negative values denote compressive stresses, while positive numbers denote tension.

Table 4.1: Summary of the Lining Stresses for All Cases

Case	Crown (MPa)	Springline (MPa)
1D	-1.3	0.7
2D	1.9	-1.3
3D	-3.0	12
Control	-3.8	7.8

4.4.2 BENDING MOMENTS

Flexural theory was used to determine the bending moments (M) based on the stresses calculated in Section 4.4.1. The following relation was used to achieve the results summarised in Table 4.2:

$$M = \frac{I\sigma}{y} \quad \text{.....(4.2)}$$

where I is the moment of inertia about the neutral axis of bending, and y is the distance from the neutral axis to the upper-most fibre of the cross-section exposed to flexure. It was assumed that the stresses were distributed symmetrically and evenly about the neutral axis, which resulted with y equating to a value of half of the cross-sectional thickness of the aluminium sheet. A positive bending moment corresponded to compressive action on the

inner surface of the lining (i.e. where the strain gauges were placed), while a negative bending moment corresponded to tensile action along the outer surface.

Table 4.2: Summary of the Bending Moments for All Cases		
Case	**Crown (N·mm/mm)**	**Springline (N·mm/mm)**
1D	-14	7.3
2D	19	-14
3D	-31	129
Control	-51	81

4.5 ANALYSIS

The experimental results indicated that the presence of a sand layer had a measured influence on the response of a cohesive soil which was exposed to tunnelling. This was best observed in the 1D case. The close proximity of the granular material to the tunnel seemed to confine the underlying soil. This was confirmed by the resulting small strain magnitudes as presented in Figure 4.8; these strains were negligible when compared with those of the control test.

As the granular stratum was moved further away from the excavation, it appeared to have a progressively declining influence on the behaviour of the underlying cohesive material which was exposed to excavation. The progressively increasing magnitudes of the strains for each of the 2D and 3D tests confirmed this trend when compared with the 1D case. However for the 2D test, the compressive strains at the crown and tensile action at the springline indicated the ovalisation pattern shown in Figure 4.4, which was a departure from the radial displacement of the other three cases. Nevertheless, in terms of strains, the magnitudes from the 2D test were still significantly less when compared with the results of the control test and were more comparable with the 1D case, whereas those of the 3D test were very similar with the control case. This indicated that the confinement of the lower cohesive stratum was more pronounced when the sandy layer was within two excavated diameters above the crown, whereas above this elevation, the influence of the granular material seemed to be negligible, and did not act to confine the lower cohesive layer significantly. Indeed, the granular stratum and overlying cohesive soil were seen to act merely as surcharge weight. ■

CHAPTER 5 – NUMERICAL ANALYSIS

5.1 INTRODUCTION

Two-dimensional finite element analyses were conducted to calculate the tunnelling-induced stresses in the lining and to compare the results with those measured in the experimental programme as detailed in Chapter 3. A brief overview of the constitutive model used to simulate the soil behaviour will be presented first. This will be followed by a description of the model properties along with the calibration and all of the parameters and assumptions used throughout the analyses. An investigation into the bending moments, axial forces and soil movements arising from tunnelling in multi-layer ground will be discussed.

5.2 CONSTITUTIVE MODEL

All numerical analyses were done using Plaxis V8 software. A second-order, elasto-plastic model known as *The Hardening Soil* model was utilised for all simulations, and it is based on the hyperbolic relationship between vertical strain, ε_1 and the deviatoric stress, q (Schanz et al., 1999). The advantage of the Hardening Soil model versus the Mohr-Coloumb model is that it allows for a control of the dependency of the stress level. This is more realistic, as the appropriate stiffness modulus depends on the stress level for real soils.

Soil usually exhibits a decreasing stiffness along with corresponding irreversible plastic strains when it is subjected to primary deviatoric loading. This relationship can be approximated by a hyperbola under drained conditions, and it can be described mathematically by (Schanz et al., 1999):

$$\varepsilon_1 = \frac{q_a}{2E_{50}} \cdot \frac{(\sigma_1 - \sigma_3)}{q_a - (\sigma_1 - \sigma_3)} \quad \text{for } q < q_f \text{.....} \textit{(5.1)}$$

where:

$$q_f = \frac{6\sin\phi}{3-\sin\phi}(p + c\cot\phi) \text{ .....} \textit{(5.2)}$$

and:

$$q_a = \frac{q_f}{R_f} \text{ .....} \textit{(5.3).}$$

The asymptotic deviatoric stress (q_a) and the deviatoric stress at failure (q_f) are related by a failure ratio (R_f) as seen in equation 5.3 (Figure 5.1). It is generally acceptable for this value to be 0.9. Equation 5.2 was derived from the Mohr-Coulomb failure criterion, involving the cohesion (c) and the angle of friction (ϕ). Perfectly plastic yielding occurs at the instance $q = q_f$, and the criterion is satisfied. E_{50} is the confining stress-dependent secant stiffness modulus for primary loading. It is used instead of the initial elastic modulus for small strains (E_i in Figure 5.1) because it is easier to determine experimentally, and can be found by:

$$E_{50} = E_{50}^{ref}\left(\frac{\sigma_3 + c\cot\phi}{\sigma^{ref} + c\cot\phi}\right)^m \quad \text{..... (5.4).}$$

E_{50} determines the magnitude of both the elastic and the plastic strains. E_{50}^{ref} is a reference secant stiffness modulus in drained conditions corresponding to the reference minor principal stress, σ^{ref}, which is usually 100 kPa. The degree of stress-dependency is given by the power, m. It can be measured both in oedometer tests and in triaxial tests and ranges between 0.4 and 1.0. A value of 0.5 is typical for sands; it is generally accepted to be unity for soft clays.

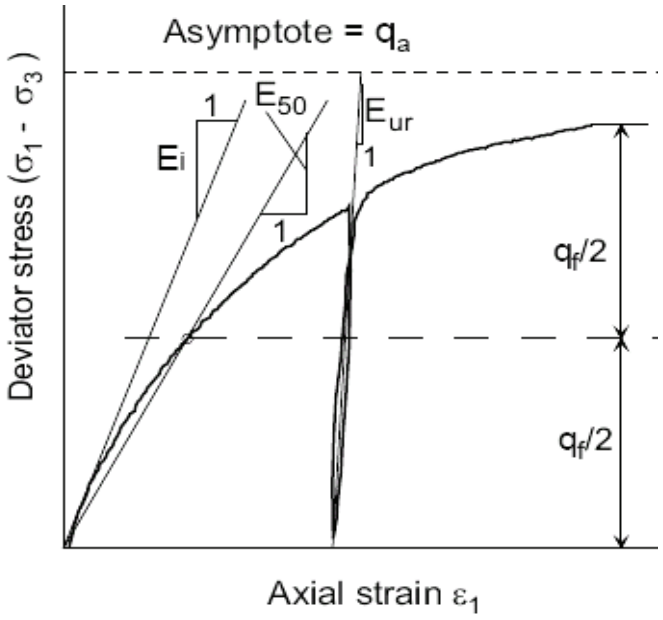


Figure 5.1: Hyperbolic stress-strain relation in primary loading for a standard drained triaxial test (Adapted from Plaxis User's Manual, 2004).

In the case of unloading and reloading (denoted by the subscript -*ur*), another stress-dependent stiffness modulus (E_{ur}) is used:

$$E_{ur} = E_{ur}^{ref}\left(\frac{\sigma_3 + \cot\phi}{\sigma^{ref} + c\cot\phi}\right)^m \quad \text{..... (5.5).}$$

E_{ur}^{ref} is the reference Young's modulus for unloading and re-loading that corresponds to σ^{ref}. The Hardening Soil model does not provide a fixed relationship between the drained triaxial stiffness (E_{50}) and the oedometric stiffness (E_{oed}). Therefore E_{oed} must be determined independently, and can be found according to:

$$E_{oed} = E_{oed}^{ref}\left(\frac{\sigma_3 + \cot\phi}{\sigma^{ref} + c\cot\phi}\right)^m \quad \text{..... (5.6)}$$

where E_{oed}^{ref} is the tangent stiffness for primary oedometer loading.

Together with the parameters m, c, ϕ, ν_{ur} and the dilatancy angle, ψ, there are a total of eight material parameters. Often, no triaxial test results are available for determining ν_{ur}, E_{50}^{ref} and E_{ur}^{ref}, in which case one has to rely on oedometer results and general empirical data, such as ν_{ur} = 0.1 – 0.2. For sands and stiff clays, one can mostly use $E_{50}^{ref} = E_{ur}^{ref}$. The elasticity modulus E_{ur}^{ref} can be determined directly from a triaxial test or indirectly with the help of oedometer results. If the unloading modulus from the oedometer test is termed E_{oed}^{ur}, according to isotropic linear elasticity the following relationship holds (Vermeer et al., 2002)

$$E_{ur} = (1-2\nu_{ur})\frac{1+\nu_{ur}}{1-\nu_{ur}} \cdot E_{oed}^{ur} \quad \text{..... (5.7)}$$

Hence the proper estimates of E_{ur} can be calculated from E_{oed}^{ur}. The stiffness properties of the saturated clay in this study are assumed based on the range of values proposed by Kempfert and Gebreselassie (2006) for $\frac{\sigma_3}{p^{ref}}$ of about 0.10 as shown in Figure 5.2. This value simulates the low overburden pressure expected in the small scale tests conducted in this study.

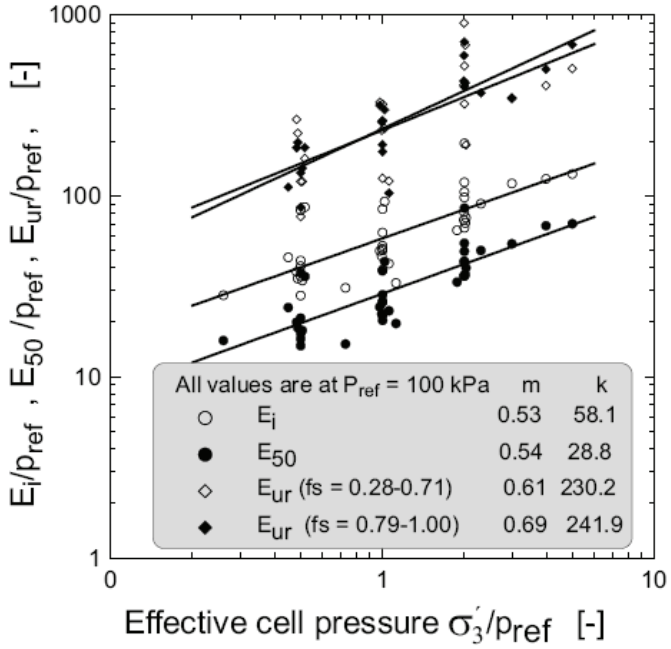


Figure 5.2: The variation of the modulus of elasticity with confining pressure under CID test condition (Kempfert and Gebreselassie, 2006).

5.3 NUMERICAL MODEL

A plane-strain finite element model was used to represent the soil and the tunnel lining. The problem was considered to be symmetrical and was therefore constructed with bisection along the axis of symmetry. Figure 5.3 provides an illustration.

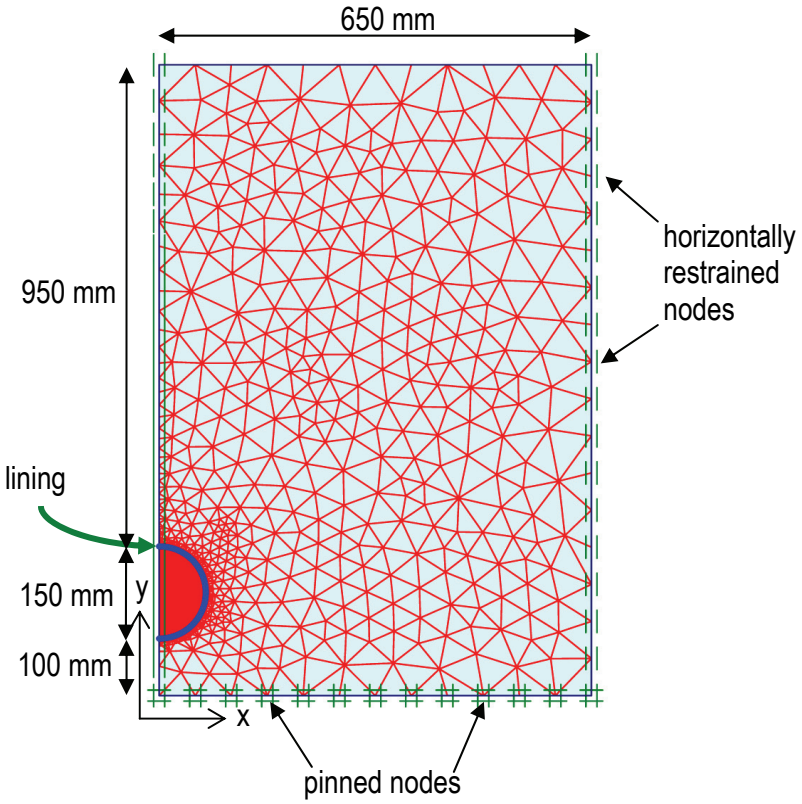


Figure 5.3: Finite element mesh depicting the position of the tunnel and the boundary conditions.

The nodes along the lower boundary were considered to be pinned, or fixed, prohibiting movement in both the *x*- and *y*-axes (rough-rigid conditions) to simulate underlying bedrock. The model was restrained in the horizontal direction for boundaries parallel with the symmetry axis (smooth-rigid conditions). The free surface was unrestricted. The lining was modelled using six-noded beam elements, whereas the soil was modelled using 15-noded triangular elements, for a total of 2,956 elements. The chosen geometry was based on the physical model; the invert of the 150 mm ϕ tunnel was located at 100 mm above the lower boundary. The crown was located at 950 mm from the free surface. The model was 650 mm wide. The specified maximum annular contraction due to tunnelling activity was 30%; this was based on the 25-mm difference in diameter between the excavated hole and the aluminum sleeve in the physical model.

5.4 PROPERTIES & ASSUMPTIONS

The material properties of the study will now be discussed, beginning with the modelled cohesive soil. A drained analysis was specified. All properties were based on the findings of Kempfert and Gebreselassie (2006) for the elastic parameters, and based on known accepted ranges for all other values. A sensitivity analysis was done to investigate the effect of varying the properties within these ranges, and it was found that the degree of deviance was negligible. Therefore the average, typical values based on this analysis are summarised below:

- $\gamma_{unsaturated}$ = 16 kN/m^3
- $\gamma_{saturated}$ = 18 kN/m^3
- c_{ref} = 0.05 kPa
- ϕ = 20°
- K_o = 0.658
- ν_{ur} = 0.20
- E_{50}^{ref} = 800 kPa
- E_{oed}^{ref} = 800 kPa
- E_{ur}^{ref} = 2400 kPa.

The sandy layer was modelled using the same properties, with the exceptions of c_{ref} (0 kPa) and ϕ (25°), which was the result of a similar sensitivity analysis as mentioned above. The lining was modelled by using accepted elastic properties as found in the literature, along with the geometric characteristics of the physical lining. The properties are summarised below:

- t (cross-sectional thickness) = 2.5 × 10^{-4} mm,
- EA = 1.60 × 10^4 kN/m,
- EI = 8.33 × 10^{-5} kN·m^2/m, and
- ν = 0.30.

The interaction between the lining and the soil was modelled using interface elements. No-slip conditions were specified at the interfaces between the cohesive and granular media. A strength factor R_{int} was introduced to define the strength parameters of the interface relative to those of the original material. Throughout this investigation, a value of 0.67 was assigned to the strength factor R_{int}, except for the interfaces separating the cohesive soil from the granular material; R_{int} was unity in this instance.

5.5 RESULTS

The model was calibrated using analytical solutions and the experimental results first before any thorough investigation could be done. It was decided to use the bending moments from the control test for this purpose, as they facilitated a simple comparison between the theoretical predictions based on Bobet's (2001) solution, the calculated values from the physical testing and those from the numerical modelling. The mesh in Figure 5.3 represents the control case. The FE analysis yielded a bending moment of 92 N·mm/mm at the springline and 73 N·mm/mm at the crown. These compared well with the values of 81 N·mm/mm and 51 N·mm/mm, respectively, that were calculated from the experiment. They were also in agreement with Bobet's (2001) predicted values of 89 N·mm/mm and 85 N·mm/mm at the springline and crown, repsectively. Figure 5.4 shows a bending moment distribution superimposed onto a naked representation of the tunnel lining. This allowed the maximum moment calculated by the numerical analysis of 104 N·mm/mm to be located by visual inspection.

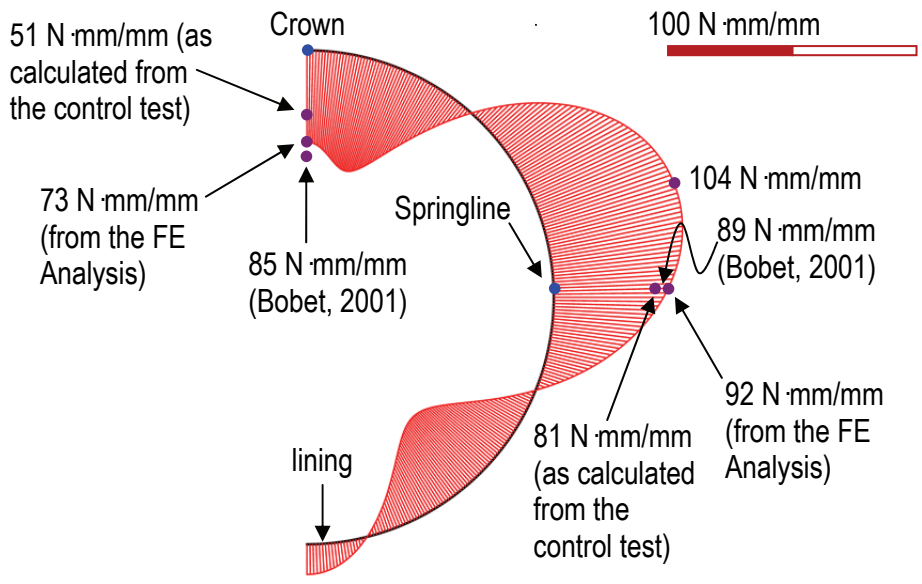


Figure 5.4: Visual comparison of the FE maximum bending moments versus those from the control 1g test and Bobet's solution (2001).

It was believed that the parameters as outlined in Section 5.4 represented the physical model sufficiently based on this result. The investigation was then expanded to the cases where a layer of coarse-grained material was present at varying elevations above the crown of the

tunnel. Figure 5.5 depicts the mesh from the 2D case. The 1D and 3D cases can be considered similar.

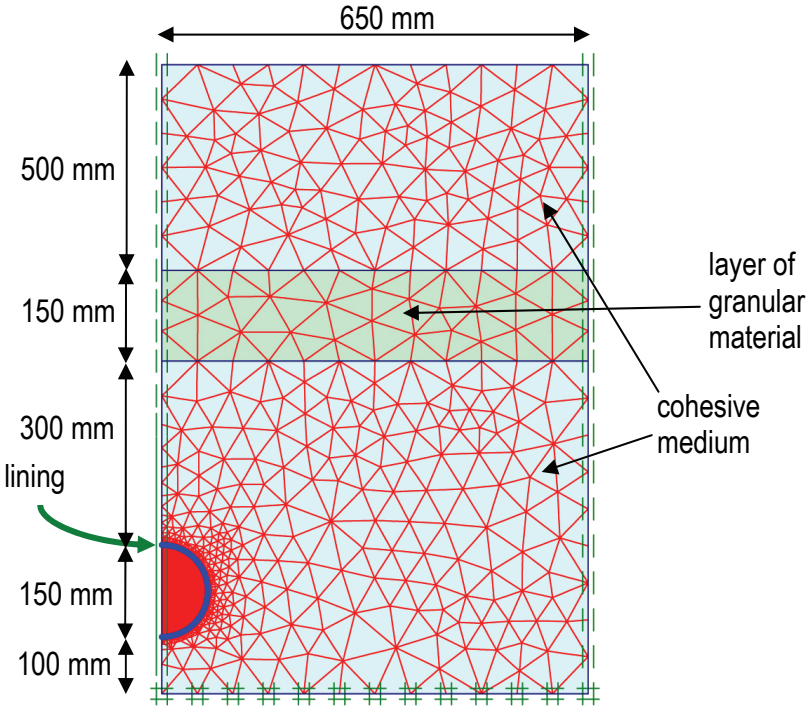


Figure 5.5: Finite element mesh illustrating the position of the sand layer for the 2D case.

Visual comparisons of the maximum bending moments with calculated experimental values can be seen in Figures 5.6 to 5.8 for the 1D, 2D and 3D cases, respectively.

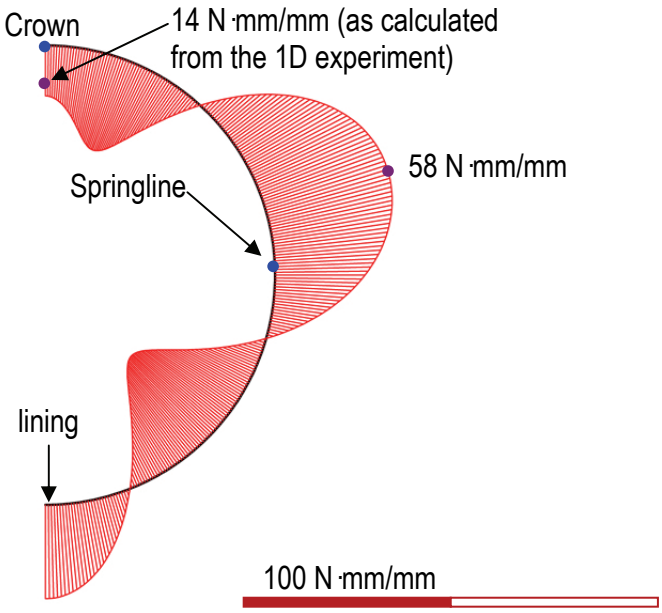


Figure 5.6: Visual comparison of the FE maximum bending moment versus that from the 1D test. The maximum bending moment from the physical test was located at the crown.

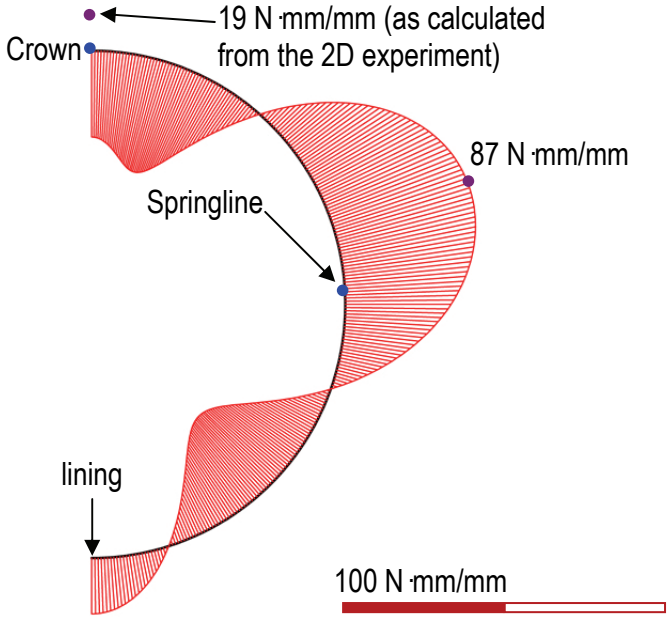


Figure 5.7: Visual comparison of the FE maximum bending moment versus that from the 2D test. The maximum bending moment from the physical test was located at the crown and was compressive.

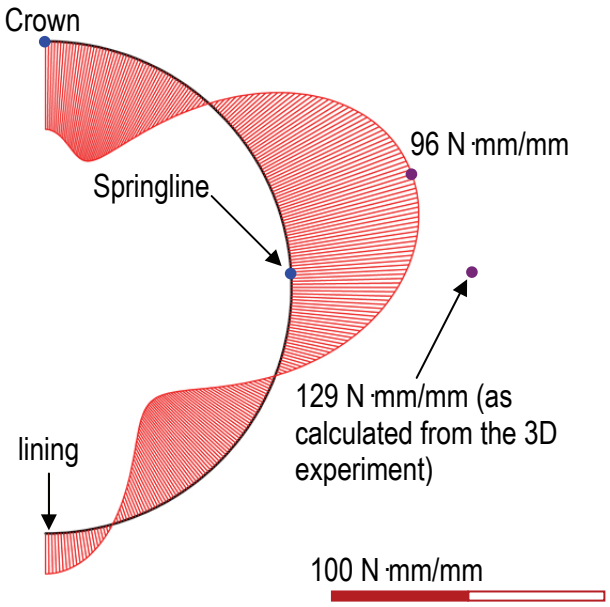


Figure 5.8: Visual comparison of the FE maximum bending moment versus that from the 3D test. The maximum bending moment from the physical test was located at the springline.

Other results provided by the FE model were axial forces and total displacements. Figure 5.9 shows a typical axial force distribution along the lining for all cases, including the model with homogenous ground. The shapes of the distributions did not differ appreciably from the one shown in Figure 5.9. Table 5.1 summarises the maximum axial forces for all cases.

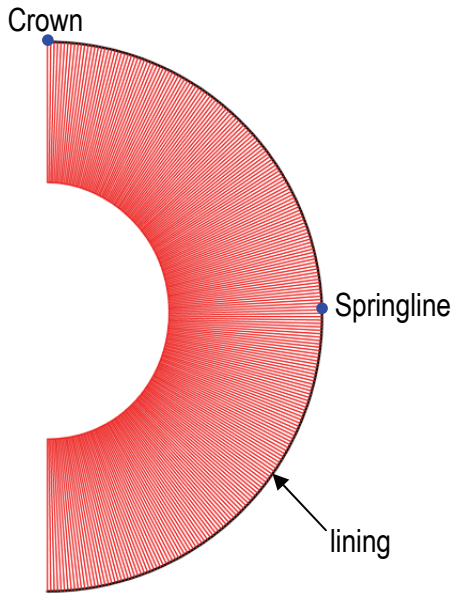


Figure 5.9: Typical distribution of the axial forces arising in the lining for all tests. All forces are compressive.

Table 5.1: Summary of FE Axial Forces	
Case	**Maximum Axial Force (N/mm)**
1D	877
2D	886
3D	891
Control	894

Finally, displacement patterns arising in the regions near the tunnel were investigated. Figures 5.10 to 5.13 show the vector diagrams of the soil movements around the excavation for each case, starting with the 1D case to the control test.

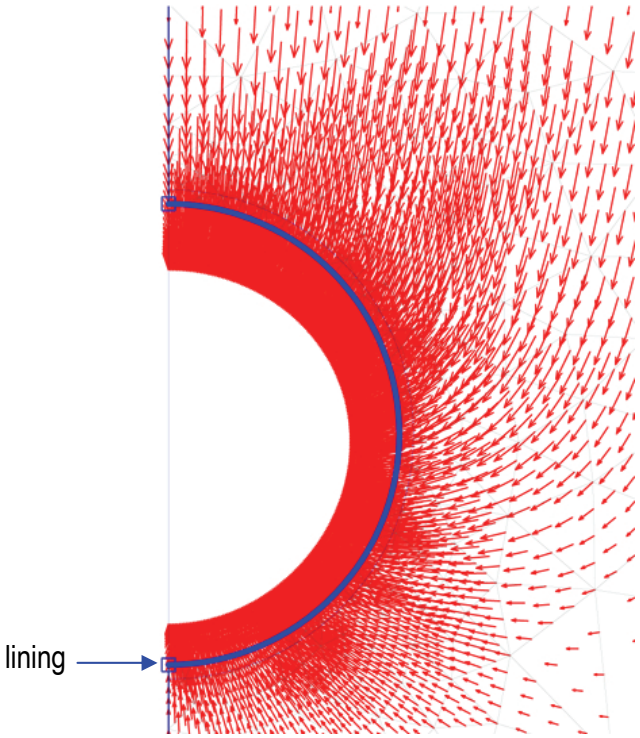


Figure 5.10: Vector diagram showing direction and magnitude of soil displacements (1D case).

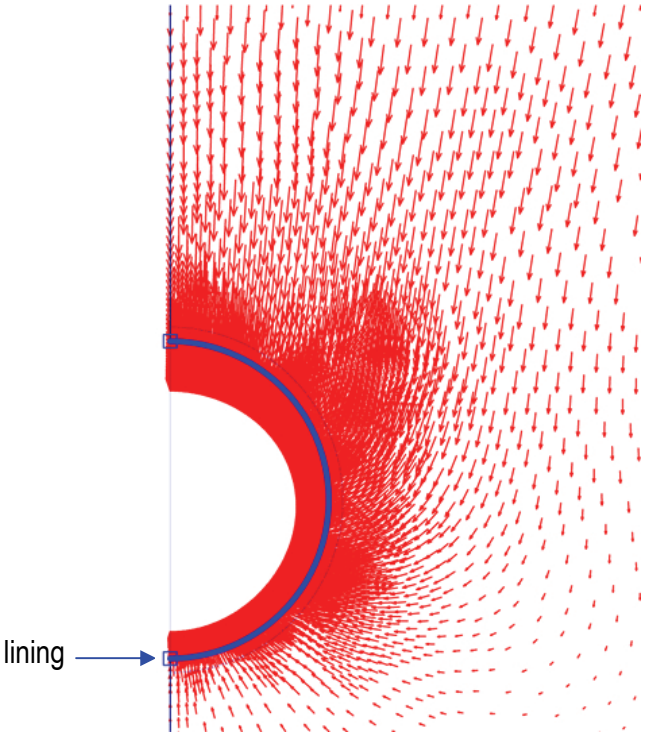


Figure 5.11: Vector diagram showing direction and magnitude of soil displacements (2D case).

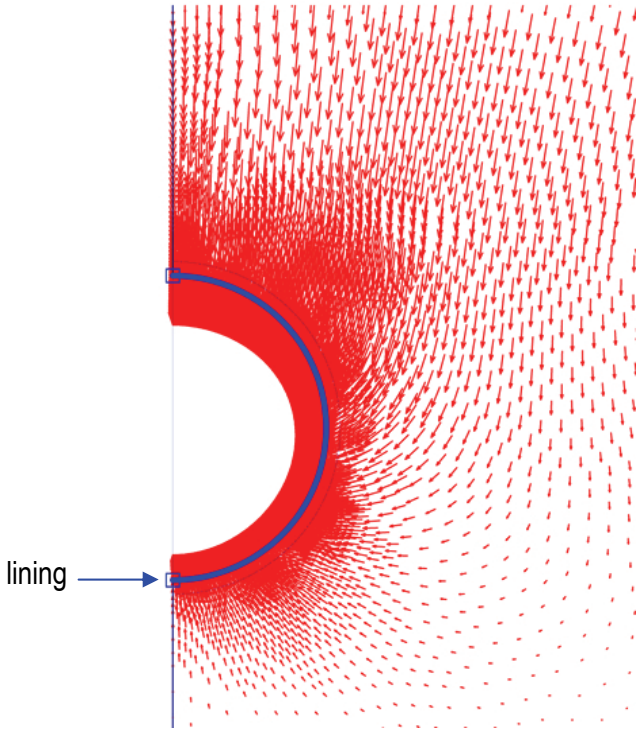


Figure 5.12: Vector diagram showing direction and magnitude of soil displacements (3D case).

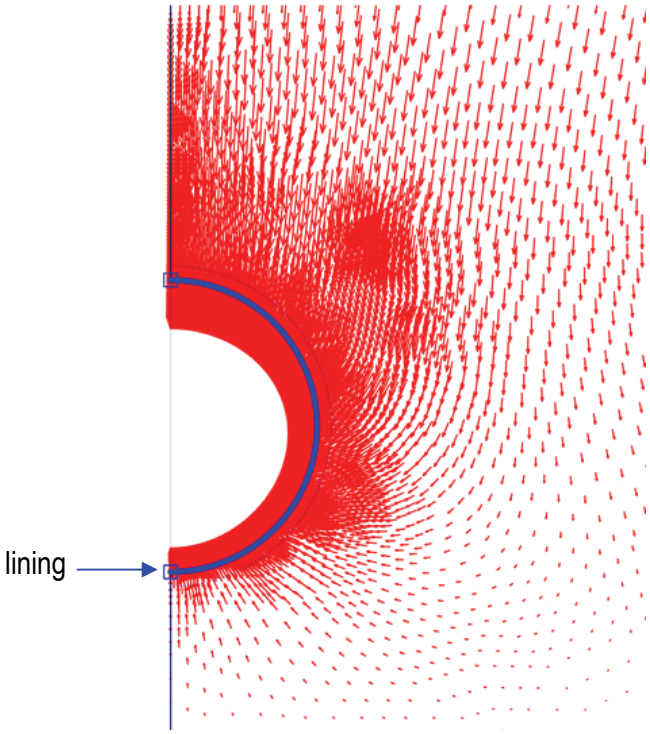


Figure 5.13: Vector diagram showing direction and magnitude of soil displacements (control case).

It can be seen in the preceding figures that horizontal movements became less pronounced as the location of the sand layer was located further away from the tunnel. Accordingly, vertical movements were seen to become more dominant. However vertical displacements dominated in general. The maximum displacements as calculated from the FE model were taken from each case. Table 5.2 is a summary of these results. Displacements appeared to increase as the sand layer was located further away from the opening, with a negligible difference between the 3D and control cases. There was a visual confirmation of this in Figures 5.12 and 5.13, as the displacement patterns were nearly identical.

Table 5.2: Summary of FE Maximum FE Displacements

Case	Maximum Displacement (mm)
1D	14.6
2D	15.9
3D	16.4
Control	16.9

5.6 ANALYSIS

This section will examine the findings presented in this chapter. First there will be an analysis of the results of the FE model. This will be followed by a contrast with the results measured in the experimental programme.

5.6.1 DISCUSSION

The presence of a layer of granular material influenced the response of the lining in the FE model once the excavation was created. The maximum bending moments increased as the granular stratum was located further from the crown of the tunnel. A similar trend was seen with the maximum axial forces and displacements. Moreover, it was noticed that there was significantly high similarity in the results of the 3D and control cases when examining the bending moments, axial forces and displacements; this was also observed in the experimental results. Furthermore, the presence of a sandy layer located within two excavated diameters above the crown had a significantly greater influence on the lining response than if it were located at a higher elevation, which was also seen in the experimental results.

The vector diagrams shown in Figures 5.10 to 5.13 also presented a considerable trend. It was noticed that as the sandy layer was moved away from the tunnel, the horizontal

components of the displacements decreased with a rise in the vertical movements. This was noticed especially in the region near the springline. The layer of granular material had the effect of reinforcing the soil against vertical movements, with decreasing influence as the layer was placed further away. The vector diagram for the 1D case (Figure 5.10) illustrates larger horizontal movements than those depicted in the control case (Figure 5.13). As it was seen from both the experimental and the FE results, the differences between the 3D and the control cases were negligible, manifested in nearly identical displacement profiles.

5.6.2 DISCREPANCIES

It was not expected that the FE results would agree perfectly with those from the experimental programme. All differences will now be detailed and explained.

1. A maximum annular contraction of 30% was assigned to the FE model. The software simulated movement so that the actual calculated contraction matched this value as closely as possible. In all cases the realised soil contraction was 27.7%.
2. Implicit in the FE model was the assumption of complete and full contact between the soil and the lining at all times, commencing immediately after the opening was created. For some cases, this was in contrast with what was observed in the laboratory. The soil was allowed to move into contact with the lining, with enough time given for a static equilibrium to develop. Transient considerations were not included in the FE model. It is for this reason that the anomalous behaviour observed in the physical 2D case was not repeated in the corresponding numerical case.
3. The FE model incorporated instantaneous excavation work. The experimental tunnelling work was done in minutes. This particular incremental response was not duplicated in the FE model.
4. The soil media in the numerical analysis were assumed to be perfectly homogeneous and uniform. Careful effort was made in the laboratory to ensure as much homogeneity as possible, since the cohesive mix was poured in batches. This included minimising air voids as well. Vibration and standardised mixing procedures were employed to mitigate any irregularities of the material once it was placed inside of the strongbox. However it was impossible to ensure that the cohesive material and sandy layer were perfectly similar from test to test.

5. The flexible lining (EI = 8.33 × 10^{-5} kN·m^2/m) allowed for localised movements that were not replicated in the FE analysis. It was noticed that slight irregularities in the soil produced corresponding irregular, unpredictable deflections at some locations of the lining. For example, this explained how one pair of springline gauges registered compressive strains, while the opposing pair would register tensile strains. The modelled lining was assumed not only to be in perfect contact with the soil, but that all deflections were the results of a perfectly homogeneous medium.
6. Perfect contact at the interfaces between the cohesive soil and granular material was assumed in the FE analysis. A fully saturated geotextile layer was placed between each layer to eliminate mixing at the interface. While it is expected that this had a minimal effect on the physical results, it should be noted that no such delineating boundary was modelled in the FE analysis, and hence was not considered.
7. Shear stresses and slip conditions at the interfaces between the cohesive medium and sand that would exist in the physical model were not considered in the FE model. It was assumed that all movements at the interface were achieved as if both materials moved as one mass as a whole.
8. Friction was minimised as much as possible at the boundaries in the physical model with the application of silicone grease on all of the surfaces that were involved in containing soil in the physical model. However friction was never eliminated completely. Smooth-rigid conditions were specified at the vertical boundaries of the FE model, which is based on the assumption of friction-free vertical movement. Rough-rigid conditions were specified at the base, prohibiting any movement in any direction there. While any movement along the base of the physical model would be considered negligible for this study, it should be noted that the soil was not restricted from movement in the manner in which it was assumed in the FE model.
9. Finally it should be noted that the strength of the soil remained constant with time, whereas the presence of cement in the physical model contributed to evolving strength with time.

Despite these discrepancies, there was still a significant agreement between the physical testing and the analogous numerical analyses, as the trends gleaned from the two sets of tests have shown. ■

CHAPTER 6 – CONCLUSIONS & RECOMMENDATIONS

6.1 CONCLUDING REMARKS

The stresses developing in a flexible tunnel lining supporting a small-diameter tunnel was investigated in cohesive multi-layer ground under 1g conditions. An innovative mix involving bentonite clay, fine sand, and cement was designed to eliminate the need for consolidating large-scale cohesive samples, thereby reducing the requirement of large overburden pressures and the time normally associated with this process. This cohesive mix strengthened adequately within hours of preparation and allowed for several tests to be done in relatively quick succession, which is normally a disadvantage of 1g testing. A strongbox was specially constructed for this purpose. A control test with uniform ground conditions was done first. A layer of coarse-grained sand with an equivalent thickness of one excavated diameter was then introduced at distances equivalent to one, two and three excavated diameters above the crown of the tunnel for the subsequent tests. Excavation was achieved by incrementally pulling a rigid casing through the model by the force of a hydraulic jack. A flexible aluminum sleeve instrumented with strain gauges at the crown and springlines served to act as a tunnel lining.

A 2D finite element analysis was conducted and was based on the physical prototype. The Hardening Soil model was used to model the soil behaviour, which was considered to be more realistic, as the response of a soil was dependent on the level of stress it experienced. A control test with uniform ground conditions was first analysed. The numerical model was calibrated by comparing the results of the control test with those from the analogous physical experiment, as well as the analytical solution given by Bobet (2001). A layer of granular material with a depth of one equivalent excavated diameter was simulated at distances of one, two and three equivalent excavated diameters above the crown of the tunnel.

The following conclusions were made from the physical experimental programme:

1. The presence of a layer of sand affects the two-dimensional deformations of an underlying cohesive medium when a tunnel is excavated out of it. The granular material effectively served to confine this layer of soil, which limited soil movements. The upper stratum of cohesive soil was seen to act merely as a surcharge, simply

providing the weight necessary to mobilise soil movements without having any significant impact on displacement patterns. The inherent stiffness of the sand combined with increased densification arising from the overburden pressures of the overlying soil contributed to this confinement phenomenon.

2. The proximity of the sandy layer to the tunnel had an effect on the movements of the soil surrounding to the cavity. It was noticed that sand located at a distance of 3D above the crown showed no discernable difference than if there were no granular layer at all. The results from the 2D case showed that the sand stratum affected movements significantly when compared with the 3D and control tests. The observations from the 1D test contrasted well with those from the 3D and control tests in that there was lesser contact with the outer skin of the lining.
3. The patterns of strains – and hence stresses and bending moments – showed a corresponding pattern with that observed from the soil displacements around the lining. The magnitudes of the strains increased as the layer of sand was positioned further away from the crown of the excavation, with negligible differences between the 3D and control cases. The major axis of ovalisation was perpendicular with the axis of symmetry for the 1D, 3D and control tests. The major axis of ovalisation coincided with the axis of symmetry for the 2D test. However the magnitudes from this case was comparable with, if not slightly greater than the 1D test, yet significantly less than the 3D and control tests. A graphical summary of the strains at the crown and springline from the physical testing can be seen in Figures 6.1 and 6.2, respectively.

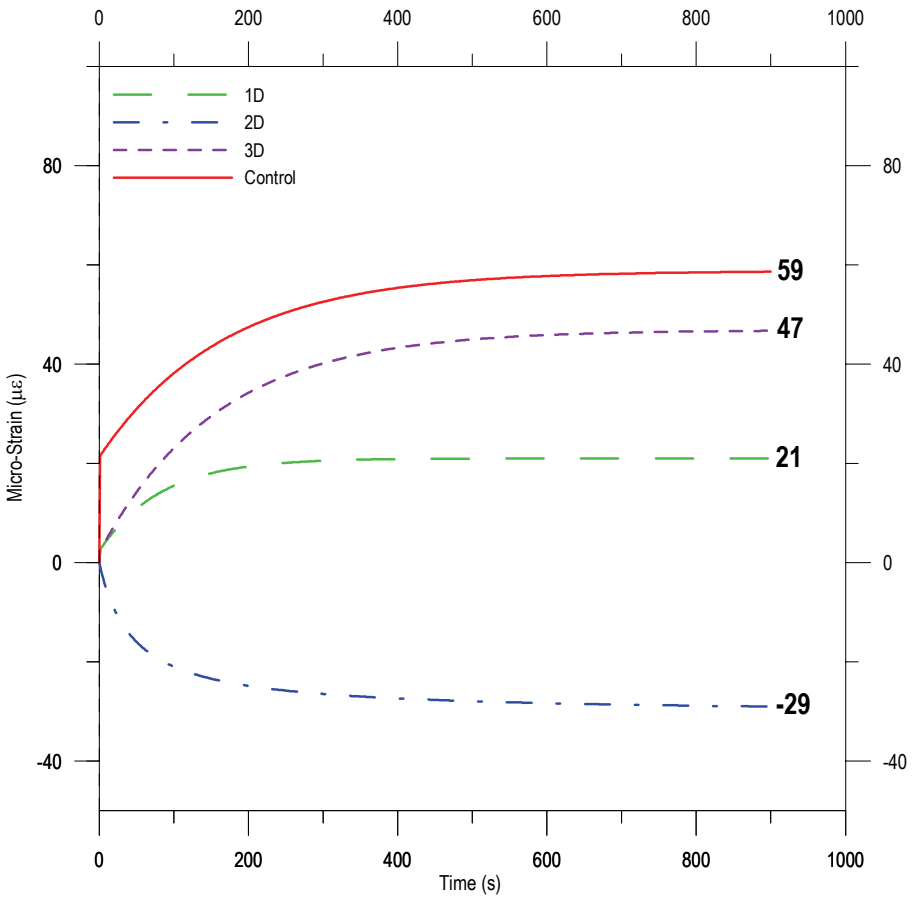


Figure 6.1: Summary of the micro-strain data at the crown for all tests.

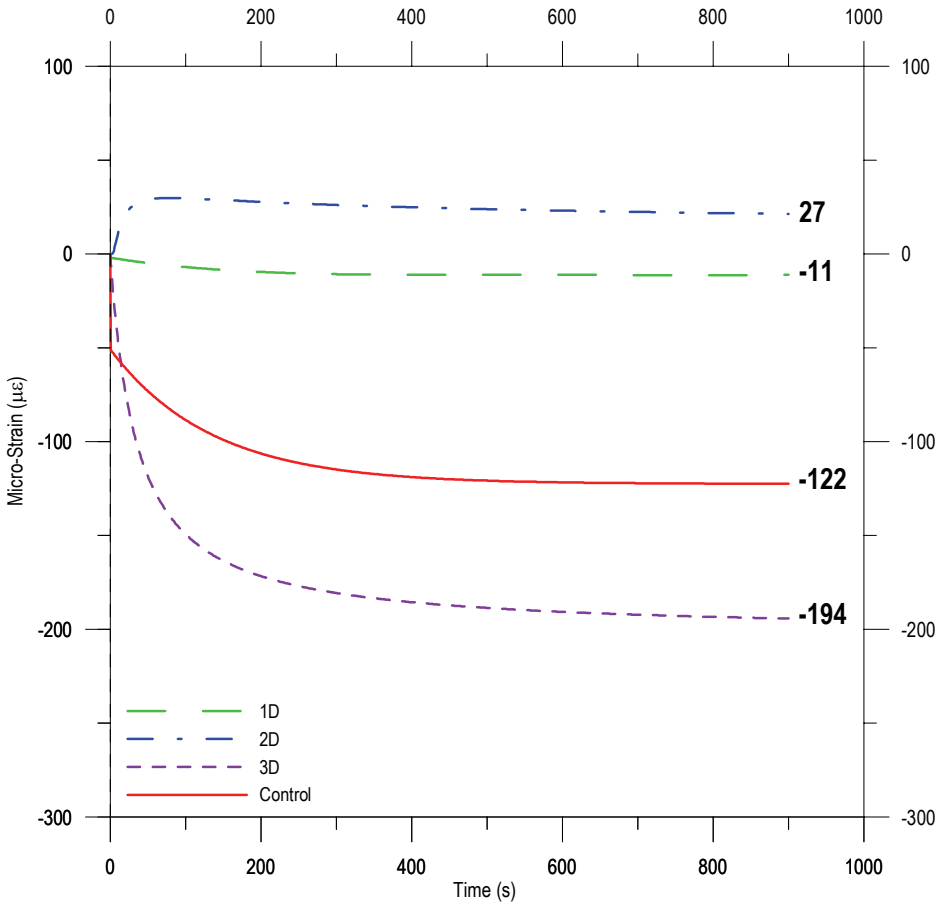


Figure 6.2: Summary of the micro-strain data at the springline for all tests.

The following conclusions were made from the numerical analyses:

1. The magnitudes of the horizontal component of the soil displacement vectors decreased as the distance between the crown of the tunnel and the layer of granular material increased. This indicated that the sandy layer indeed served to confine the underlying soil against displacements. Furthermore, the upper stratum of cohesive soil had no appreciable effect, and merely acted as a surcharge.
2. The maximum displacements increased as the distance between the sand layer and the crown increased. The most significant increase was observed over the interval between the 1D and 2D cases, with an 8% increase in maximum soil displacements. There were negligible differences in maximum displacements over the successive intervals, as the calculated displacements increased by 3% between the 2D, 3D and control cases (Figure 6.3). This was a consequence of lessened confinement as the granular layer was situated further away.

3. The maximum axial forces and bending moments followed the same trend as that of the maximum displacements (Figure 6.4). The maximum bending moments and axial forces increased as the distance between the sand layer and the crown increased. Once again, the values for the 3D and control cases were comparable. This validated the results from the physical testing, where appreciable effects on plane-strain behaviour were seen for the 1D and 2D cases. Furthermore, the greatest increase in bending moments and forces occurred between the 1D and 2D cases, as it was noticed with the pattern of maximum displacements. When the sandy layer was located at distances greater than 2D above the crown, the behaviour was similar with that of the control case. This confirmed the results as reported by Grant and Taylor (2000).
4. The numerical analysis also confirmed the pattern observed from the experimental programme; if the anomalous results from the 2D case were to be discounted, the patterns of increasing magnitudes of displacements, moments and forces with decreasing proximity of the sandy stratum still would be valid.

Figure 6.3 shows the general trend of increasing maximum displacement with increasing distance of the sandy stratum from the crown. Figure 6.4 shows the similar patterns for both the maximum axial forces and the maximum bending moments as calculated by the FE model. It should be noted that the symbol representing infinity (∞) was chosen for the values corresponding to the control test. The reason for this was that the control test could be considered to simulate the case where either there was no sandy layer at all or simply that such a layer existed at a distance very far away from the crown of the excavation. The values along the ordinate axis for the maximum displacements (u) were normalised by relating them to the radius (r) of the excavation. Similar normalisations were used for the maximum bending moments (M) and axial forces (N); γ symbolises the unit weight of the soil; h is the depth of soil cover as measured from the free surface to the elevation of the springline. Attention is directed to the appropriate figures for further details.

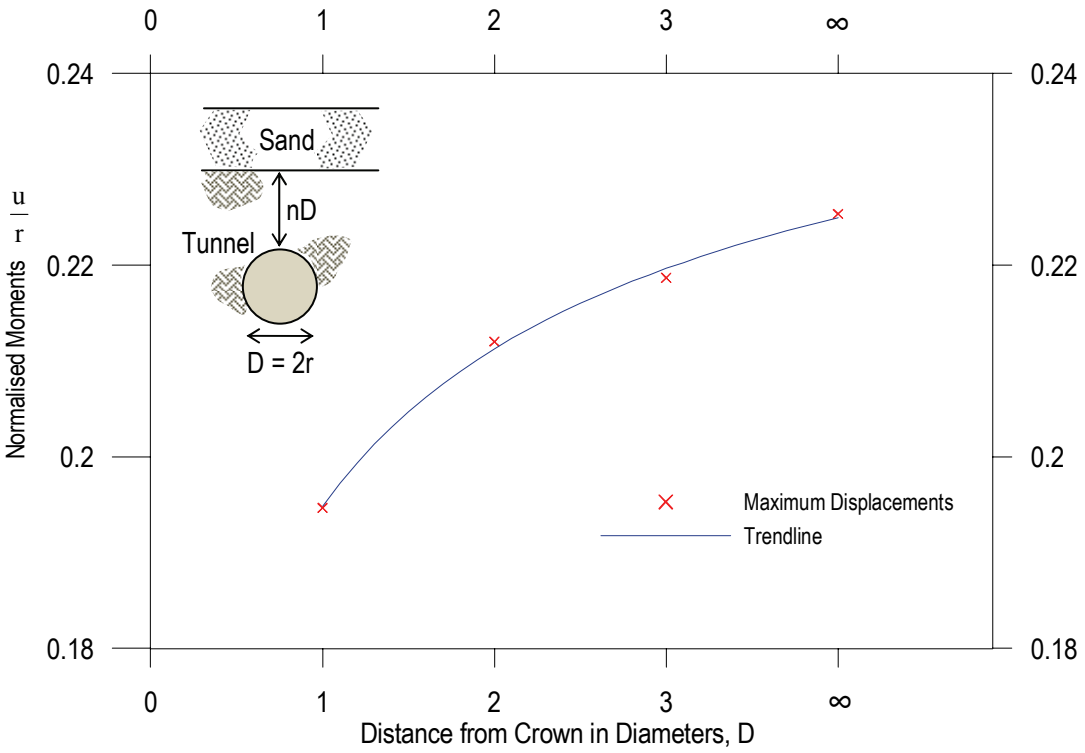


Figure 6.3: Summary of the maximum displacements for all cases from the FE analyses.

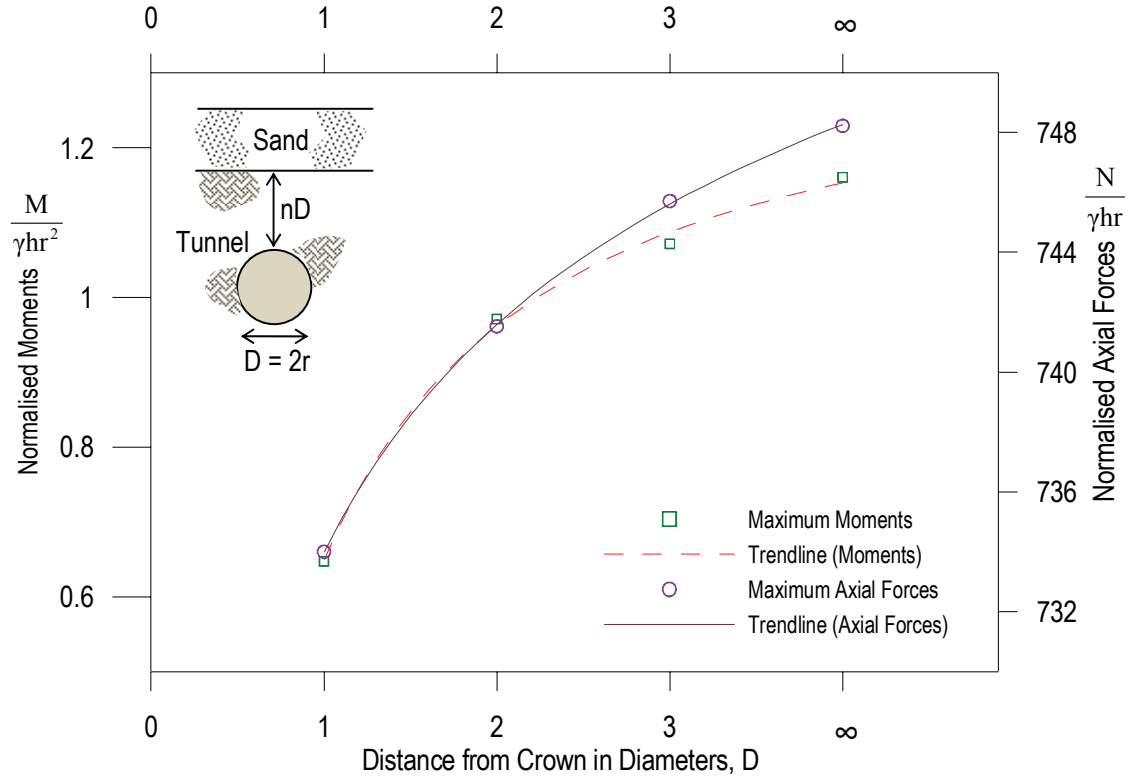


Figure 6.4: Summary of the maximum bending moments and axial forces for all cases from the FE analyses.

6.2 RECOMMENDATIONS FOR FUTURE WORK

Investigation into tunnelling in multi-layer ground is scant, as evidenced by a review of the literature. The following recommendations list the primary areas of research which require further study.

1. Drainage from the strongbox should be controlled as much as possible. There should be flow only through a defined exit point and quantified through the use of a valve system. This will help to investigate the effects of tunnelling in fully drained soils, as well as soils with varying degrees of drainage.
2. A stiffer lining should be used. The response of the lining to the surrounding mass of soil was not known *a priori* as the properties of the cohesive mix were untested on a large-scale. A flexible lining section was chosen on purpose to ensure that appreciable strains would register. However a stiffer section would mitigate localised movements caused by the unforeseen irregularities, or the slight heterogeneity of the soil.
3. A larger lining sleeve should be used. Before testing, it was not known how the cohesive mass would respond to tunnelling under 1g conditions. Therefore a conservative decision was made to exaggerate greatly the soil movements around the lining by creating a lining diameter significantly smaller than that of the excavation. It was also originally proposed to monitor the movement at the free surface, and the large gap would have served to accomplish this. However it was felt that this particular point of study was not within the scope of this project.
4. More focus should be placed on the scenario when the layer of sand is located in the vicinity of distance of two equivalent excavated diameters away from the crown of the tunnel. It may be necessary to study the incremental positioning of the granular layer in this region, as it appeared to be a point of transition between the sand stratum having significant influence on the behaviour of the soil cavity, and having negligible influence.
5. The thickness of the sand layer as well as the grain sizes of the constituent sand should be varied to investigate the changes in these parameters.
6. The shear strength of the cohesive soil is another variable to consider. The presence of sand in a stiffer medium should be investigated. The use of cement in the

cohesive mix coupled with a brief mould-testing scheme will enable researchers to predict shear strength, thereby controlling this particular parameter.

7. The depth of the soil cover should also be studied. All tunnelling in this project was done under deep-tunnel conditions. Shallow tunnels are of interest in order to examine the subsidence patterns that may arise, and how these might affect existing structures at the surface.
8. Pore-water pressure monitoring is recommended as well. It may be of interest to study the effect of pore-water pressure changes as excavation work is done, and also how they vary as strains develop. Pore-water pressure readings can also aid in determining drainage conditions.
9. More trials for each case should have been done. However the limitations of time and the availability of resources allowed for only one test to be done for each case.
10. Particle Image Velocimetry (PIV) is suggested for monitoring the soil movements around the excavation in a physical model. This will facilitate the quantification of and direction of displacements after the tunnel is created. ■

REFERENCES

Adachi, T., Tamura, T., Kimura, K., Nishimura, T. (1995). "Axial symmetric trap door tests on sand and cohesion soil [in Japanese]." *Proc. of the 30th Jap. Natl. Conf. on Geot. Eng*, 1973 - 1976.

Adachi, T., Kimura, M., Nishimura, T., Koya, N., Kosaka, K. (1997). "Trap door experiment under centrifugal conditions." *Deformation and Progressive Failure in Geomechanics*, 725 - 730.

Adachi, T., Kimura, M., Kishida, K. (2003). "Experimental study on the distribution of earth pressure and surface settlement through three-dimensional trapdoor tests." *Tunneling and Underground Space Technology*, 18, 171 - 183.

Allersma, H. G. B. (1996). "Using digital image processing field measurement." *Géotechnique*, 46(3), 561.

ASTM. (2007). "ASTM D854-06 (Test Methods for Specific Gravity of Soil Solids by Water Pycnometer)."

ASTM. (2007). "ASTM D4318-05 (Test Methods for Liquid Limit, Plastic Limit, and Plasticity Index of Soils)."

ASTM. (2007). "ASTM D6913-04e1 (Test Methods for Particle-Size Distribution (Gradation) of Soils Using Sieve Analysis)."

Atkinson, J. H., Brown, E.T., Potts, M. (1975). "Collapse of shallow unlined tunnels in dense sand." *Tunnels and Tunnelling*, 81.

Atkinson, J. H., Potts, D.M., Schofield, A.N. (1977). "Centrifugal model tests on shallow tunnels in sand." *Tunnels and Tunnelling*.

Atkinson, J. H., Potts, D.M. (1977). "Stability of a Shallow Circular Tunnel in Cohesionless Soil." *Géotechnique*, 27(2), 203 - 215.

Bobet, A. (2001). "Analytical Solutions for Shallow Tunnels in Saturated Ground." *J. Engrg. Mech.*, 127(12), 1258-1266.

Bolton, M. D., Lu, Y.C., Chin, C.Y. "Compensation grouting." *Proceedings of the Centrifuge'94*, Singapore, 719 - 724.

Bray, J. W., Goodman, R.E., 1981. (1981). "The theory of base friction models." *International Journal of Rock Mechanics and Mining Science and Geomechnics Abstract*, 18, 453 - 468.

Bucky, B. P. (1931). "The Use of Models for the Study of Mining Problems. Technical Publication." *American Institute of Mining Engineers*, 425.

Burland, J. B. (1997). "The teaching of soil mechanics-a personal view." *Proc. 9th European Conf. on Soil Mech. And Foundation Engineering*, Dublin, 1427 - 1447.

Cairncross, A. M. (1973). "Deformations around Model Tunnels in Stiff Clay," Cambridge University.

Carter, J. P., J.R. Booker. (1990). "Sudden Excavation of a Long Circular Tunnel in Elastic Ground." *Int. J. Rock Mech. Min. Sci. & Geomech.*, 27, 129 - 132.

Chambon, P., Corte, J.F., Garnier, J. (1991). "Face stablity of shallow tunnels in granular soils."

Chambon, P., Corte, J.F. (1994). "Shallow tunnels in cohesionless soil: Stability of tunnel face." *Journal of Geotechnical Engineering*, 120(7), 1148 – 1165.

Chapman, D. N., Ahn, S.K., Hunt, D.V.L., Chan, H.C. (2006). "The use of model tests to investigate the ground displacement associated with multiple tunnel construction in soil." *Tunnels and Tunnelling*, 21(3), 413.

Chen, W., Baldauf, S. "Prediction of ground deformations due to excavation – application to tunnel lining design in weak rock." *Proceedings of the Eighth International Conference on Analytical and Computational Methods in Geomechanics*, West Virginia, 2565 – 2570.

Corbetta, F., D. Bernaud, D. Nguyen-Mihn. (1991). "Contribution à la Méthode Convergence-Confinement par le Principe de la Similitude." *Rev. Franç. Géotech.*, 54, 5 - 11.

Craig, W. H. (1989). "The use of a centrifuge in geotechnical engineering education." *Geotechnical Testing Journal, ASTM*, 12(4), 288 - 291.

Duncan J.M., C. C. Y. (1970). "Nonlinear analysis of stress and strain in soil." *J. Soil Mech. Found. Div. ASCE*, 96, 1629–1653.

Dunham, L., Valsangkar, AJ, Schriver, AB. (2004). "Centrifuge Modeling of Rigid Square Footings on Weak Jointed Rock." *ASTM geotech. test. j.*, 28(2), 133-143.

Dykeman, P., Valsangkar, A.J. (1996). "Model studies of socketed caissons in soft clay." *Can. Geotech. J.*, 33, 747-759.

Egger, P., Gindroz, C. "Anchored tunnels at shallow depth – a comparative study with physical and mathematical models." *Proceedings of the Fourth Congress of International Society for Rock Mechanics*, Montreux, 121 - 136.

Einstein, H. H., Schwartz, C.W. (1978). "Simplified Analysis for Tunnel Supports." *American Society of Civil Engineers, Journal of the Geotechnical Engineering Division*, 105(4), 499-518.

Eringen, A. C. (1957). "Elasto-Dynamic Problem Concerning the Spherical Cavity." *Q. J. Mech. Appl. Math.*, 10, 257 - 270.

González, C., Sagaseta, C. (2001). "Patterns of soil deformations around tunnels. Application to the extension of Madrid Metro." *Computers and Geotechnics*, 28, 445 - 468.

Goodman, R. E. "Geological investigations to evaluate stability. In: Geotechnical Practice for Stability in Open Pit Mining." *Proceedings of the Second International Conference on Stability in Open Pit Mining*, Vancouver, BC, 125 - 132.

Grant, R. J., Taylor, R.N. (1996). "Centrifuge Modelling of Ground Movements Due to Tunnelling in Layered Ground." *Geotechnical Aspects of Underground Construction in Soft Ground: Proceedings*, Rotterdam, NL, 507-512.

Grant, R. J. (1998). "Movements around a tunnel in two-layer ground," City University, London, UK.

Grant, R. J., Taylor, R.N. (2000). "Stability of Tunnels in Clay with Overlying Layers of Coarse Grained Soil." *GeoEng2000: An International Conference on Geotechnical & Geological Engineering*, Melbourne, Australia.

Hagiwara, T., Grant, R.J., Calvello, M., Taylor, R.N. (1999). "The effect of overlying strata on the distribution of ground movements induced by tunneling in clay." *Soils and Foundations*, 39(3), 63 - 73.

Harris, D. I., Mair, R.J., Love, J.P., Taylor, R.N., Henderson, T.O. (1994). "Observations of ground and structure movements for compensation grouting during tunnel construction at Waterloo station." *Géotechnique*, 44(4), 691 - 713.

Hefny, A. M., K.Y. Lo. (1999). "Analytical Solutions for Stresses and Displacements Around Tunnels Driven in Cross-Anistropic Rocks." *International Journal for Numerical and Analytical Methods in Geomechanics*, 23, 161 - 177.

Hoek, E. (1971). "Rock Engineering (Inaugural Lecture)." Imperial College, University of London.

Hoek, E., Brown, E.T. (1980). "Empirical strength criterion for rock masses." J. Geotech. Engng Div., ASCE 106 (GT9), 1013-1035.

Iai, S., Tobita, T., Nakahara, T. (2005). "Generalised scaling relations for dynamic centrifuge tests." *Géotechnique*, 55(5), 355 - 362.

Jacobsz, S. W., Standing, J.R., Mair, R.J., Hagiwara, T., Sugiyama, T. (2004). "Centrifuge modeling of tunneling near driven piles." *Soils and Foundations*, 44(1), 49 - 56.

James, R. G. (1965). "Stress and Strain Fields in Sand," Cambridge University, Cambridge, UK.

Kamata, H., Masimo, H. (2003). "Centrifuge model test of tunnel face reinforcement by bolting." *Tunneling and Underground Space Technology*, 18(2), 205.

Kempfert, G. a. G., B. (2006). "Excavations and Foundations in Soft Soils." Springer, Berlin, 57-116.

Kim, S. H. (1996). "Interaction between closely spaced tunnels in clay," Oxford University.

Kimura, T., Kusakabe, O. (1987). "Centrifuge model tests, 2 (in Japanese)." *Tsuchi-to-kiso*, 35(11), 68 - 74.

Kline, S. J. (1986). "Similitude and Approximation Theory."

Kondner R.L., Z. J. S. (1963). "A hyperbolic stress strain formulation for sands." *Proc. 2nd Pan Am. Int. Conf. Soil Mechods Found. Engng.*, 1, 289–394.

Kumar, P. (1986). "Stress Concentration Due to Underground Excavation in Cross-Anisotropic and Nonhomogeneous Elastic Halfspace." *Computers & Structures*, 25, 687 - 694.

Ladanyi, B., Hoyaux, B. (1969). "A study of the trap door problem in a granular mass." *Canadian Geotechnical Journal*, 6(1), 1 - 14.

Langhaar, H. L. (1951). *Dimensional Analysis and Theory of Models*, Wiley.

Leca, E., Clough, G.W. (1992). "Prehminary design for NATM tunnel support in soil." *Journal of Geotechnical Engineering Division, ASCE*, 118(4), 558 - 575.

Lee, C. J., Wu, B.R., Chen, H.T., Chiang, K.H. (2006). "Tunneling stablity and arching effects during tunneling in soft clayey soil." *Tunneling and Underground Space Technology*, 21(2), 119.

Lee, K. M., Rowe, R.K., Lo, K.Y. (1992). "Subsidence owing to tunnelling. I. Estimating the gap parameter." *CAN. GEOTECH. J.*, 29, 929 - 940.

Lee, S. W., Bolton, M.D., Mair, R.J., Hagiwara, T., Soga, K., Dasari, G. R. (2001). "Centrifuge modeling of injection near tunnel lining." *Int. Jour. of Phy. Mod. In Geo.*(9 - 24).

Lee, C.-J., Wu, B.-R., C., Shean-Yau. (1999). "Soil Movements around a Tunnel in Soft Soil." *Proceedings of the National Scientific Council*, Chungli, Taiwan, R.O.C., 23(2), 235 - 247.

Lo, K. Y., B. Lukajic. (1984). "Predicted and Measured Stresses and Displacements Around the Darlington Intake Tunnel." *Can. Geotech. J.*, 21, 147 – 165.

Loganathan, N., Poulos, H.G. (1998). "Analytical prediction for tunneling-induced ground movements in clays." *Journal of Geotechnical and Geoenvironmental Engineering*, 124(9), 846 – 856.

Love, J. P. (1984). "Model testing of geogrid in unpaved roads," D.Phil. thesis, University of Oxford, Oxford, England.

Mair, R. J. (1979). "Centrifugal Modelling of Tunnel Construction in Soft Clay," PhD thesis, University of Cambridge.

Mair, R. J. (1982). "Ground Movement around Shallow Tunnels in Soft Clay." *Tunnels and Tunnelling*, 14(5), 45 – 48.

Mair, R. J., Taylor, R.N., Bracegirdle, A. (1993). "Subsurface settlement profiIes above tunnels in clays." *Géotechnique*, 43(2), 315 – 320.

Meguid, M. A., Mattar, J., Nunes, M., Saxe, S. (2006). "On the physical modeling of tunnels in soft ground." *59th Canadian Geotechnical Conference*, Vancouver, BC.

Meguid, M. A., Saada O., Nunes, M.A., and Mattar, J. (2008). "Physical modeling of tunnels in soft ground: A review." *Tunneling and Underground Space Technology*, 23, 185 – 198.

Meymand, P. J. (1998). "Shaking table scale model tests of nonlinear soil-pile-superstructure interaction in soft clay," Ph.D. Thesis, University of California, Berkeley.

Mindlin, R. D. (1940). "Stress distribution around a tunnel." *ASCE*, 1117 – 1153.

Morgan, H. D. (1961). "A Contribution to the Analysis of Stress in a Circular Tunnel." *Géotechnique*, 11, 37 - 46.

Muir Wood, A. M. (1975). "The Circular Tunnel in Elastic Ground." *Géotechnique*, 25, 115 – 127.

Murayama, S., Matsuoka, H. (1971). "Earth pressure on tunnels in sandy ground [in Japanese]." *J. Geotech. Eng.*, 187, 95 – 108.

Murayuma, S. (1968). "Earth pressure on vertically yielding section in sand layer [in Japanese]." *Disaster Prevention Research Institute Annuals*, 11B, 123 – 138.

Nakai T., S. H. M., Hinokio M., Sada T. (2000). "Tunnel Excavations Considering Building Loads: 2D Model Tests and Numerical Analysis." *Nagoya Institute of Technology, Japan.*

Newson, T., White, D. (2005). "Modeling geotechnical problems in soft clays using the mini-centrifuge." *The Univesity of Western Ontario, K.Y. Lo Symposium*.

Nomoto, T., Imamura, S., Hagiwara, T., Kusakabe, O., and Fujii, N. (1999). "Shield Tunnel Construction in Centrifuge." *Journal of Geotechnical and Geoenvironmental Engineering*, 125(4), 289 - 300.

O'ReiIIy, M. P., New, B.M. "Settlements above tunnels in the UK – their magnitude and prediction." *Proceedings of Tunnelling'82*, IMM, London, UK, 173 - 181.

Orr, T. L. L. (1976). "The Behavior of Lined and Unlined Model Tunnel in Stiff Clay," Ph.D. thesis. Cambridge University, Engineering Department, UK.

Panet, M., A. Guenot. "Analysis of Convergence Behind the Face of a Tunnel." *Tunnelling '82*, The Institution of Mining and Metallurgy, London, 197 - 204.

Park, S. H., Adachi, T., Kimura, M., Kishida, K. "Trap door test using aluminum blocks." *Proceedings of the 29th Symposium of Rock Mechanics. J.S.C.E.*, 106 - 111.

Peck, R. B. (1969) "Deep excavations and tunneling in soft ground." *Proceedings of the Seventh International Conference On Soil Mechanics and Foundation Engineering*, Mexico City, 225 - 290.

Pender, M. J. (1980). "Elastic Solutions for a Deep Circular Tunnel." *Géotechnique*, 30, 216 - 222.

Plaxis. (2007). "Plaxis V8 User's Manual."

Pokrovsky, G. I., Fedorov, I.S. "Studies of soil pressures and soil deformations by means of a centrifuge." *Proceedings of the First International Conference ISSMFE (Harvard)*, 70.

Potts, D. M. (1977). "Behavior of Lined and Unlined Tunnels in Sand," Cambridge University.

R.J.A., W. (1973). "Study of progressive hanging wall caving at Chambishi copper mine in Zambia using the base friction model concept," Imperial College, University of London.

Randolph, M. F., House, A.R. (2001). "The complementary roles of physical and computational modeling." *Int. Jour. of Phy. Mod. In Geo.*, 1 - 8.

Rocha, M. "The possibility of solving soil mechanics problems by use of models." *Proc. 4th Intl. Conf. Soil Mech Fdn. Eng.*, London, 183 - 188.

Romero, V. (2002). "NATM in Soft Ground: A Contradiction of Terms?" *World Tunnelling*, 338-343.

Roscoe, K. H., Arthur, J.R.F., James, R.G. (1963). "The determination of strains in soils by an X-ray method." *Civil Engineering & Public Works Review*, 58, 1009 - 1012.

Rowe, P. W. (1962). "The stress-dilatancy relation for static equilibrium of an assembly of particles in contact." *Proc. R. Soc. A.*, 269, 500-527.

Rowe, R. K., Kack, G.J. (1983). "A theoretical examination of the settlements induced by tunneling: from cases history." *Can. Geotech. J.*, 20(2), 299 - 314.

Rowe, R. K., Lee, K.M. (1989). "Deformations caused by surface loading and tunnelling: the role of elastic anisotropy." *Géotechnique*, 39(1), 125 - 140.

Sagaseta, C. (1987). "Analysis of Undrained Soil Deformation Due to Ground Loss." *Geotechnique*, 37(3), 301-320.

Sakai, T. (1996). "A study of a particle size effect of a trap-door problem with glass beads." Proc. IS-Nagoya'97 - Deformation and progressive failure in geomechanics, A. Asaoka et al. (eds), 145-150.

Schanz, T., Vermeer, P.A., Bonnier, P.G. (1999). "The hardening soil model: Formulation and Verification." In: Brinkgreve RBJ, editor. Beyond 2000 in Computational Geotechnics. Balkema.

Schmidt, B. "Prediction of settlements due to tunneling in soil: three case histories." *Proceedings of the Second Rapid Excavation and Tunneling Conference*, San Francisco, CA, 1179 - 1199.

Scott, R. (1989). "Centrifuge and modeling technology: A survey." *Rev. Franc. Geotech.*, 48, 15 - 34.

Selberg, H. L. (1952). "Transient Compression Waves from Spherical and Cylindrical Cavities." *Ark. Fys.*, 5, 97 - 108.

Seneviratne, H. N. (1979). "Deformations and Pore Pressure Dissipation around Tunnels in Soft Clay." PhD thesis, University of Cambridge, UK.

Sharan, S. K. (1989). "Finite-Element Analysis of Underground Openings." *Int. J. Num. & Ana. Meth. Geomech.*, 13, 565 - 570.

Sharma, J. S., Bolton, M.D. (1995). "A new technique for simulation of collapse of a tunnel in a drum centrifuge." *CUED/D-Soils/TR286*, Cambridge University Engineering Dept., Cambridge.

Sharma, J. S., Bolton, M.D., Boyle, R.E. (2001). "A new technique for simulation of tunnel excavation in a centrifuge." *Geotechnical Testing Journal*, 24(4), 343 - 349.

Sharpe, J. A. (1941). "The Production of Elastic Waves by Explosion Pressures." *Geophys.*, 7, 144 - 154.

Singh, B., R.K. Goel, V.K. Mehrotra, S.K. Garg, M.R. Allu. (1988). "Effect of Intermediate Principal Stress on Strength of Anisotropic Rock Mass." *Tunnelling and Underground Space Technology*, 13, 71 - 79.

Singh, M., B. Singh, J.B. Choudhari, R.K. Goel. (2004). "Constitutive Equations for 3-D Anisotropy in Jointed Rocks and Its Effect on Tunnel Closure." *Int. J. Rock Mech. Min. Sci.*, 41, 1 - 6.

Sleby, A. R. (1988). "Surface Movements Caused by Tunnelling in Two-Layer Soil." *Engineering Geology of Underground Movements*(5), 71-77.

Sterpi, D., Cividini, A., Sakurai, S., Nishitake, S. (1996). "Laboratory model tests and numerical analysis of shallow tunnels." in G. Barla (ed.), Proc. Int. Symp. Eurock'96, Balkema, Rotterdam, pp. 689-696.

Sterpi, D., Cividini, A. (2004). "A physical and numerical investigation on the stability of shallow tunnels in strain softening media." *Rock Mechanics and Rock Engineering*, 27(4), 277 - 298.

Stimpson, B. (1970). "Modelling materials for engineering rock mechanics." *Int. J. Rock Mech. Min. Sci.*, 7, 77 - 121.

Swoboda, G., Mertz, W., Schmid, A. "Three dimensional numerical models to simulate tunnel excavation." *Proceedings of NUMLOG III*, London, UK, 536 - 548.

Take, A., Bolton, M.D. (2003). "Soil deformation measurement using particle image velocimetry (PIV) and photogrammetry." *Géotechnique*, 53(7), 619 - 631.

Tanaka, T., Sakai, T. (1993). "Progressive failure and scale effect of trapdoor problem with granular materials." *Soils and Foundations*, 33(1), 11 - 22.

Taylor, R. N. (1995). *Geotechnical Centrifuge Technology*, Blackie Academic & Professional, Chapman & Hall, London.

Terzaghi, K. "Stress distribution in dry and in saturated sand above a yielding trap-door." *Proceedings of the International Conference on Soil Mechanics*, Cambridge, MA, 307 - 311.

Terzaghi, K. (1943). *Theoretical Soil Mechanics*, Wiley, New York.

Tonon, F., B. Amadei. (2002). "Effect of Elastic Anisotropy on Tunnel Wall Displacements Behind a Tunnel Face." *Rock Mech. Rock Engng*, 35, 141 - 160.

Vardoulakis, I., Graf, B., Gudehus, G. (1981). "Trap-door problem with dry sand: a statical approach based upon model test kinematics." *International Journal for Numerical and Analytical Methods in Geomechanics*, 5, 57 - 78.

Venkatachalam, G. N., A. V. (1977). "Interaction in tunnels in stratified media." *International Symposium on Soil Structure Interaction*, Roorkee, India, 33-38.

Vermeer, P. A., Marcher, T., Ruse, N. (2002). "On the Ground Response Curve." *Rock and Soil Engineering*, 20(6), 19-24.

Verruijt, A., Booker, J.R. (1996). "Surface settlements due to deformation of a tunnel in an elastic half plane." *Geotechnique*, 46(4), 753-756.

Verruijt, A. (1997). "A Complex Variable Solution for a Deforming Circular Tunnel in an Elastic Half-Plane." *International Journal for Numerical and Analytical Methods in Geomechanics*, 21, 77 - 89.

White, D., Take, A. (2002). "GeoPIV: Particel Image Velocimetry (PIV) Software for use in Geotechnical Testing." ***CUED/D-SOILS/TR322***, Cambridge University, Cambridge, UK.

Wu, B. R., Lee, C.J. (2003). "Ground movement and collapse mechanisms induced by tunneling in clayey soil." *Int. Jour. of Phy. Mod. In Geo.*, 15 - 29.

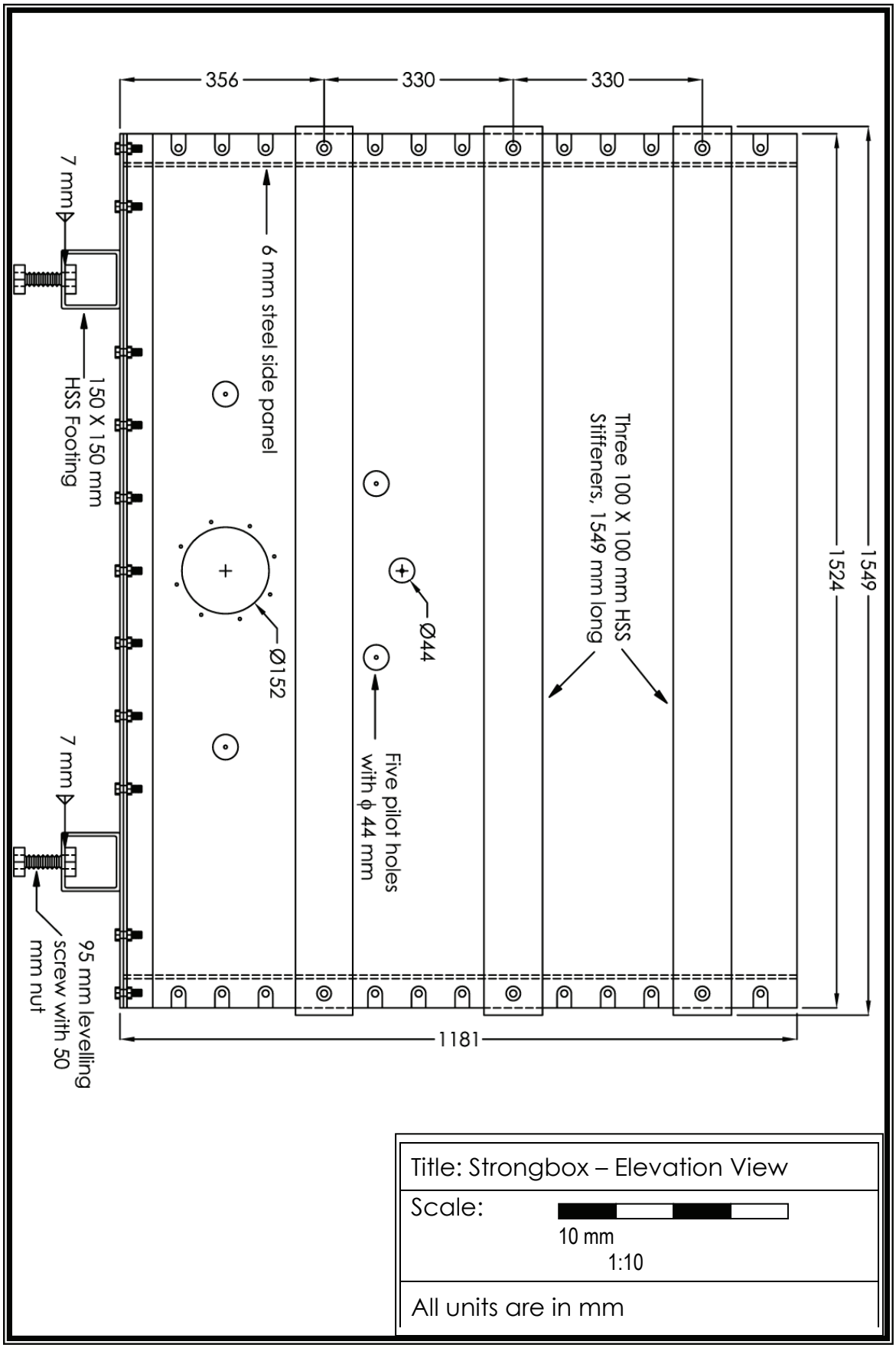
Xiao, B., J.P. Carter. (1993). "Boundary Element Analysis of Anisotropic Rock Masses." *Engineering Analysis with Boundary Elements*, 11, 293 - 303.

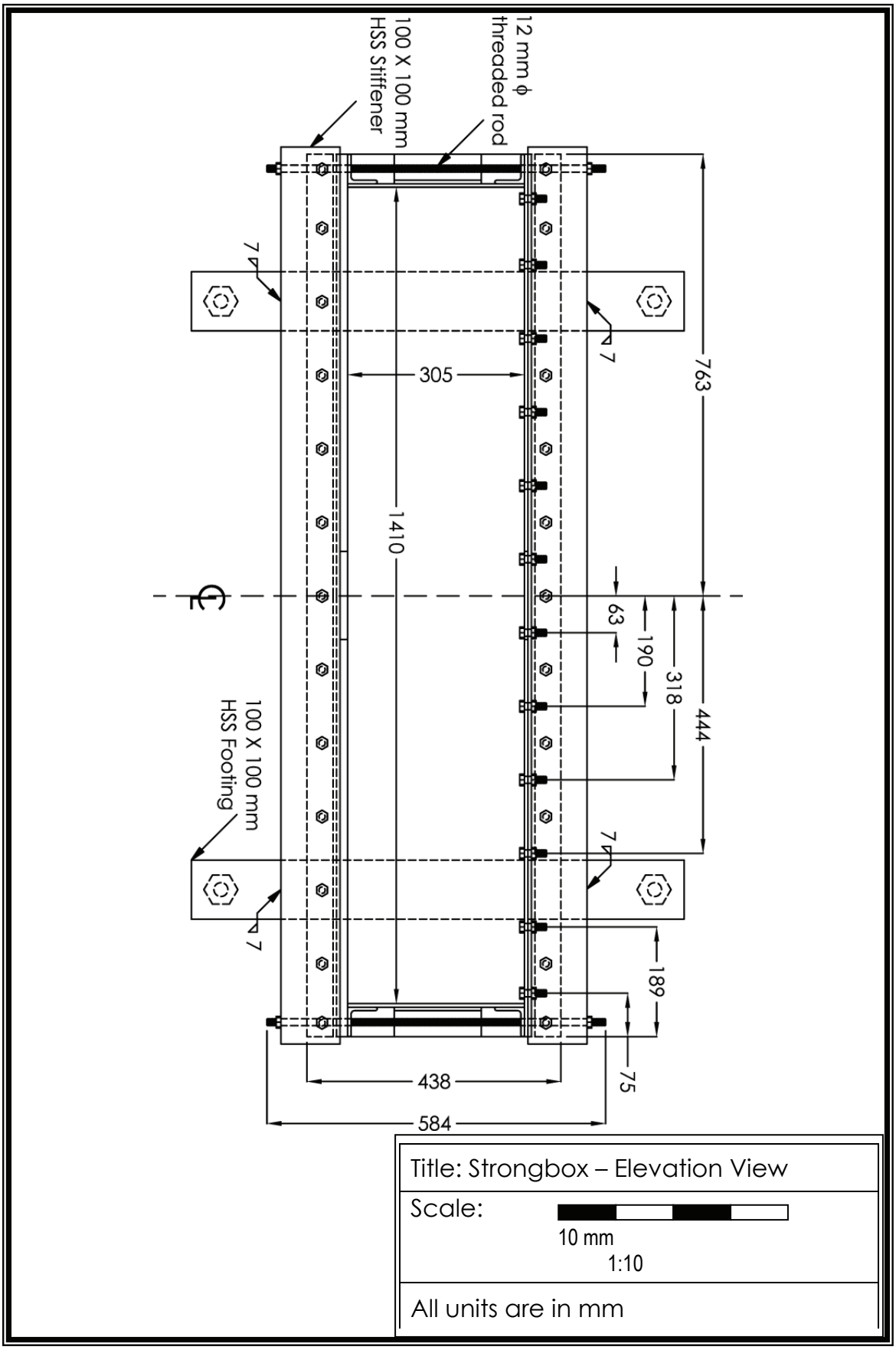
Xu, L. M., Nakai, T., Yamazaki, H. "Three dimensional model tests and analyses of lowering basement [in Japanese]." *Proc. of the 30th Jap. Natl. Conf. on Geot. Eng.*, 504 - 505.

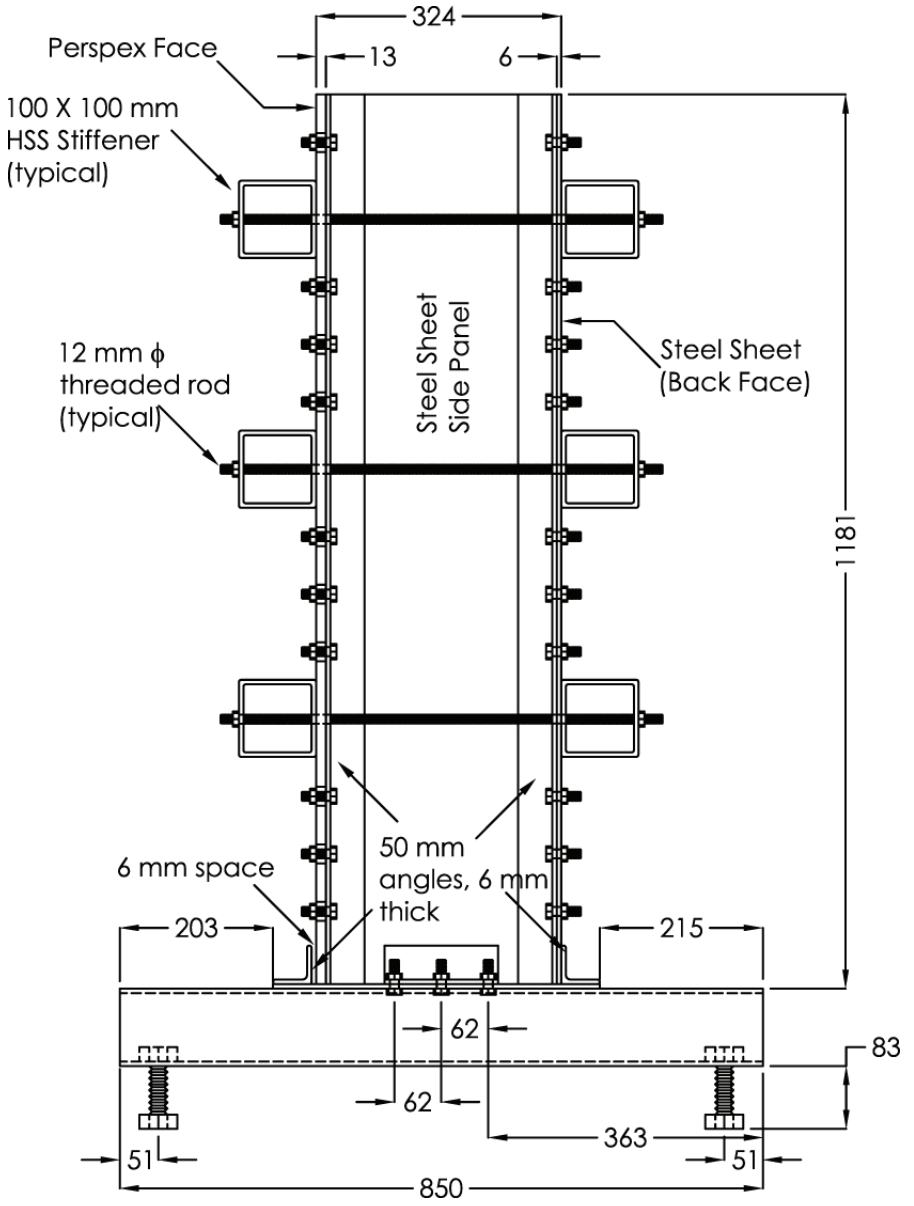
Yoshimura, H., Miyabe, K., Tohda, J. (1994). "Response of a tunnel lining due to an adjacent twin shield tunneling." *Proceedings of the Centrifuge'94 Conference*, Singapore, 69 - 698.

APPENDIX A

SCHEMATICS


356
330
330
1549
1524
1181
7 mm
7 mm
6 mm steel side panel
150 X 150 mm
HSS Footing
Three 100 X 100 mm HSS
Stiffeners, 1549 mm long
Ø44
Ø152
Five pilot holes
with ϕ 44 mm
95 mm levelling
screw with 50
mm nut
Title: Strongbox – Elevation View
Scale:
10 mm
1:10
All units are in mm


100 X 100 mm
HSS Stiffener
12 mm ϕ
threaded rod
7
7
305
763
1410
63
190
318
444
100 X 100 mm
HSS Footing
7
7
189
75
438
584
Title: Strongbox – Elevation View
Scale:
10 mm
1:10
All units are in mm



Title: Strongbox – Elevation View
Scale: 10 mm 1:10
All units are in mm

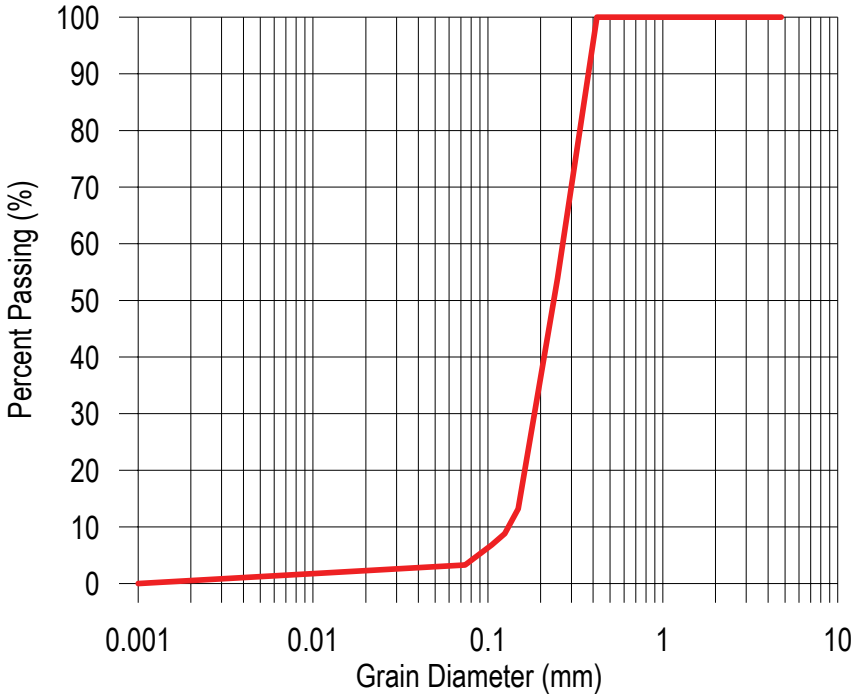
APPENDIX B

PARTICLE-SIZE DISTRIBUTION

Two different grades of silica-based sand were used in the testing of this study. This appendix provides the particle-size distributions for these soils according to ASTM D6913-04e1 (*Test Methods for Particle-Size Distribution (Gradation) of Soils Using Sieve Analysis*).

Quartz Industrial "7030" (30% retained on a no. 70 mesh) soil was used as a constituent of the cohesive mix. Five samples of approximately 500 g were taken from a randomly selected bag of "7030" sand. Each individual sample was weighed and placed into a stack of sieves prepared according to ASTM D6913-04e1. The stack was then secured within a sieve-shaking machine for ten minutes. The particle-size distribution based on an average of all five trials can be seen in Figure B.1 below.

Figure B.1: Particle size distribution for the fine (7030) sand

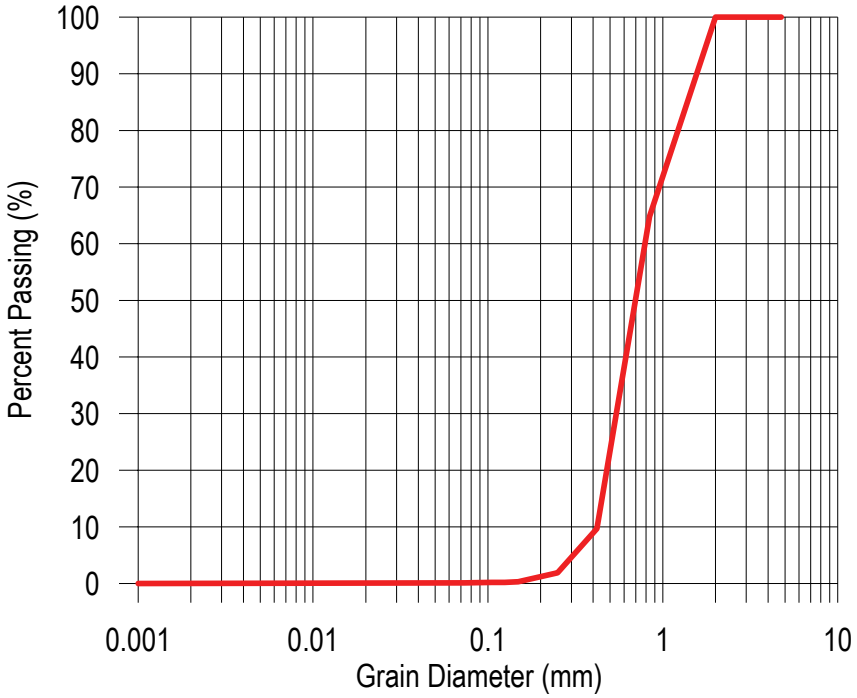


D_{10}, D_{30}, and D_{60} were found to be approximately 0.14 mm, 0.18 mm, and 0.26 mm, respectively. Accodingly, C_u and C_c were 1.86 and 0.90, respectively.

Quartz Industrial "2075" (75% retained on a no. 20 mesh) soil was used to simulate a layer of granular soil within a surrounding cohesive medium. Five samples of approximately 500 g were taken from a randomly selected bag of "2075" sand. Each individual sample was weighed and placed into a stack of sieves prepared according to ASTM D6913-04e1. The stack was then secured within a sieve-shaking machine for ten

minutes. The particle-size distribution based on an average of all five trials can be seen in Figure B.2 below.

Figure B.2: Particle size distribution for the coarse (2075) sand



D_{10}, D_{30}, and D_{60} were found to be approximately 0.42 mm, 0.55 mm, and 0.79 mm, respectively. Accodingly, C_u and C_c were 1.88 and 0.91, respectively.

APPENDIX C

SPECIFIC GRAVITY

The results presented in this appendix were obtained by conducting tests to determine the specific gravity of the two grades of silica sand that were used in this project. The testing was done according to ASTM D854-06 (*Test Methods for Specific Gravity of Soil Solids by Water Pycnometer*).

Three samples of Quartz Industrial "7030" (30% retained on a no. 70 mesh) sand having a mass of approximately 100 g were taken from a freshly cut bag. The water that was used in this experiment was de-ionised, distilled and de-aired. The specific gravity of the "7030" sand, based on three trials was found to be 2.66.

Three samples of Quartz Industrial "2075" (75% retained on a no. 20 mesh) sand having a mass of approximately 100 g were taken from a freshly cut bag. The water that was used in this experiment was de-ionised, distilled and de-aired. The specific gravity of the "2075" sand, based on three trials was found to be 2.65.

APPENDIX D

ATTERBERG LIMITS

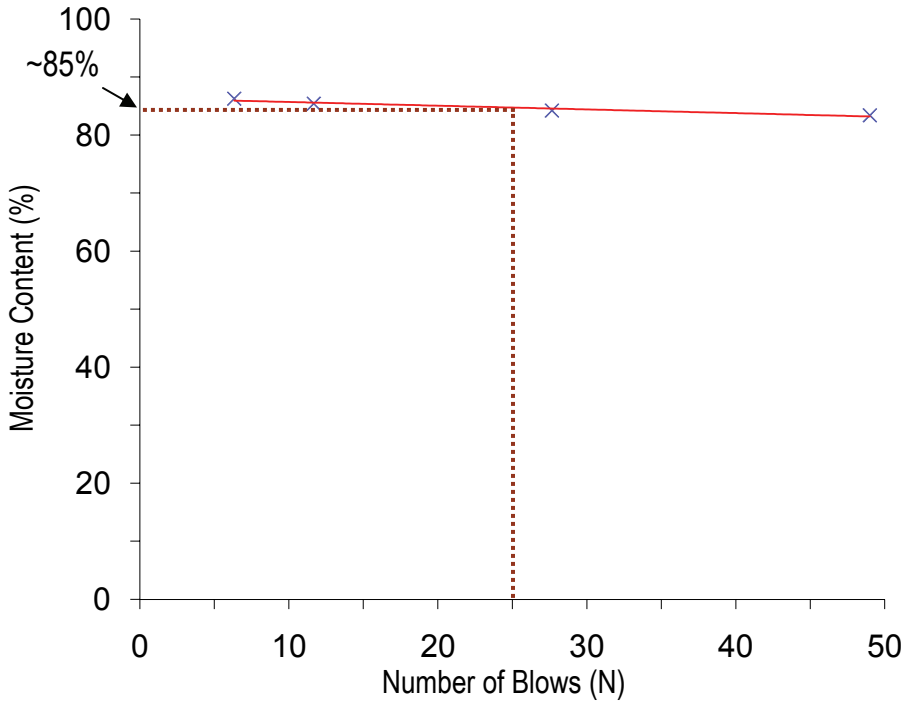
This appendix presents the results of tests that were done to determine the Atterberg Limits of the bentonite clay that was used in the cohesive mix. All work was done according to ASTM D4318-05 (*Test Methods for Liquid Limit, Plastic Limit, and Plasticity Index of Soils*).

Samples to determine the liquid limit (*LL*) were prepared by mixing pre-determined proportions (by mass) of water and clay for testing in the Casagrande device. The nominal proportions that were used were as follows (percentages denote the mass fraction of water): 82%, 83%, 84% and 85%. These values were chosen based on prior initial ad-hoc testing that was done in order to appraise roughly the liquid limit of the soil.

All test batches that were used were 300 g of total mass and were mixed using a commercial household electronic mixer for at least ten minutes. Three separate soil pats were taken from each batch and were tested in the Casagrande device in succession. Actual moisture content values were determined by taking four individual samples from each pat. The wet soil was weighed and then placed into an oven to dry for at least 24 hours before determining the dry mass. The averaged moisture content values for each pat were then recorded.

The number of blows from each group of three pats (i.e. for each batch) was determined by averaging the number of blows observed from each individual pat. Similarly, the actual water content for each batch was found by averaging the average values for each pat. A plot of moisture content against the number of blows can be seen in Figure D.1.

Figure D.1: Moisture Content vs. Blows



The liquid limit by convention is the moisture content which corresponds to 25 blows. This was found to be about 85% based on linear interpolation. This result was confirmed by the ad-hoc testing mentioned above which yielded a similar result.

The plastic limit (*PL*) was also found according to ASTM D4318-05. A test batch of 33% mass fraction of water was prepared, having a total mass of 300 g. This proportion was determined based on prior ad-hoc testing. Four samples were removed from the batch and were rolled separately by hand until the prescribed disintegration of the 3-mm rolled beads. Moisture content values were determined by weighing the beads and oven-drying them for at least 24 hours. The plastic limit was found to be approximately 31% which confirmed the value acquired from the previous ad-hoc testing. The plasticity index (*PI*) of the bentonite clay used in this project was therefore 54.

APPENDIX E

ELASTIC MODULUS OF ALUMINUM

This appendix presents the results of coupon-testing that was done in order to determine the Elastic Modulus of the aluminum sheet metal that was used in this project.

Seven pieces of aluminum were cut by using a guillotine apparatus, creating rectangular specimens approximately 225 mm by 19 mm. These were machined to "dog-bone" styled coupons having the dimensions as shown in Figure E.1 below.

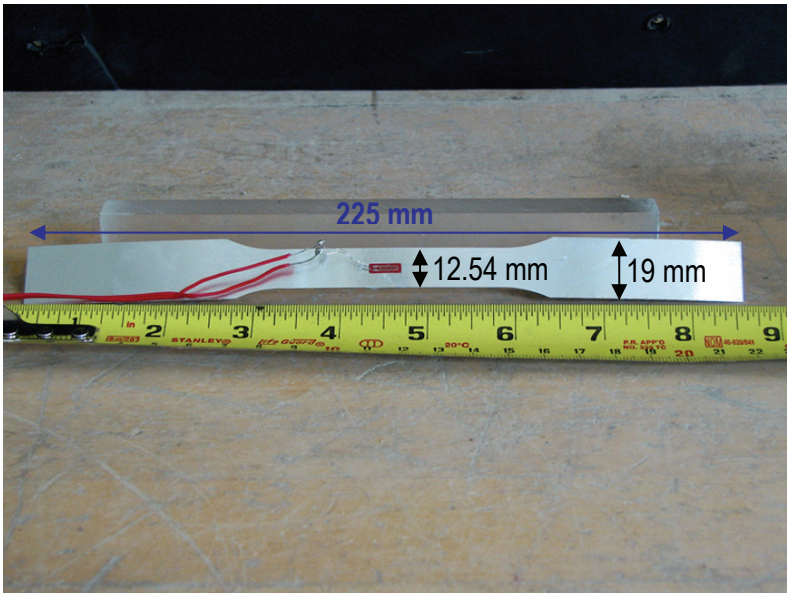


Figure E.1: A typical specimen used in the coupon testing.

The coupons were measured in three places along the thin neck section (Points A, B and C in Figure E.2) for width and thickness. An average of these three values was used to determine the average cross-sectional area that was to be exposed to the tensile axial load. Each specimen was then secured within the opposing grippers of the MTS machine (*Sintech 30/G*) and a digital calliper was used to determine the initial separation of the grippers, or "grip length." The specimens were instrumented with strain gauges (as shown in Figure E.1), however these were never used.

The software controlling the MTS machine (Testworks 4.0) allowed for the control of the separation rate (or crosshead movement), as well as for the sampling rate. The rate of separation of the crosshead was set to 0.1 mm/min with a sampling rate of 10 Hz for all tests. All specimens were tested until failure (see Figure E.2).

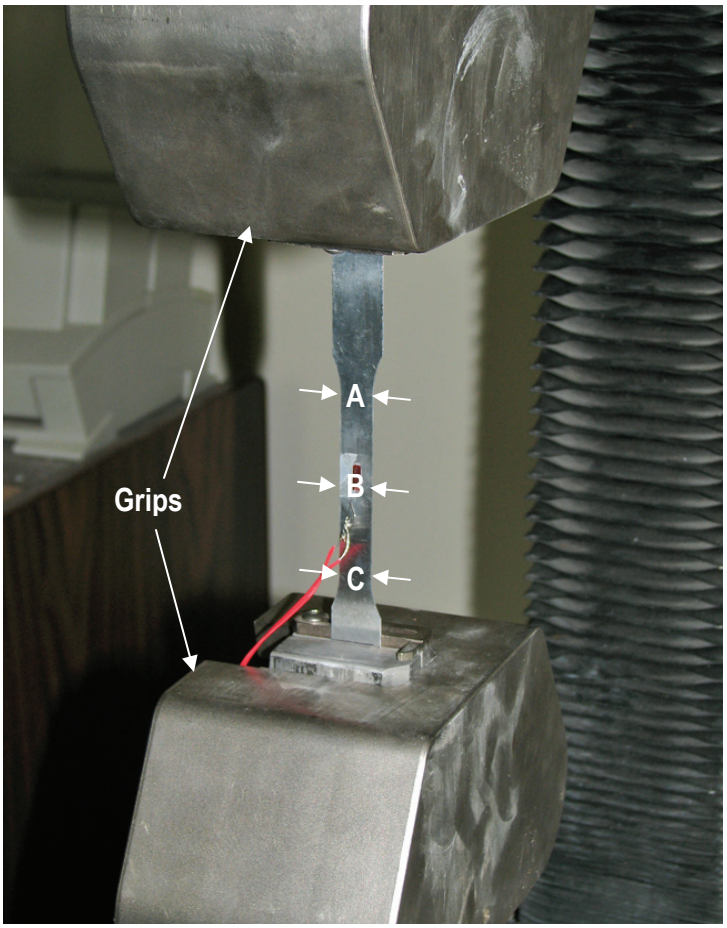


Figure E.2: Coupon held by grips.

The output from Testworks 4.0 was given in tabular form and presented axial tensile force against both time and the incremental movement of the crosshead. The axial force was divided by the appropriate cross-sectional area of the coupon under study to obtain the stress. The strains were determined by using the appropriate recorded incremental crosshead separation with respect to the initial position. Stress-strain curves were then generated (Figures E.3 to E.9). The elastic zone for each analysis was identified and linear regression was performed over this region, which yielded the elastic modulus (E) for each coupon. The average of these moduli was found to be 64 GPa, which is more than 90% of the accepted value for aluminum, 70 GPa.

Figure E.3: Stress-Strain Curve (Coupon 1)

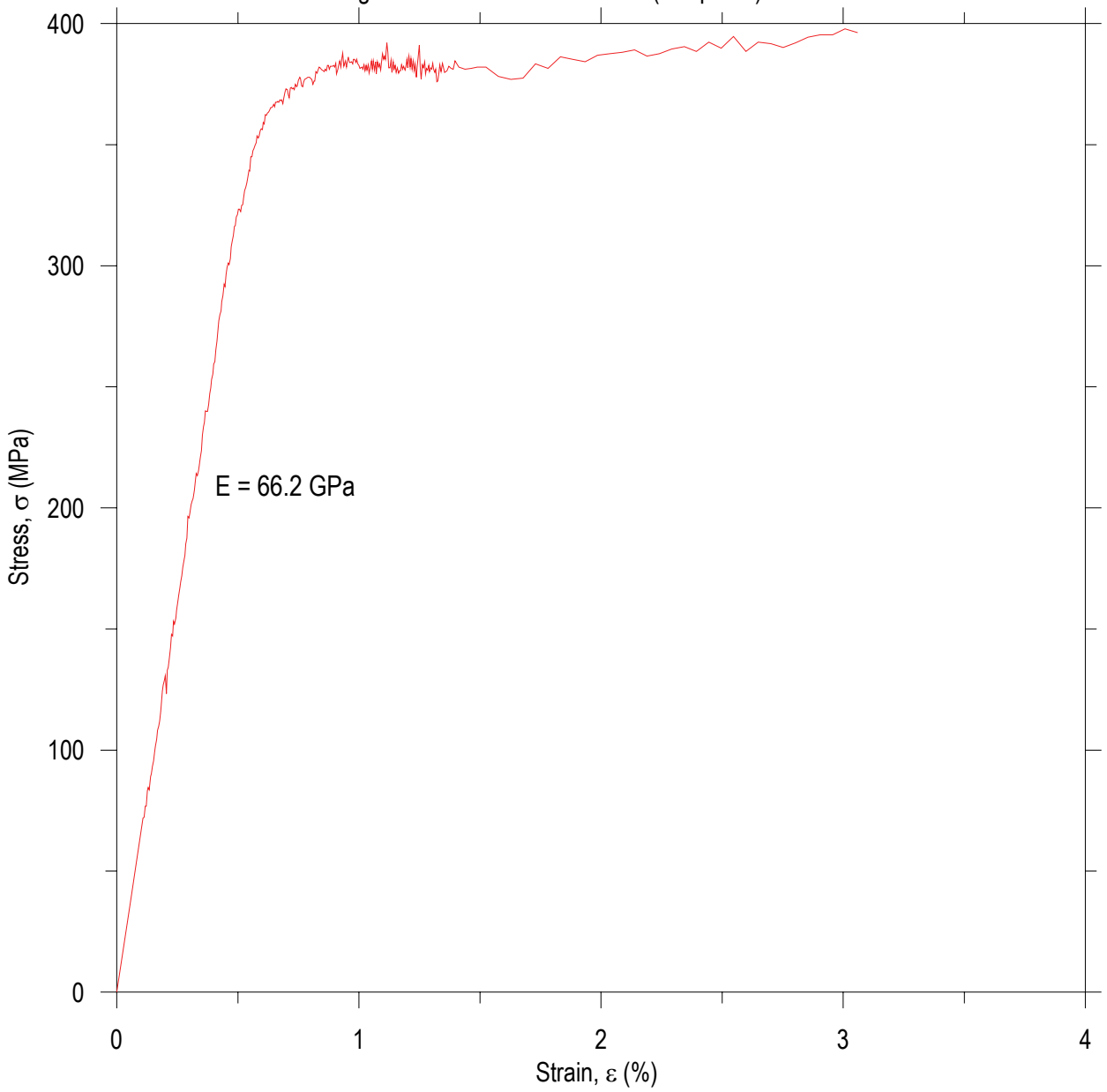


Figure E.4: Stress-Strain Curve (Coupon 2)

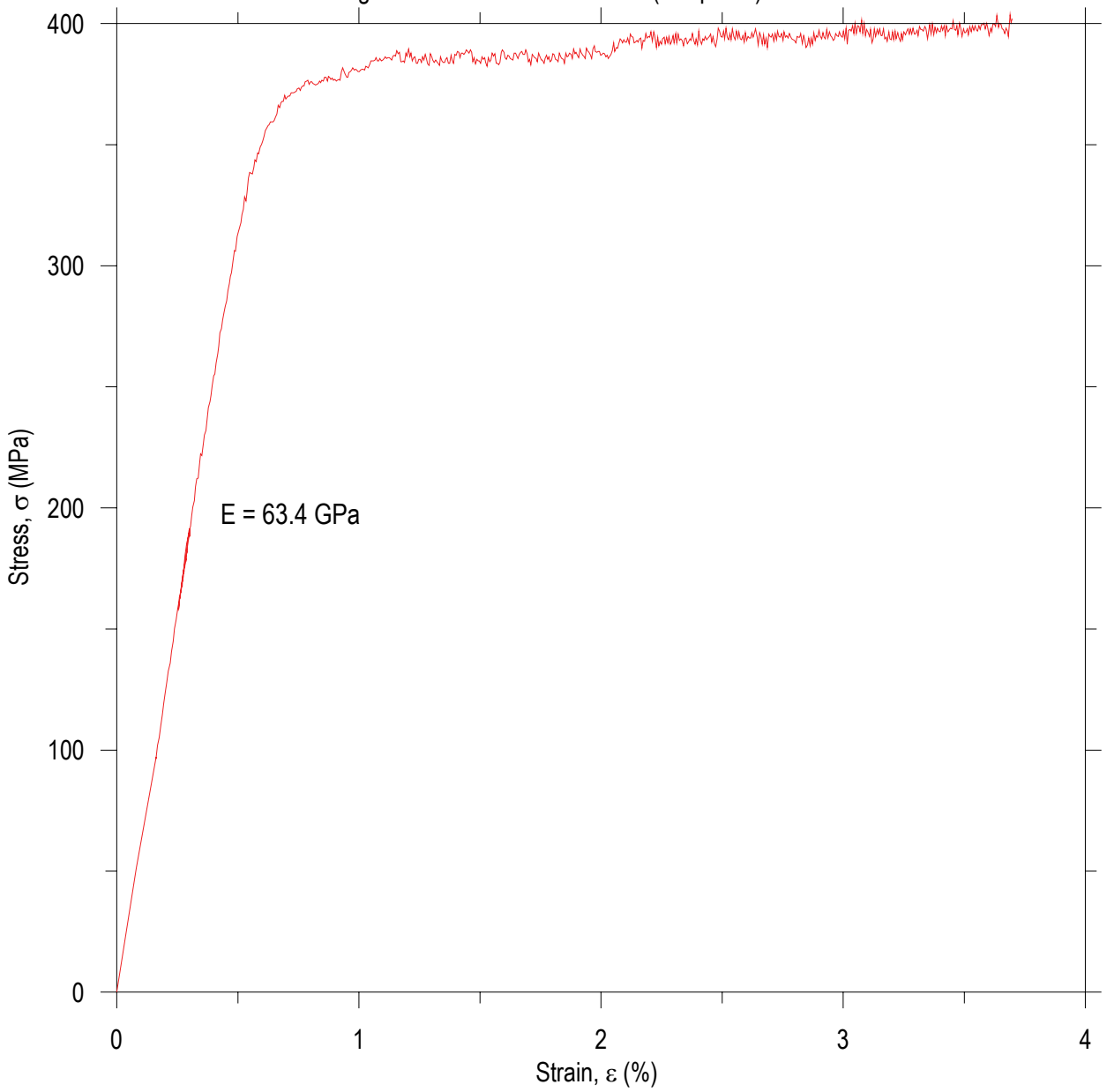


Figure E.5: Stress-Strain Curve (Coupon 3)

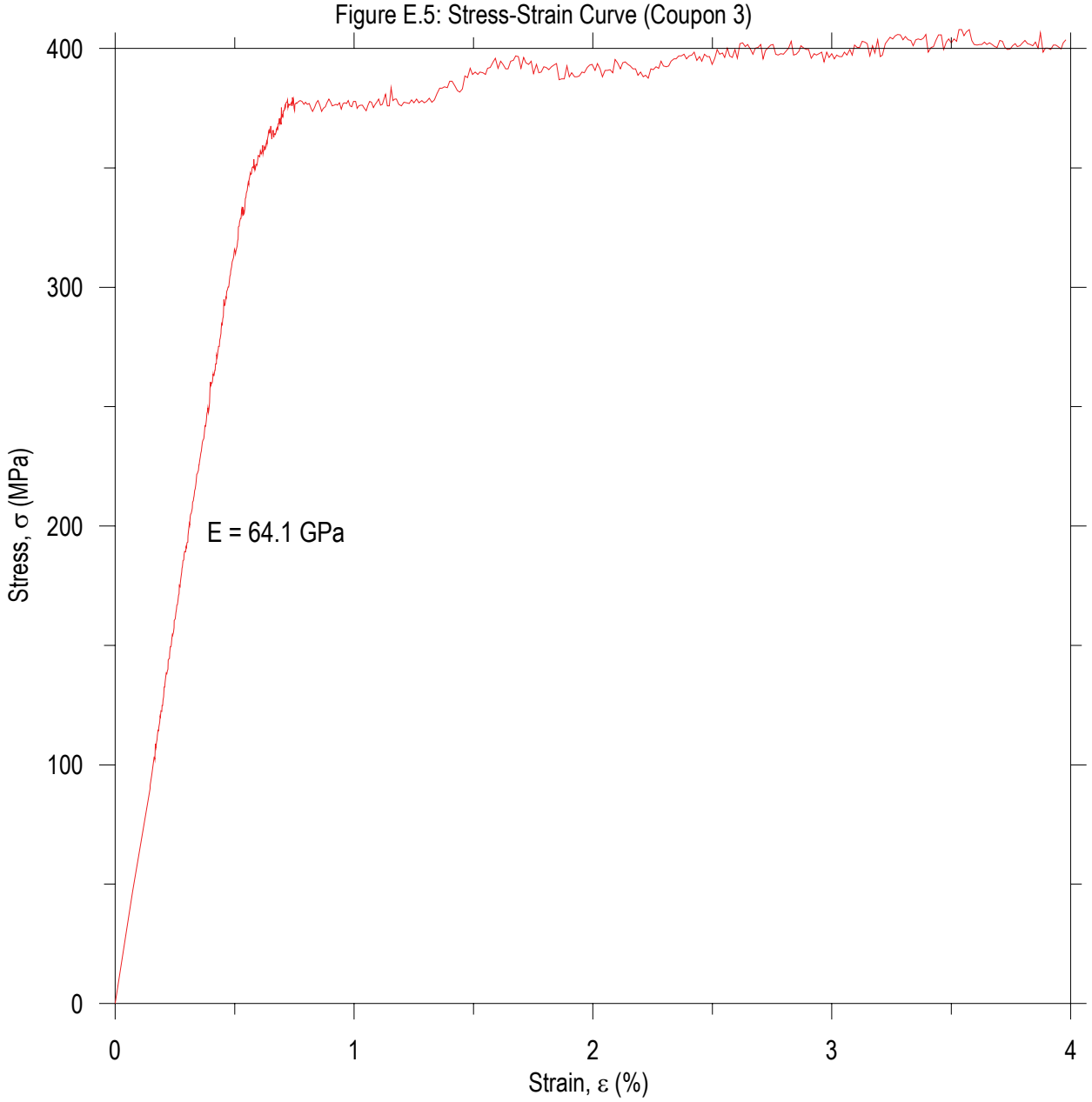


Figure E.6: Stress-Strain Curve (Coupon 4)

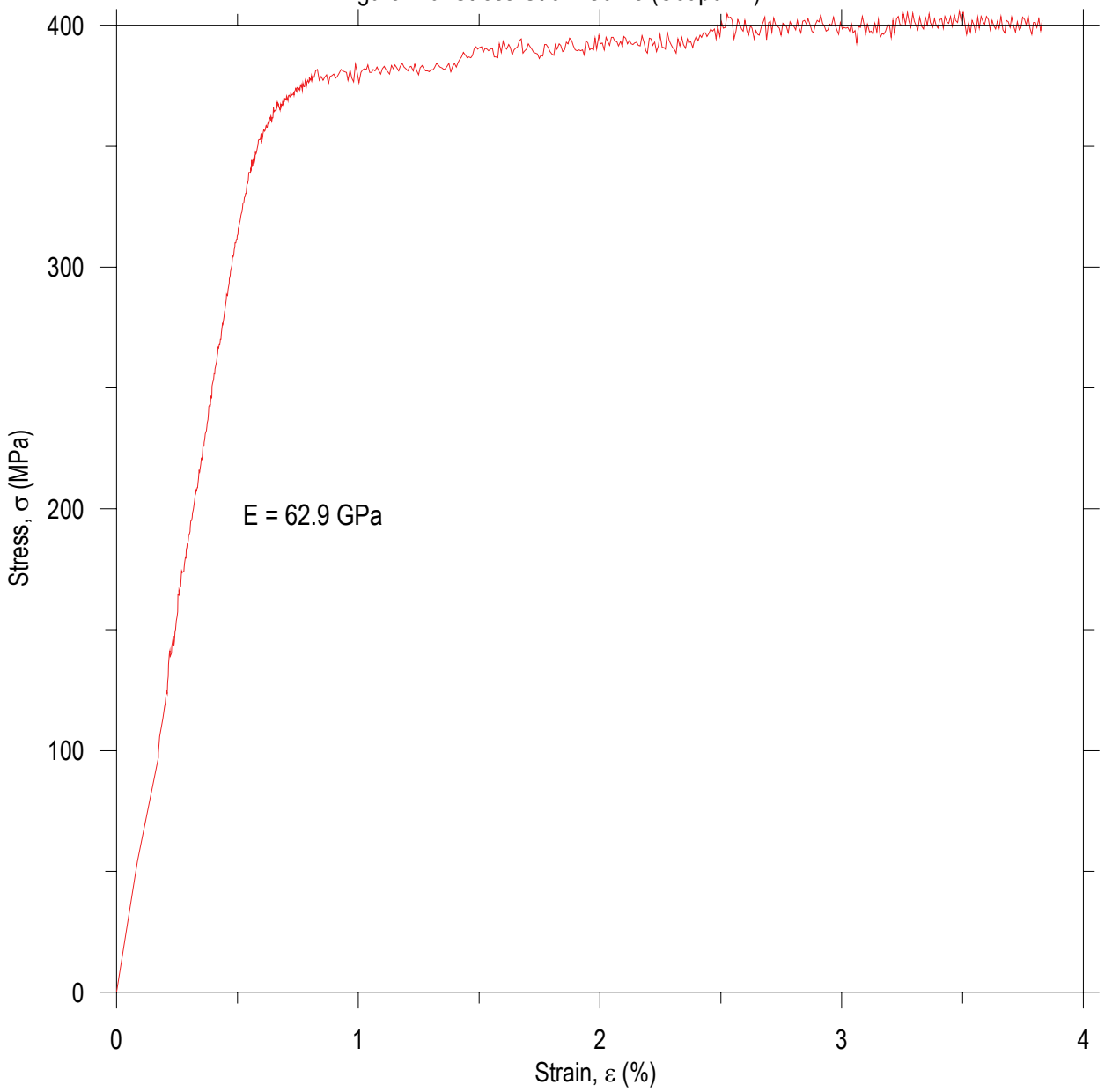


Figure E.7: Stress-Strain Curve (Coupon 5)

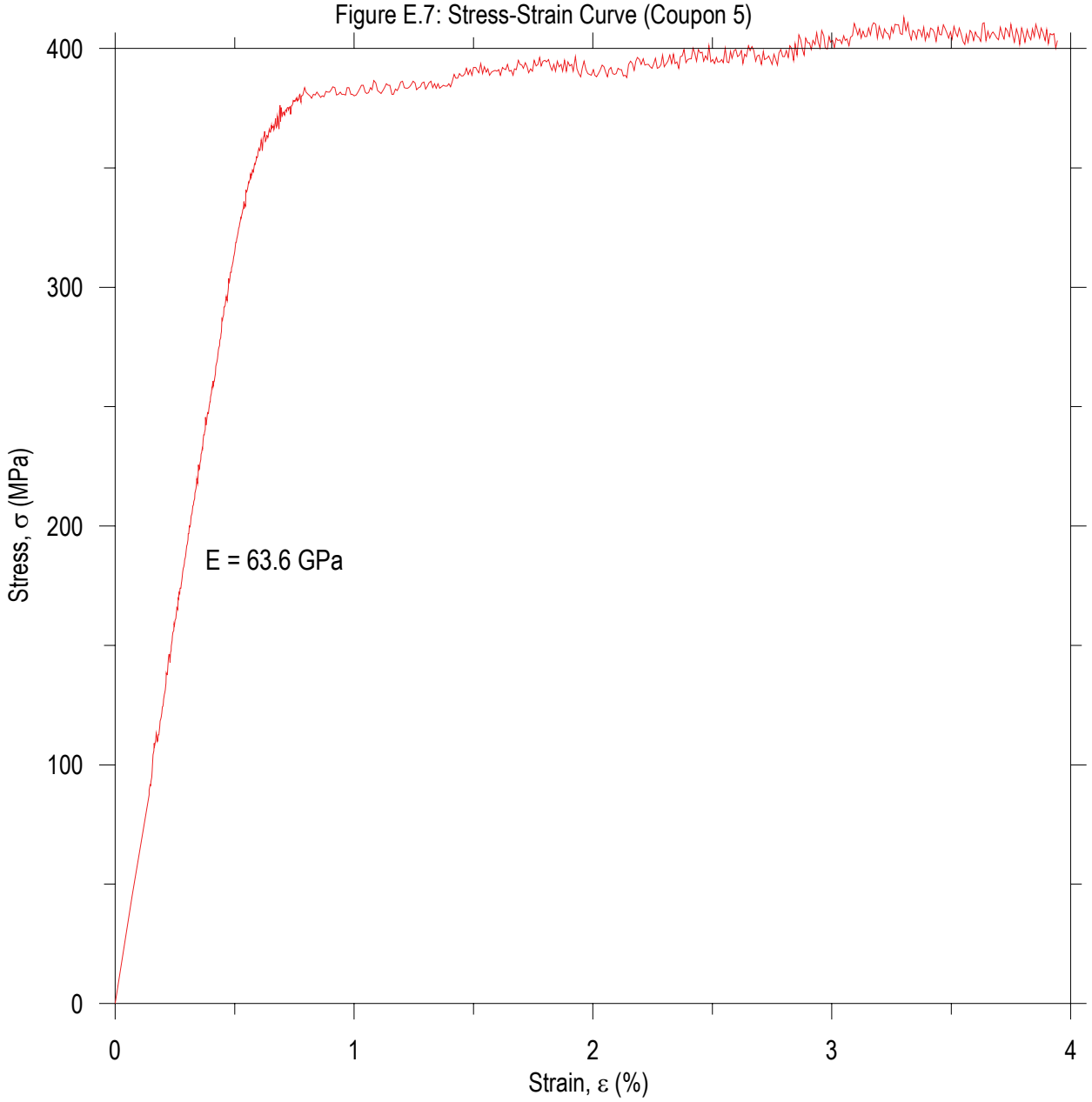


Figure E.8: Stress-Strain Curve (Coupon 6)

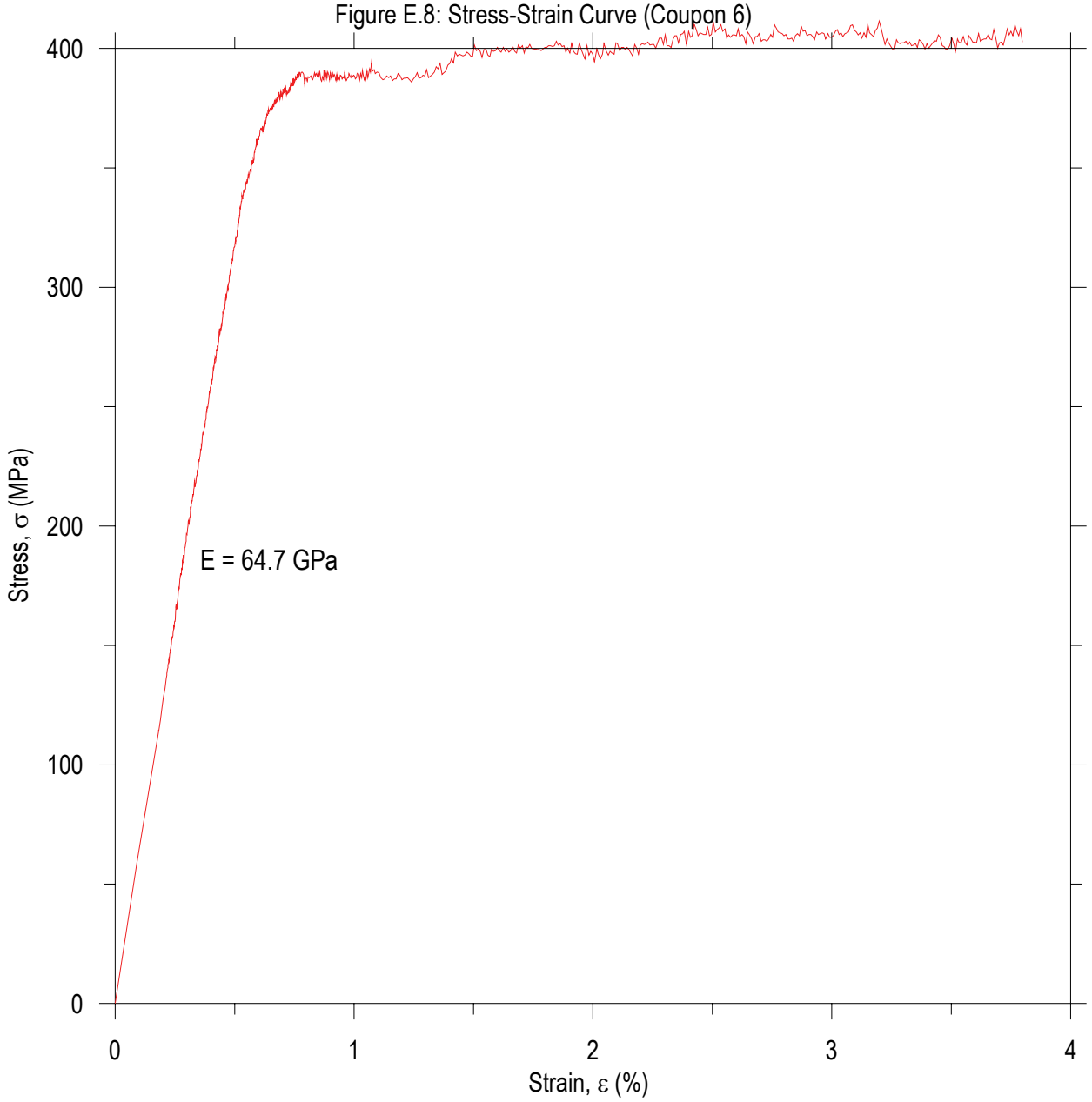
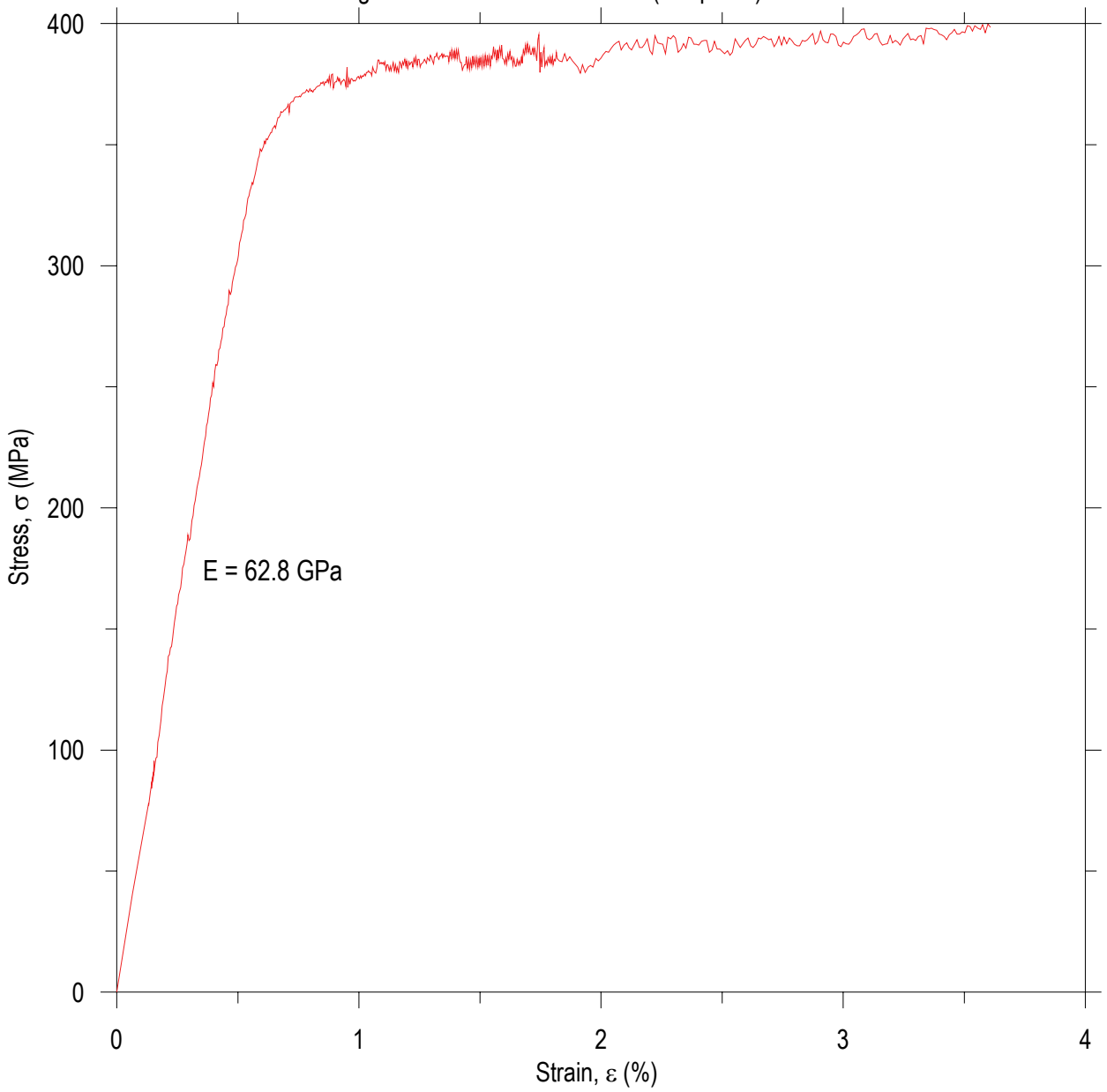


Figure E.9: Stress-Strain Curve (Coupon 7)



APPENDIX F

DENSITY OF THE COHESIVE MIX

The density of the cohesive mix used in this project was found by weighing a known volume. A cut plastic graduated cylinder was used as the vessel of known volume. It was sawn at approximately the "225 mL" mark. It was calibrated first by pouring water that had been de-ionised, distilled and de-aired to the lip of the cylinder. Care was taken to ensure that the entrainment of air was kept to a minimum. The dry mass of the cut cylinder had been determined prior to pouring water into it. The mass of the cylinder filled with water was taken three times. The temperature of the water was determined for each trial. Once the mass of the net amount of water was determined, the volume was found by using the density adjusted for temperature. The volume of the cut cylinder based on an average of the three trials was 223.13 mL.

Six samples of 500 g of total mass were prepared according to the mix design that was used in this project. Each batch was mixed for a minimum of five minutes to achieve homogeneity and to ensure that no clumps were present. The cylinder was filled nearly to the lip (approximately five mm from the lip), and tamped 25 times to force any trapped air to the free surface. The cylinder was then filled completely and weighed. The average unit weight was found to be 17.9 kN/m^3, with a specific gravity of 1.83.

APPENDIX G

STRAIN GAUGES & CALIBRATION CHARACTERISTICS

The strains were read directly in real time via the data acquisition system. The signals were converted instantly by using engineering units, otherwise known as '$mx + b$' units. The slope (m) is used to convert the raw electronic data into strains (ε), while the intercept value (b) accounts for any initial offsets that might exist; it was always zero for this project. The strains (ε) were found by using the following equation which is based on a Wheatstone bridge circuit involving four resistors:

$$\varepsilon = \frac{4}{GF \cdot V_e} \cdot 10^6 \quad \text{.....} (G.1)$$

where GF is the gauge factor and V_e is the excitation voltage. GF and V_e were always 2.11 and ± 2.0 V for this project, respectively. The conversion factor was found to be 9.47×10^5. Figure G.1 is a graphical summary of other strain gauge test data as provided by the manufacturer.

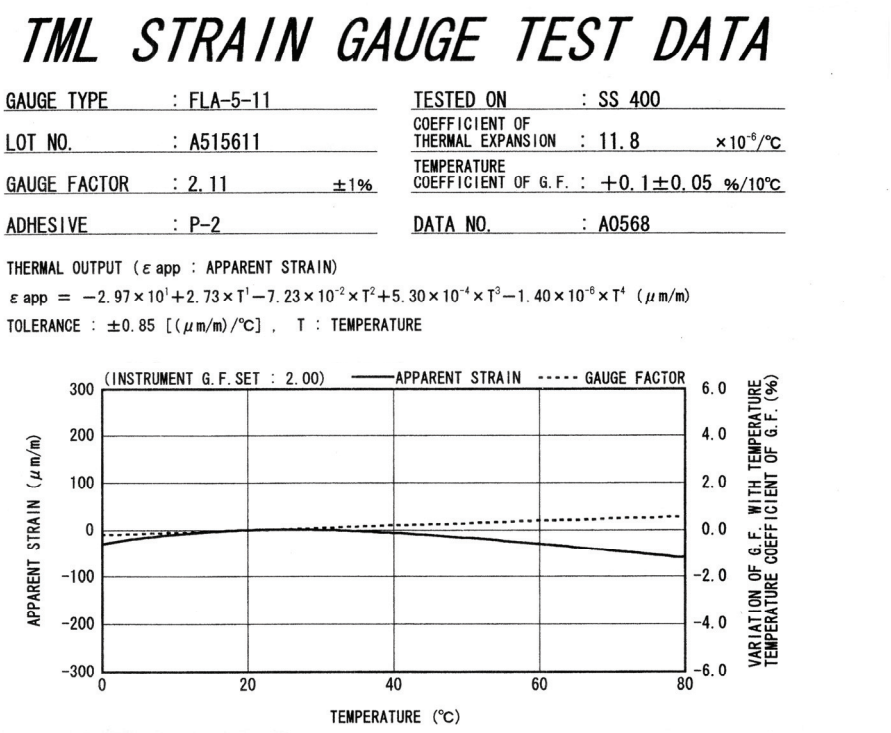


Figure G.1: Summary of test data for the strain gauges used (Tokyo Sokki Kenkyujo Co., Ltd)